Miguel Ângelo Machado Caiola

# Age and growth of the longfin mako shark, *Isurus paucus*, in the Equatorial Atlantic Ocean.

**Mestrado em Biologia Marinha**

**Supervisor:**

Rui Pedro Andrade Coelho (IPMA)

**Co-supervisors:**

Jorge Afonso Martins da Palma (UALG)

Daniela Rosa (CCMAR)


Faculdade de Ciências e Tecnologia

2024/2025

**Statement of authorship and copyright**

I hereby declare that I am the sole author of this master's thesis and have not recurred to any alternative sources other than those listed in my bibliography, and identified as references, for the elaboration of this work. I further declare that I have not submitted this thesis work at any other institution, with the purpose of obtaining a master's degree.



**Resumo**

O tubarão-anequim-de-gadanha (*Isurus paucus*) da família Lamnidae é uma espécie que é ocasionalmente capturada na pesca de palangre pelágica portuguesa, que tem como alvo principal espécies de grandes pelágicos comerciais, como o espadarte e o atum. Assim como para várias espécies de tubarão pelágico capturadas por esta indústria, existem poucos estudos publicados até à atualidade para *I. paucus*, especialmente a nível dos seus ciclos de vida, o que compromete a sua eficiente gestão pesqueira e proteção considerando a sua vulnerabilidade e baixa densidade populacional. Este estudo providência as primeiras estimativas de parâmetros de idade e crescimento para *I. paucus* no Oceano Atlântico Equatorial, contribuindo para o conhecimento científico atual acerca da espécie. Foram analisadas 294 amostras de vértebras recolhidas por observadores científicos a bordo de palangreiros comerciais portugueses entre 2012 e 2019. Os indivíduos amostrados tinham entre os 99 e os 230 cm de comprimento furcal (CF), sendo as amostras limpas e preservadas em álcool com a devida identificação. As vértebras foram imersas numa preparação de resina e catalisador em moldes de silicone, formando um bloco sólido de resina de forma a prevenir a quebra das vértebras durante a sua montagem e corte. Estes blocos foram seccionados recorrendo a uma máquina Buehler Isomet num corte sagital passando pelo centro da vértebra, produzindo secções entre 0.3-0.5 mm, sendo uma das secções coloridas por imersão em corante violeta de cristal. Após este processo, as preparações dos cortes foram observadas sob luz transmitida e microfotografadas utilizando um microscópio de dissecação equipado com uma câmara digital. As imagens foram editadas para melhorar o contraste entre as bandas de crescimento, e posteriormente transferidas para um computador. As leituras de bandas de crescimento foram feitas recorrendo ao software ImageJ, onde até aos seis anos de idade as bandas foram contadas de dois em dois pares, e de um em um par após esta idade. Após

uma contagem inicial de treino para aprender o método, as contagens foram feitas em triplicado. Apenas contagens diferindo por não mais que um ano foram consideradas válidas, levando ao descarte de três amostras que não corresponderam ao critério. Efetuaram-se medições desde o centrum da vértebra a cada banda de crescimento considerada válida e até ao bordo da vértebra ao longo do *corpus calcareum* de forma a obter o raio vertebral (RV) a cada idade e o RV total com uma macro do ImageJ. O enviesamento entre contagens foi avaliado graficamente, e a precisão entre leituras avaliada através do coeficiente de variação (CV) e do erro médio percentual (EMP), onde se obteve um CV = 5.6% e EMP = 4.3%, considerados aceitáveis de acordo com valores reportados na literatura. No entanto, detetou-se um enviesamento direcional negativo entre a primeira e segunda leitura e entre a primeira e terceira leitura. Foi feita uma regressão entre CF e o comprimento total (CT), uma vez que alguns estudos reportados na literatura usam CT em vez de CF. Assim, o tamanho à nascença ($L_0$) é de 99.3cm CF (108 cm CT), baseado na média entre o $L_0$ máximo e mínimo reportados na literatura e o tamanho máximo ($L\infty$) é 387 cm CF (427 cm CT), baseado no tamanho máximo reportado para fêmeas. Foram ainda feitas regressões lineares e quadráticas entre o CF e o RV de forma a obter o raio vertebral à nascença ($RV_0$), onde a regressão linear se apresentou mais apta na representação dos dados, obtendo-se um $RV_0$ de 3.31 mm. Foi utilizado retrocálculo para expandir os dados devido à falta de amostras de indivíduos pequenos, recorrendo a uma abordagem multi-metódica com o Dahl-Lea de proporções diretas (DL), Dahl-Lea com modificação linear (LDL), Dahl-Lea com modificação quadrática (QDL) e Fraser-Lee com interceção biológica (MFL). Os valores de CF retrocálculados foram avaliados através do desvio médio aos valores em CF observados a cada idade, onde o LDL e o QDL tiveram o melhor desempenho. Vários modelos de idade e crescimento foram aplicados aos dados originais e dados retrocálculados com o LDL e QDL, como o von Bertalanffy de dois parâmetros (2P-VBGF), von Bertalanffy de três parâmetros (3P-VBGF), o Gompertz (GOMP), Logístico (LOG) e Richard's (RICH). O desempenho dos modelos foi comparado recorrendo aos Critérios de Informação de Akaike (AIC) e Bayesiano (BIC). Para os mesmos modelos, comparou-se ainda a representação do crescimento dos sexos em conjunto e em separado através de testes de rácio de probabilidade, e apesar de não existir diferença significativa entre os sexos, os modelos foram apresentados para os sexos combinados e para os sexos em separado. O 3P-VBGF aplicado aos dados retrocálculados com o LDL produziu as estimativas de parâmetros consideradas biologicamente mais plausíveis para o crescimento dos machos ($L\infty$ =

363.466 cm CF, $k = 0.061$ $y^{-1}$, $L_0 = 96.075$ cm CF). Por outro lado, o 2P-VBGF, com o $L_0$ fixo em 99.3 cm CF aplicado ao LDL produziu as estimativas de parâmetros mais plausíveis biologicamente para o crescimento das fêmeas ($L\infty = 399.700$ cm CF, $k = 0.050$ $y^{-1}$) apesar de não ser suportado pelo AIC e BIC. A metodologia Bayesiana foi ainda aplicada recorrendo a informação prévia acerca da biologia da espécie, como tentativa de superar o obstáculo imposto às estimativas de $L\infty$ por falta de amostras de indivíduos maiores, gerando uma distribuição de posteriores prováveis com base nos dados originais. Apesar das distribuições posteriores permitirem uma melhor visualização das limitações impostas pelas amostras, a metodologia Bayesiana não teve sucesso em produzir estimativas de parâmetros biologicamente mais plausíveis para o crescimento de *I. paucus* comparado com o método LDL. Este trabalho contribui com informação importante acerca dos parâmetros de idade e crescimento e ciclo de vida de *I. paucus*. É recomendado que se continuem os estudos da biologia para esta espécie, em particular estudos de idade e crescimento em que a amostra abranja a distribuição de tamanhos conhecida da espécie. É ainda necessário realizar estudos de validação de idades que incluam amostras de indivíduos maiores, de forma a melhorar a precisão de futuros modelos demográficos e os dados usados nos modelos de avaliação e gestão de stocks de pesca para esta espécie.

**Palavras-chave** – Tubarão-anequim-de-gadanha; Vértebras; Parâmetros de história de vida; Crescimento; Retrocálculo; Estatística Bayesiana.

**Abstract**

The longfin mako shark (*Isurus paucus*, Lamnidae) is a species of mackerel shark often bycaught in pelagic longlines and one of the least studied pelagic sharks, hindering its effective management in fisheries. This study provides the first study on age and growth parameter estimates for *I. paucus* in the Equatorial Atlantic Ocean. Data from 291 individuals was collected between 2012 and 2019, with specimens ranging from 99 to 230 cm in fork length (FL) and analyzed. Vertebrae were sectioned and stained with crystal violet dye, age counts were performed, and the vertebral radius (VR) was measured from the centrum to each band and to the edge of the vertebra. Back-calculation methods such as Dahl-Lea (DL), linear Dahl-Lea (LDL), quadratic Dahl-Lea (QDL), and biological intercept Fraser-Lee (MFL) were applied to account for the lack of younger small individuals and evaluated based on their mean average deviation. Several growth models were fitted to the original sample data and back-calculated LDL and QDL data, such as the two-parameter von Bertalanffy (2P-VBGF), three-parameter von Bertalanffy (3P-VBGF), Gompertz (GOMP), Logistic (LOG), and Richards (RICH). The 3P-VBGF fitted to LDL data produced the most biologically accurate estimates for male growth ($L\infty$ = 363.466 cm FL, $k$ = 0.061 $y^{-1}$, $L_0$ = 96.075 cm FL) and the 2P-VBGF, with a fixed $L_0$ at 99.300 cm FL for females ($L\infty$ = 399.700 cm FL, $k$ = 0.050 $y^{-1}$). A Bayesian framework ,using priors developed from previous biological knowledge, was used to attempt to overcome the lack of large individuals in the sample, but failed to produce estimates biologically more plausible. These findings contribute with essential *I. paucus* life history parameter estimates and highlight the need for age validation studies and expanded sampling of large individuals to enhance the accuracy of future demographic and ultimately stock assessment models.

**Keywords** - Longfin mako shark; Vertebrae; Life history parameters; Growth; Back-calculations; Bayesian framework.

**Table of Contents**

**Aknowledgments**

First, I would like to thank my mother for all the support she has given me throughout my life, for being a great role model and true fighter, it is with love and admiration that this son dedicates this achievement to you. I would like to sincerely express my gratitude to Dr. Rui Coelho and Daniela Rosa for the chance to work with such a wonderful shark species, a childhood dream come true, and for all the advice, help and patience throughout the elaboration of this thesis. I would also like to thank the rest of my family and partner for all the love and support through these hard times, and without whom none of this would have ever been possible. Finally, I would also like to thank all the wonderful people and friends I made during not only my Marine Biology degree, but also during my masters, which provided some of the funniest moments and craziest studying sessions. So, from the bottom of my heart, thank you all for this wonderful journey.

## List of abbreviations, acronyms, and symbols

| | |
|---|---|
| Akaike information criterion | AIC |
| Average percent error | APE |
| Bayesian information criterion | BIC |
| Biological intercept Fraser-Lee method. | MFL |
| Bomb radiocarbon | $\Delta^{14}C$ |
| Coefficient of variation | CV |
| Confidence intervals | CI |
| Convention on International Trade of Endangered Species of Wild Fauna and Flora | CITES |
| Credibility interval | CrI |
| Dahl-Lea direct proportions method | DL |
| Degrees of freedom | df |
| Fork length | FL |
| Gompertz growth model | GOMP |
| International Commission for the Conservation of Atlantic Tunas | ICCAT |
| International Union for Conservation of Nature | IUCN |
| Instituto Português do Mar e da Atmosfera, I.P | IPMA |
| Leave-one-out information criterion | LOOIC |
| Linear-modified Dahl-Lea method | LDL |
| Logistic growth model | LOG |
| Longfin mako shark | *I. paucus* |
| Markov Chain Monte Carlo | MCMC |
| Mean average deviation | MAD |
| Methyl ethyl ketone | MEKP |
| Oxytetracycline | OTC |
| Porbeagle shark | *L. nasus* |
| Quadratic-modified Dahl-Lea method | QDL |
| Residual standard error | RSE |
| Richards growth model | RICH |

| | |
|---|---|
| Shortfin mako shark | *I. oxyrinchus* |
| Simple fisheries stock assessment methods | FSA |
| Standard error | SE |
| Three-parameter von Bertalanffy growth function | 3P-VBGF |
| Total length | TL |
| Two-parameter von Bertalanffy growth function | 2P-VBGF |
| Vertebral Radius. | VR |
| Von Bertalanffy growth function | VBGF |

## 1. Introduction

Sharks occupy a wide diversity of ecological niches varying based on species, behaviors, migration patterns, physiology, and dietary preferences (Carrier et al., 2022; Dedman et al., 2024; Heupel et al., 2014; Roff et al., 2016). For example, whale sharks (*Rhincodon typus*) are large and feed on small fish and zooplankton, while blackmouth catsharks (*Galeus melastomus*) are small and prey on euphausiaceans and small fish (Montero-Quintana et al., 2021; Rodríguez-García et al., 2024). Large apex predators consume a wide range of teleosts and cephalopods, playing a key role in regulating marine food webs (Cortés, 1999; Hairston et al., 1960; Lopez et al., 2010; Navia et al., 2010). The longfin mako shark (*Isurus paucus*) (Guitart Manday, 1966) is a rare, migratory apex predator species of mackerel shark within the Lamnidae family (Estupiñán-Montaño & Delgado-Huertas, 2022; Froese & D. Pauly, 2025).

*I. paucus* distribution spans the tropical and warm temperate Pacific, Atlantic, and Indian open oceans, and is rarely sighted in coastal waters (Bustamante et al., 2009; Compagno, 2008; Mucientes et al., 2013; Nelson et al., 2016; Ruiz-Abierno et al., 2021a; Wakida-Kusunoki & de Anda-Fuente, 2012). Additional sightings of the species include the Mediterranean Sea, where it is considered a cryptogenic species, as well as in the Arabian sea (Hemida & Capapé, 2008; Varghese et al., 2017; Zenetos et al., 2011).

Its coloration varies as it ages, with juveniles having a lighter ventral region, becoming dark blue like the dorsal region in adults (Castro, 2011). Its diet is generalistic, consisting of teleosts, squids, and other elasmobranchs, such as *Carcharhinus sp.*, which is likely linked to vertical migration patterns in the water column (Bowman, 2000; Bustamante et al., 2009; Gong et al., 2023). Information on dietary variations across geographic regions and different depths remains, however, underreported.

Morphologically, *I. paucus* shares many similarities with its congener, the shortfin mako shark (*Isurus oxyrinchus*), often being confused, but distinguishable by *I. paucus* slender and fusiform body, larger eyes, and pectoral fins longer than the length of its head (Castro, 2011; Chang et al., 2013; Compagno, 2001; ICCAT, 2016). Another distinguishing feature is the morphology of the teeth, with anterior teeth cusps of *I. paucus* being straighter and lacking reversed tips (Garrick, 1967; Whitenack & Gottfried, 2010). However, the similarities between both species hinder the proper identification of *I. paucus* for the

untrained eye, which might contribute to underreporting of *I. paucus* bycatch (Mandelman et al., 2008; Mucientes et al., 2013).

The pelagic longline fishing practice has long been employed in the capture of large pelagic commercial fish, such as tunas (*Thunnus sp.*), swordfish (*Xiphias gladius*), and other billfish species (Mandelman et al., 2008; Santos et al., 2024). Longlines are baited with prey preferred by these larger predators, such as squids, mackerel, and sardines (National Oceanic & Atmospheric Administration, 2025), often leading to the unintentional bycatch of several other species with similar dietary preferences, such as sea birds, cetaceans, sea turtles, and sharks (Anderson et al., 2011; Gallagher et al., 2014; Gilman et al., 2008; Queiroz et al., 2016; Santos, et al., 2023).

The low fecundity and low abundance of *I. paucus* make it highly vulnerable to bycatch, which may result in mortality, requiring the implementation of capture and retention restrictions for better management (Cortés et al., 2015; Pan et al., 2024; Gallagher et al., 2014). Using only nylon leaders instead of wire leaders in pelagic long lines has been shown to reduce the retention of elasmobranchs, even though most studies have not been able to collect sufficient and definitive data for rare species such as *I. paucus* (Gilman et al., 2008; Sales et al., 2010; Santos et al., 2024, Ward et al., 2009). Unregulated activities such as illegal fishing in poorly monitored international waters, as well as the pressure from finning industries, exacerbate challenges regarding the efficient management of shark species, despite many having an overall relatively low commercial value (Kai, 2021).

As most sharks adopt a K life-history strategy, a low reproductive potential is expected for the longfin mako, which together with a slow growth, may lead to fast declines in populations from overfishing (Cortés, 2008; Mucientes et al., 2013). Cortés et al. 2015 stated that *I. paucus* shows a very low productivity, making it one of the most vulnerable sharks to pelagic longline fisheries, along with the bigeye thresher (*Alopias superciliosus*). Additionally, the IUCN red list criteria attributed the Endangered status to *I. paucus* in 2019 (Rigby et al., 2018). This species was also listed in the Appendix II of CITES (Convention on International Trade in Endangered Species) (Sellheim, 2020). Furthermore, ICCAT (International Commission for the Conservation of Atlantic Tunas) also put forth a document recommending the monitorization of *I. paucus* captures in the North Atlantic Ocean (ICCAT, 2021), alongside a zero TAC (total allowable catch) for *I. oxyrinchus*. Despite these regulations, more robust measures and policies are required, as

illegal shark harvesting practices, including for fins, still occur and still appear in oriental markets as highly desirable products, especially larger fins like those of *I. paucus* (Cardeñosa et al., 2022; Oktaviyani et al., 2022; Saigal et al., 2024; Ward-Paige, 2017).

Data on sizes, life history, and reproduction of *I. paucus* remains limited, being an aplacental viviparous species, with oophagy present in embryos (Gilmore, 1983; Varghese et al., 2017). It gives birth to litters of 2 to 8 pups, ranging from 86 - 135 cm total length (TL), however, information on *I. paucus* nursery locations and its reproductive seasons remains unknown (Castro et al., 1999; Gilmore, 1983; Ruiz-Abierno et al., 2021a).

Ruiz-Abierno et al., 2021a reported on the length-at-maturity of *I. paucus*, with a median TL of 215 and 230 cm for males and females, respectively. As for the largest sizes, the most common sizes in landings range between 310 and 345 cm TL (Bustamante et al., 2009; Dodrill & Gilmore, 1979; Ruiz-Abierno et al., 2021b), with the largest specimen recorded being a female with 427 cm TL (Castro, 2011).

Information on the age and growth of *I. paucus* remains unknown, in part due to its rarity and difficulty of sample acquisition after the species CITES listing (CITES, 2019). Ageing studies are essential in developing age-length keys and growth models. In sharks these studies are commonly conducted using elasmobranch vertebrae (similarly to teleost otolith readings) which exhibit differential patterns in calcified material accumulated as sharks age (Cailliet et al., 2006; Goldman, 2005; Raoult et al., 2016; Régnier et al., 2021). Considering many shark species, such as *I. paucus*, are listed as data deficient for stock assessments and conservation efforts, studies describing their life history, age, and growth are essential for their efficient management in fisheries (Smart et al., 2012).

This thesis focused on the analysis of *I. paucus* vertebral samples, collected by onboard fishery observers along the Equatorial Atlantic Ocean. Various statistical methods were employed, such as back-calculations, to increase the sample size especially at younger age classes (Goldman & Cailliet, 2004). Several growth models, such as the modified versions of the von Bertalanffy growth function (VBGF) (Von Bertalanffy, 1938) were explored to estimate growth parameters both with the original data and back-calculated data. These models were fitted using a frequentist approach, and also a Bayesian inferential framework with the use of priors (Gelman et al., 2013). Thus, this work aims to contribute to a better understanding of *I. paucus* life history, providing new information

to current scientific knowledge for this species, which ultimately allows for better scientific advice to be provided and a more efficient and sustainable management of fisheries.

## 2. Materials and methods

### I. Sampling and sample characteristics

Samples of *I. paucus* were taken from individuals that were dead on capture, prior to the species CITES listing (CITES, 2019) (Figure 2.1). These samples were collected aboard Portuguese commercial longline fishing vessels targeting swordfish by scientific observers from IPMA (Instituto Português do Mar e da Atmosfera, I.P.) in the Equatorial Atlantic Ocean. A total of 294 samples were collected over the span of seven years, between July 2012 and November 2019, with sampling conducted in different vessels throughout the period. These samples were taken between 5ºS and 13ºN (latitude) and between 0ºW and 24ºW (longitude) (Figure 2.2).

Biological data, such as the fork length (FL), measured in a straight line to the nearest centimeter from the shark snout to the fork of their tail, and the sex of each specimen was recorded (Rosa et al., 2017). Samples were collected by removing a section of 4-8 vertebrae from the anterior region of the carcass (directly behind the head) and were kept frozen during transportation to the IPMA-Olhão laboratory, where preparations of vertebral sections were made. The frequency of males and females across different size classes was plotted, based on their recorded FL to assess the number of males and females within 10 cm size classes. The normality assumption was tested for FL using Shapiro-Wilk's test (Shapiro & Wilk, 1965), and the mean and standard deviation for the FL range of each sex was calculated.

Vertebral samples were collected by removing a section of 4-8 vertebrae from the anterior region of the carcass (directly behind the head) and were kept frozen during transportation to the IPMA-Olhão laboratory, where preparations of vertebral sections were made.

Additionally, measurements of 102 individuals were taken for both FL and total length (TL), measured in a straight line to the nearest centimeter from the tip of the snout to the tip of the tail.

**Figure 2.1**– Picture of a longfin mako shark (*I. paucus*) on-board longline fishing vessels targeting swordfish in the equatorial Atlantic Ocean. The distinctive larger eyes and longer fins are visible, providing a distinction from the shortfin mako shark. Credits: Image provided by Sérgio Goes (IPMA-Olhão).

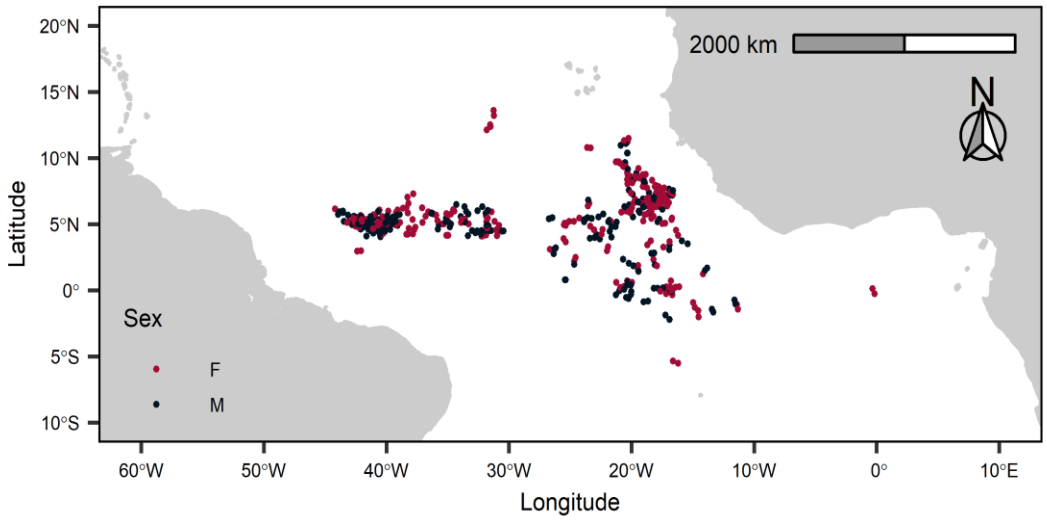


**Figure 2.2**– Map of longfin mako shark (*I. paucus*) vertebral samples collected for this study. Red dots represent sampled females, while black dots represent sampled males. Coordinates were jittered by 0.5x0.5 degrees.

## II. Vertebral sample processing, imaging, and editing

All samples were processed, analyzed, and made available by the Highly Migratory Species Group from DivRP (*Divisão de Modelação e Gestão dos Recursos da Pesca*) at

IPMA-Olhão. The vertebrae were cleaned by first removing larger pieces of connective tissue and flesh using scalpels. Smaller remnants of connective tissue were then removed by soaking the vertebrae in a 4-6% sodium hypochlorite solution (NaClO), with the immersion time depending on the size of the vertebral sample. The samples were then preserved in plastic flasks filled with 70% ethanol ($C_2H_6O$). A pencil-written label containing information on the sample code, species, FL, and sex, was placed inside the flask until processed (Figure 2.3).

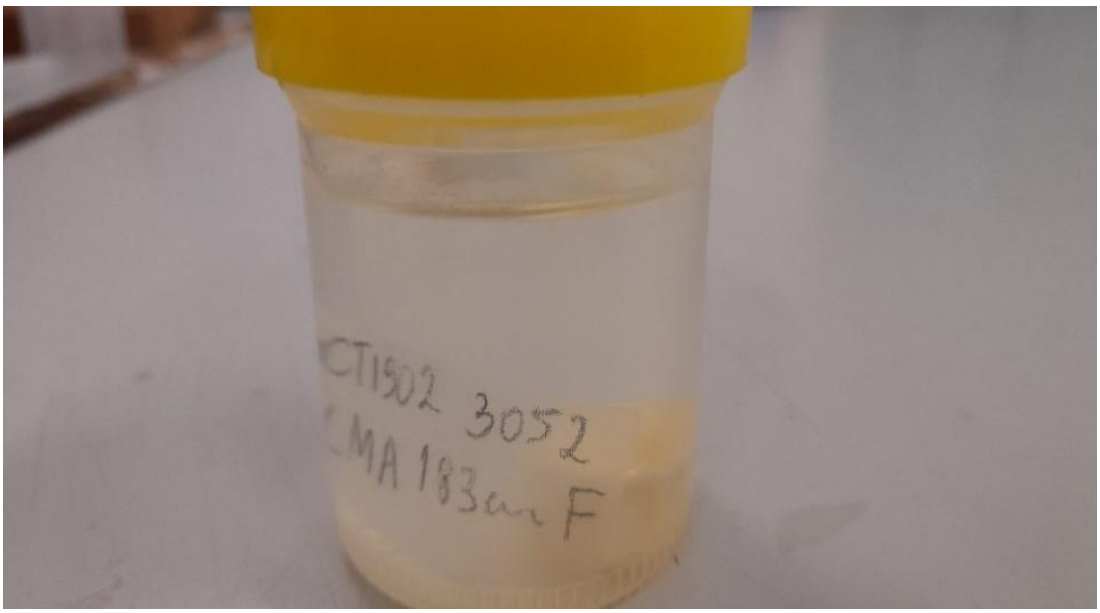


**Figure 2.3**– Example of a longfin mako shark (*I. paucus*) vertebrae, preserved in 70% ethanol. This sample contained a label with the following information: CT19023052 (sample unique ID), the species (LMA- longfin mako shark, FAO species code), the fork length (FL; 183 cm), and sex (F- female).

For sectioning, the method described in Coelho et al. (2011), Rosa et al. (2017), and Rosa et al. (2021) were followed. A modification of this method was applied in cases where a second preparation of the vertebrae had to be made, due to broken sections and difficulties while counting concentric growth bands. This modification consisted in encasing the vertebrae in resin blocks before sectioning, making them less susceptible to breaking. This second method is described hereafter.

First, samples were removed from their respective flasks and left to air-dry for approximately 24h. Once dry, polyester resin was mixed with methyl ethyl ketone peroxide (MEKP) ($C_8H_{18}O_6$) catalyst and added in small amounts to wells in a silicon mold, creating a bottom layer where the sample codes were inserted for sample identification. This layer was left to partially curate for 30 minutes to 1 hour until it had a more viscous consistency. The vertebral samples were then dipped in the same resin

mix and placed in the respective wells in the desired cutting orientation. An important factor to note is that vertebral facets are concave, so the bottom layer was made deep enough to fill this cavity and avoid air bubble retention. Dipping the samples in resin ensures that large air bubbles do not cause the vertebrae to float or rotate, which would make cutting through the center impossible once the block hardens.

The orientation of the lamellae (calcified areas in the intermedialia of lamnid sharks) towards the blades is crucial for obtaining a complete vertebral section with accurate age and growth information. Less calcified areas can result in incomplete age band data, leading to errors during age readings. After positioning the samples on the bottom layer, they were covered with the same resin mixture and left to fully harden over 3 to 5 days, depending on temperatures and humidity (Figure 2.4).

**Figure 2.4**– Longfin mako shark (*I. paucus*) vertebral samples within assigned silicon mold wells after being encased in a polyester resin coating.

Each hardened resin block containing the encased vertebral sample was then individually mounted in a Buehler Isomet (Lake Bluff, IL) low-speed saw using an adjustable holding piece to secure the block in place while cutting (Figure 2.5). The machine arm, to which the block holder was attached, is also adjustable, allowing for an easy alignment of the circular diamond-wafering blades with the center of the vertebrae. This arm can also be weighed to accelerate the cutting process, but excessive weight was avoided to prevent damage to the blades or sample. Two wafering blades were mounted on a lower rotating cylinder and separated by a 0.3-0.5mm gap using a thin spacer at the center, defining the thickness of the sagittal section.

The machine's well was filled with tap water up to the edge of the wafering blades, to keep them wet. As the blades rotate at a specified speed, they gradually erode the block and vertebrae, cutting them into a "bowtie" shaped sagittal section, with both ends meeting at the focus. The proper maintenance of these blades is also crucial, as these can easily deteriorate and break if not washed and dried correctly after extensive use.

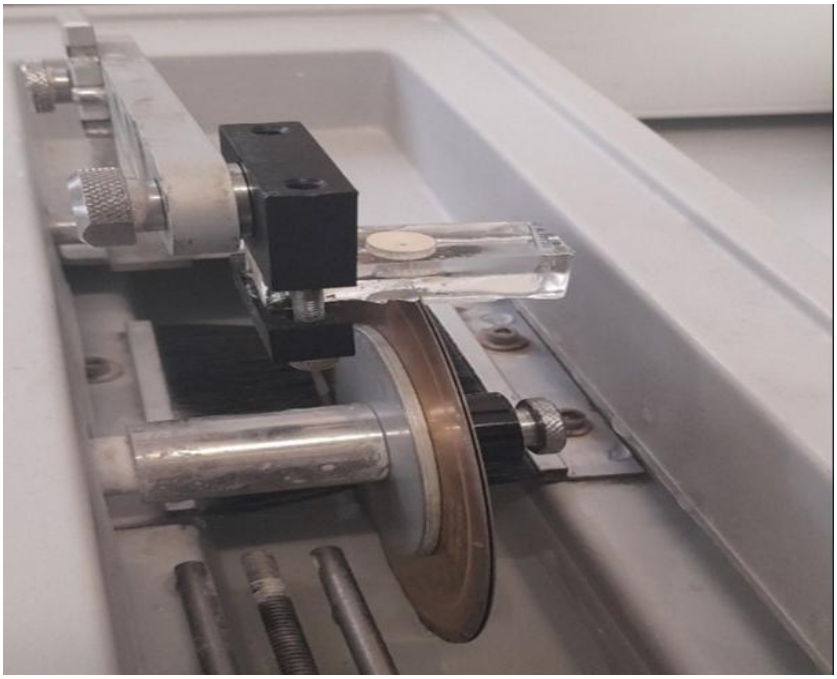

**Figure 2.5**- Buehler Isomet model low-speed saw, equipped with two diamond wafering blades. The lower chamber of the machine was filled with water to keep the blade tips wet, performing a centered 0.3 mm sagittal section of the longfin mako shark (*I. paucus*) vertebra.

The use of dyes in elasmobranch vertebral cuts can be especially useful, as the visibility of growth bands in certain species, including *I. paucus*, is particularly challenging (Cailliet et al., 1983). Therefore, one of the two halves of the "bowtie" sagittal cut was immersed in crystal violet dye (Sigma-Aldrich Co., St Louis, MO) for approximately 3 minutes, as this die was recommended as being the most effective at enhancing the contrast between opaque and translucent concentric bands for pelagic shark species, such as the smooth hammerhead shark (*Sphyrna zygaena*) by Coelho et al. (2011). The other half section was left undyed to assess the ease of band visualization between dyed and undyed.

The dyed sections were then placed in paper, which was folded over the sections and compressed between two sample slides to dry. After completing the staining process, the sections were carefully mounted on microscope slides, which were pre-labeled with the

specimen information, using anhydrous Neo-Mount™ mounting medium (Sigma-Aldrich Co., St Louis, MO) (Figure 2.6) and then stored.

**Figure 2.6**– Labeled longfin mako shark (*I. paucus*) vertebral sections mounted on microscope slides with NeoMount™ after the application of crystal violet dye. One side of the section is undyed, and the other is dyed with the crystal violet dye.

The slides were observed using a Nikon P-DSL32 dissecting microscope with white transmitted light, equipped with a Nikon Digital Sight DS-L3 camera (Figure 2.7).

**Figure 2.7**- Nikon P-DSL32 dissecting microscope used to visualize vertebral sample slides of longfin mako sharks (*I. paucus*) and Nikon Digital Sight DS-L3 camera and screen for image and scale adjustments.

This digital camera transmits images to a screen attachment, allowing adjustments of magnification and scale to capture detailed pictures of the vertebral sections, where a 1mm scale was added to the images (Figure 2.8). These images were then stored in a

memory card and later transferred to a computer for further editing using the open-source software ImageJ (Schneider et al., 2012).

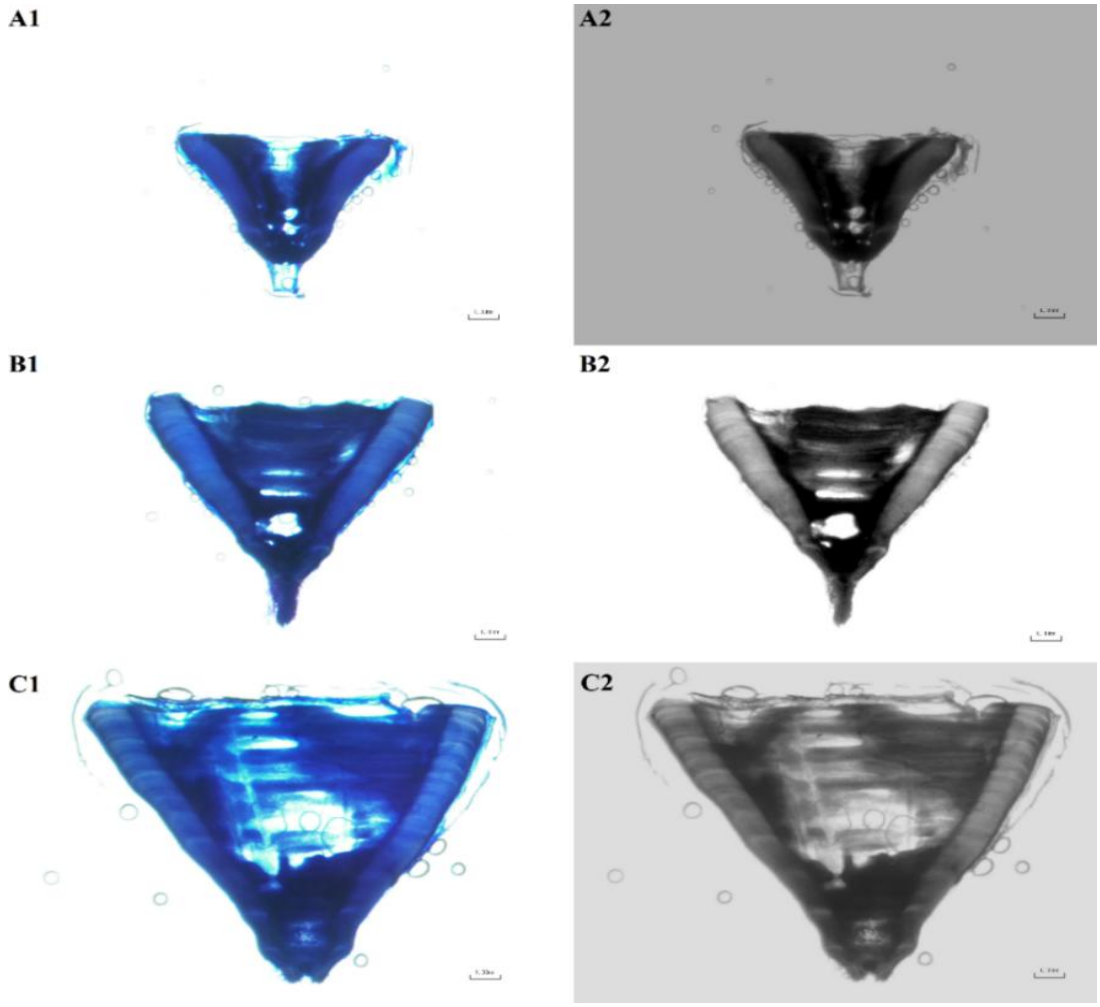


**Figure 2.8**- Side by side comparison of three different vertebral sections microphotographs from longfin mako sharks (*I. paucus*) with a 1mm imprinted scale taken with a camera coupled to a dissecting microscope (A1, B1, C1) and edited versions to enhance contrast using the ImageJ software (A2, B2, C2).

### III. Length-length relationship

A linear regression between the TL measurements (range: 114 to 363 cm TL) and their respective FL (range: 101 to 328 cm) value was fitted (n=102), to obtain the regression formula. Residuals were analyzed graphically and the $R^2$ (coefficient of determination) calculated. These parameters were used to transform the size-at-birth from TL to FL, which was used in the back-calculations and growth modelling, and maximum recorded size, to be compared with the asymptotic maximum length ($L\infty$) from growth models, that are reported in the literature in TL. The known birth size ranges between 86 cm (free

swimming) and 135 cm (largest recorded embryo) TL (Castro et al., 1999; Gilmore, 1983; Ruiz-Abierno et al., 2021a). The mean length-at-birth ($L_0$) was obtained by first converting the known pup maximum and minimum TL-at-birth to FL with the regression formula, and then calculating the mean FL as follows, respectively:

$$\mathbf{FL(cm) = (TL(cm) - b) \div m}$$

$$\boldsymbol{L_0 = (FL135 + FL86) \div 2}$$

The TL value of the largest recorded female (427 cm TL; Castro, 2011) was also converted to FL using the TL/FL formula above. Considering data on the maximum size of males is limited, with the largest reported male being a 303 cm TL (276 cm FL) male south of the Gulf of Mexico, the same initial L∞ used for females was assumed for males (Wakida & de Anda-Fuente, 2012).

**IV. Age band readings, precision, and bias plots**

The 294 samples were initially counted once as training to become familiarized with the method and vertebral sections. Based on the fact that for its closely related congener, *I. oxyrinchus*, two band pairs are deposited per year in its first 6 years of life, the same was assumed for these *I. paucus* age readings, which is a common practice when species-specific age validation is unavailable (Chin et al., 2013; Kinney et al., 2016; Wells et al., 2013). Three age counts for *I. paucus* were conducted by a single reader and an age estimate was only assigned when there were two out three concordant age readings, which is hereafter considered the agreed age (Andrade et al., 2019; Campana, 2005). To minimize personal bias during counts, the sex, FL, and results of prior readings were withheld, and each count was finalized before initiating a new count, reducing the influence of familiarity or memory with previous counts (Campana, 2005).

A feature observed in *I. paucus* sagittal sections is that often the intermedialia was incomplete, turning the visualization of bands in this region difficult, and as such, counts were made along the *corpus calcareum* (Cailliet et al., 2006). In sharks, the first band pair is considered to be a birthmark. Birthmarks are usually also found through a visible change in the *corpus calcareum* angle (Goldman, 2005), however for the longfin mako the angle change was not prominent in most vertebral samples. To reduce the chance of under/overestimation of age, the position of the birthmark was defined by measuring the

vertebral radius (VR) of specimens with a capture size close to the defined size-at-birth and considered as young-of-the-year.

A challenge in age counts is the occurrence of "false checks" or "split banding", where deviations in a sharks' typical growth pattern creates gaps mistakenly interpreted as additional age bands (Goldman, 2005). Additionally, age estimates for larger individuals are often underestimated due to the compression of terminal bands, which can overlap during deposition or be absent once growth ceases (Cailliet et al., 2006; D'Alberto et al., 2016).

Bias plots were then used as a measure to assess the personal bias, directional bias (positive or negative), consistency, and precision of age readings, following a similar approach to that of other shark ageing studies (Campana, 2005; Emmons et al., 2021; Goldman, 2005; Rosa et al., 2017; Rosa et al., 2021). McNemar's test was also employed (McNemar, 1947) to assess pairwise differences between readings. The coefficient of variation (CV) and the average percent error (APE) were also estimated, with estimates being used to assess the precision of age readings.

Potential differences in length-at-age between male and female *I. paucus* were analyzed by comparing the length-at-age of each sex. The normality and homogeneity of variances assumptions were tested for each sex for both FL and agreed ages using Shapiro-Wilk's and Levene's test (Levene, 1960; Shapiro & Wilk, 1965), respectively, and a non-parametric Mann-Whitney U test was used to test size-at-age differences between sexes (Mann & Whitney, 1947).

## V. Back-calculations

Back-calculations were used to estimate the length-at-previous-ages of sampled individuals based on known species measurements, such as the VR and FL (Francis, 1990; Goldman, 2005; Goldman & Cailliet, 2004). This method is usually applied when species size ranges are incomplete, or for smaller sample sizes (Goldman et al., 2006; Goldman & Cailliet, 2004). As this was the case, especially for FL < 120 cm, back-calculations were performed to expand the dataset, and possibly improve growth model fits.

For back-calculations, a multi-method approach was applied following Goldman and Musick (2006), where the mean average deviation (MAD) of the back-calculated FL-at-age was compared to the sample mean FL-at-age to determine the most statistically and biologically appropriate method to use for growth model parameter estimates (Goldman & Cailliet, 2004).

While these methods are commonly used in fisheries research to expand fish life history databases, these methods lack critical assessments to the accuracy of data outputs, with few extant critiques on the realism of produced fish length-at-previous-age patterns, which requires a careful interpretation of results (Vigliola & Meekan, 2009).

### V.I. FL-VR regression

Parameters from an FL-VR equation are necessary for use in some back-calculation methods as detailed below. The measurements were obtained using the ImageJ software with a macro designed for otoliths and modified to work with vertebral bands (Schneider et al., 2012). This software also converted pixels into millimeters, according to the 1 mm scale previously implemented in vertebral photographs with the dissecting microscope camera. Measurements were made between the focus and each subsequent accepted band-pair, as well as the total VR (Figure 2.9), and were only taken for vertebrae with accepted band counts.

The FL-VR was fitted with a linear and quadratic regressions as follows:

$$\mathbf{FL = a + (b \times VR)}$$

$$\mathbf{FL = a + (b \times VR) + (c \times VR^2)}$$

Both were compared using their $R^2$ values, the Akaike Information Criterion (AIC) (Akaike, 1973), and Bayesian Information Criterion (BIC) (Schwarz, 1978) to assess how well each fitted the data. The residuals of the chosen regression were graphically evaluated and tested for their normality and homoscedasticity using Shapiro-Wilk's and Breusch-Pagan's tests, respectively (Breusch & Pagan, 1979; Shapiro & Wilk, 1965).

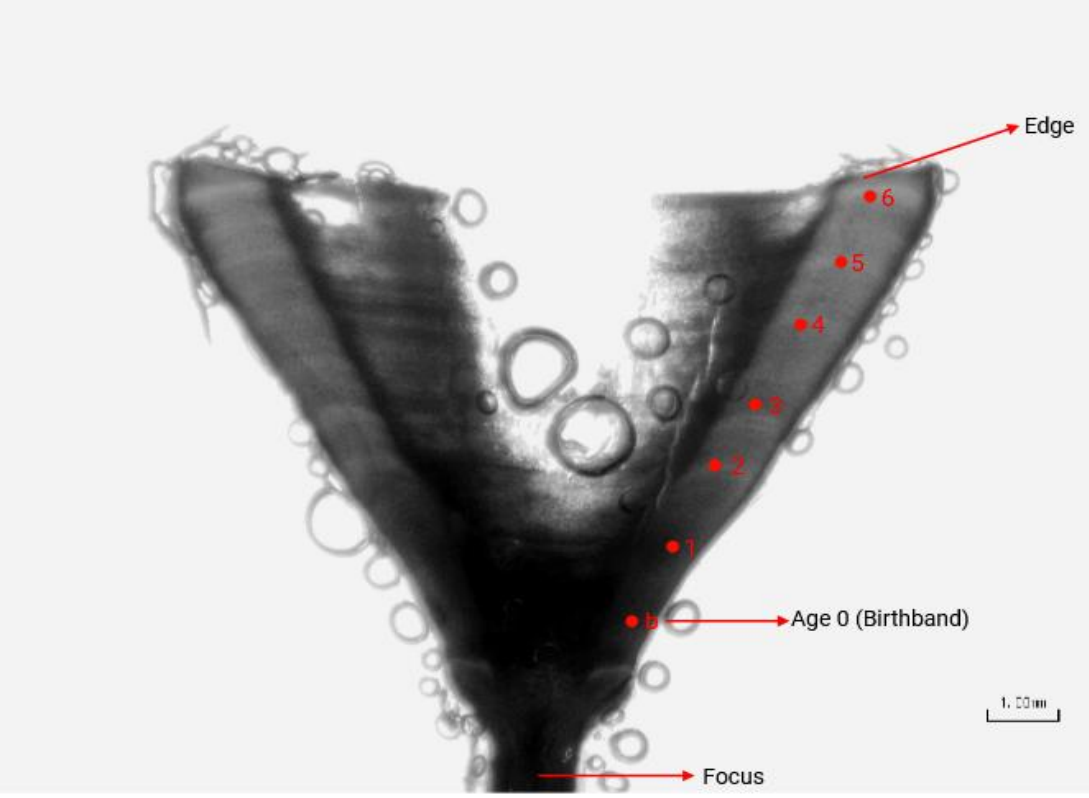


**Figure 2.9** – Microphotograph of a female longfin mako shark (*I. paucus*) vertebra with age count estimates. The image was edited with the ImageJ software, including the focus, birthmark (b), and edge markings. Red dots represent the increments and the numbers the band counts. This is a vertebra of a 187 cm fork length longfin mako shark, estimated to be six years old.

## V.II. Dahl-Lea direct proportions method

The Dahl-Lea direct proportions method (DL) (Carlander, 1969) is a commonly used method to back-calculate the fish length-at-previous-age. This method assumes a direct proportion between a sharks' FL at capture and VR, implying that the species grows isometrically as time passes (Vigliola & Meekan, 2009). The following equation was applied for the DL back-calculation method:

$$\boldsymbol{Li} = (\boldsymbol{VRi} \div VR_T) \times \boldsymbol{Lc}$$

***Lc*:** Length-at-capture.

***Li*:** Length-at-age i.

***$VR_T$*:** Total vertebral radius.

***VRi*:** Vertebral radius at age i.

### V.III. Linear-modified Dahl-Lea method

The linear-modified Dahl-Lea method (LDL) (Francis, 1990), is an alternative version to the DL method to back-calculate fish length-at-previous-age, which assumes a linear relationship between the FL and VR and uses parameters from an FL/VR linear regression, rather than a proportional growth assumption. For this, the following equation was applied:

$$\boldsymbol{Li = [(a + b \times VRi) \div (a + b \times VR_T)] \times Lc}$$

***a*:** Linear fit parameter estimate.

***b*:** Linear fit parameter estimate.

***Lc*:** Length-at-capture.

***Li*:** Length-at-age i.

***$VR_T$*:** Total vertebral radius.

***VRi*:** Vertebral radius at age i.

### V.IV. Quadratic-modified Dahl-Lea method

The quadratic-modified Dahl-Lea method (QDL) (Francis, 1990), uses the parameters of a quadratic FL/VR regression to back-calculate the length-at-previous-age in fish. This method is suitable for back-calculations of species with complex growth patterns. The following equation was used with this back-calculation method:

$$\boldsymbol{Li = Lc \times [(a + b \times VRi + c \times VRi^2) \div (a + b \times VR_T + c \times VR_T^2)]}$$

***a*:** Quadratic fit parameter estimate.

***b*:** Quadratic fit parameter estimate.

*c*: Quadratic fit parameter estimate.

***Lc*:** Length-at-capture.

***Li*:** Length-at-age i.

***$VR_T$*:** Total vertebral radius.

***VRi*:** Vertebral radius at age i.

### V.V. Biological intercept Fraser-Lee method

The biological intercept Fraser-Lee method (MFL) (Campana, 1990) much like the prior methods, is used to back-calculate the length-at-previous-age of fish. This method assumes a proportional relation between the fish FL and VR, while accounting for the fact that the shark has a size different from zero when the vertebrae are formed, which is why $L_0$ and vertebral radius at birth ($VR_0$) estimates are necessary. For this purpose, the following equation was used with the back-calculation method:

$$Li = Lc + (VRi - VR_T) \times [(Lc - L_0) \div (VR_T - VR_0)]$$

***L*$_0$:** Mean length-at-birth.

***Lc*:** Length-at-capture.

***Li*:** Length-at-age i.

***VR*$_0$:** Vertebral radius at birth.

***VR*$_T$:** Total vertebral radius.

***VRi*:** Vertebral radius at age i.

The $VR_0$ was calculated from the $L_0$ by applying either the linear or quadratic equation, depending on which presented the best fit to the data.

### VI. Frequentist growth modelling

A multi-model approach as suggested by Cailliet et al. (2006) was employed to estimate the growth of *I. paucus*, using data from age readings and FL measurements. By fitting various models, it is possible to compare and evaluate them, allowing the selection of a model which presents an optimal goodness-of-fit to the data, while avoiding less likely candidate models.

Models were fit to the original sample data and back-calculated data. These models were used to estimate growth for both sexes separately and in combination, to avoid missing

relevant growth differences between sexes and properly test them if present (Goldman, 2005).

For the models, the normality of distributions was evaluated through various methods. These involved normal Q-Q plots and residual analysis to detect any outliers and assess issues with their distributions (Anscombe, 1973; Wilk & Gnanadesikan, 1968). Lastly, likelihood ratio tests were conducted to compare the sex-separated and combined growth model outputs and assess if growth differences exist between sexes (Wilks, 1938).

### VI.I. Three-parameter von Bertalanffy growth model

The three-parameter von Bertalanffy growth model (3P-VBGF) (Ricker, 1975) is extensively used in elasmobranch age and growth studies (Andrade et al., 2019; Gervelis & Natanson, 2013; Harry et al., 2011; Rosa et al., 2017).

While the original model uses $t_0$ (age/time when length is zero), $L_0$ was introduced as the mean size at birth by Fabens (1965) and used in this study as a replacement for $t_0$ (Cailliet et al., 2006; Goldman, 2005; Rosa et al., 2017). Unlike the two-parameter Von Bertalanffy (2P-VBGF), $L_0$ values are estimated, granting the model more flexibility. The originally proposed function by Von Bertalanffy (1938) with the modification by Fabens (1965) was applied:

$$L_a = L\infty - (L\infty - L_0) \times e^{(-k \times \text{Agreed Age})}$$

$L_a$ = Length-at-age (cm).

$L\infty$ = Asymptotic maximum FL (cm).

$k$ = Relative growth coefficient ($year^{-1}$).

$L_0$ = Mean FL at birth (cm).

**Agreed age** = Agreed age for the individual from observer counts ($year^{-1}$).

The model was provided with initial values for the parameters, which allowed it to estimate $L\infty$ and the rate at which $L_a$ approaches $L\infty$ through $k$ (Brody, 1945). The resulting curve should be sigmoidal (or S-shaped), describing an initial exponential growth phase, followed by a gradual deceleration in growth as the individual ages, and a horizontal asymptote as the curve approaches L∞.

### VI.II. Two-parameter von Bertalanffy growth model

The 2P-VBGF (Von Bertalanffy, 1938) is a growth model often used in fisheries to estimate growth parameters (Andrade et al., 2019; Harry et al., 2011; Hsu et al., 2014; Thorson & Simpfendorfer, 2009). Since $L_0$ value is known, the $L_0$ obtained from the literature (see section 2.III) was fixed at 99.3 cm FL. The same formula for the 3P-VBGF was applied, with $L_0$ being fixed instead of estimated.

### VI.III. Gompertz growth model

The Gompertz growth model (GOMP) (Gompertz, 1825) is used to describe the length-at-age of an organism or population over time, and is often used to describe larval and early life stage growth of fishes (Smart & Grammer 2021; Emmons et al., 2021). Like the 2P-VBGF and 3P-VBGF, the GOMP can model growth, but instead of using the $L_0$ parameter, it instead uses an initial size variable ($\alpha$), influencing the growth rate. The modified version of the GOMP function used was as follows:

$$\boldsymbol{L_a = L\infty \times e^{(-\alpha \times e\text{^}(-k \times \text{Agreed Age}))}}$$

$\boldsymbol{L_a}$= Length-at-age (cm).

$\boldsymbol{L\infty}$ = Asymptotic maximum FL (cm).

$\boldsymbol{k}$ = Instantaneous growth rate at inflection point (year$^{-1}$).

$\boldsymbol{\alpha}$ = Initial size variable.

**Agreed age** = Agreed age for the individual from observer counts (year$^{-1}$).

### VI.IV. Logistic growth model

Logistic growth models (LOG) (Verhulst, 1838) are commonly used to describe the growth rate of organisms subject to challenges imposed by the environment such as, for example, resource limitations (Carlson et al., 2007; Grant et al., 2018; Hueter et al., 2006). Although environmental limitations were not a primary focus of this study, the LOG was fitted to the data for comparisons with prior models. The LOG produces a sigmoidal curve, which is instead symmetrical, as the growth slows consistently through time. The function used for the LOG was as follows:

$$L_a = L\infty \div (1 + e^{(-k \times (\text{Agreed Age} - t))})$$

$L_a$= Length-at-age (cm).

$L\infty$ = Asymptotic maximum FL (cm).

$k$ = Instantaneous growth rate at negative infinity (year$^{-1}$).

$t$ = Time at inflection point (year$^{-1}$).

**Agreed age** = Agreed age for the individual from observer counts (year$^{-1}$).

### VI.V. Richard's growth model

Richard's growth model (RICH) (Richards, 1959) is an elaborate variant of the LOG, designed to accommodate more complex growth patterns (Barreto et al., 2011; Hernandez-Llamas & Ratkowsky, 2004). This is achieved by introducing a curve shaping parameter ($b$), which allows the growth curve to exhibit asymmetry, offering greater flexibility compared to the symmetric growth offered by the LOG. The function used for the RICH was as follows, with $L_0$ being fixed at 99.3 cm FL, instead of estimated:

$$La = L\infty \times (1 + ((L_0^{(1-b)}) \div L\infty)) - 1) \times e^{(-k \times \text{Agreed Age}))^{(1 \div (1-b))}}$$

$L_a$= Length-at-age (cm).

$L\infty$ = Asymptotic maximum FL (cm).

$k$ = Growth coefficient at inflection point (year$^{-1}$).

$L_0$ = Mean FL at birth (cm).

$b$ = Curve shaping parameter.

**Agreed age** = Agreed age for the individual from observer counts.

### VI.VI. AIC and BIC for model selection

Each growth model fit was assessed using AIC (Akaike, 1973) and BIC (Schwarz, 1978). The AIC evaluates model parsimony and goodness-of-fit, by scoring models with a better goodness-of-fit higher, but penalizing model complexity (number of parameters), which is useful to compare candidate models and conduct model selection. BIC provides a

comparable evaluation, albeit more sensitive towards larger sample sizes, penalizing models based on their complexity with more rigor than the AIC.

While the AIC and BIC are useful for model comparisons in relative terms, the values themselves do not provide a definitive measure to the goodness-of-fit to data in an absolute sense. In other words, a model being comparatively better than another according to these criteria does not necessarily mean a better fit for the data based on the value alone, which is done by assessing the biological realism and statistical accuracy of model outputs (Arif & MacNeil, 2022).

## VII. Bayesian framework models

A Bayesian framework (Bayes, 1763) uses probabilistic inference and posterior distributions to quantify uncertainty in model parameters and predictions. By incorporating prior knowledge to observed data, the Bayesian method offers a quantification of uncertainty in key biological processes (Martin et al., 2015). This approach is applied in fisheries research when data is limited or incomplete, especially for larger sizes, treating data and parameters as random variables based on probability (Gelman et al., 2013; Siegfried & Sansó, 2006; Smart & Grammer, 2021). Given that few individuals larger than 180 cm FL were present in data, this approach was used to account for this and generate probabilistic growth parameter estimates.

Informative priors that were not too restrictive were designed for each parameter based on limited exiting biological knowledge (Castro et al., 1999; Castro, 2011; Gilmore, 1983; Ruiz-Abierno et al., 2021a). The priors had a normal distribution and were centered at $L_0$ = 99.3 cm (SE = 10 cm), and $L\infty$ = 387 cm (SE = 50 cm) for both sexes. A careful selection of priors is critical, as overly strong or poorly justified priors can bias posterior estimates (Doll & Jacquemin, 2019). The predictive accuracy of fitted models was then assessed using the Leave-One-Out information criterion (LOOIC), to select the Bayesian model with the most relevant weight (Vehtari et al., 2017).

Posterior probability distributions were then estimated and compared to priors for each parameter and sex of the selected model, which were obtained from a Bayesian 3P-VBGF To ensure the convergence of Markov Chain Monte Carlo (MCMC) chains, three chains per parameter were run, each with 10000 iterations and an initial burn-in period of 2000

iterations, allowing chain stabilization within the high-probability region of posterior distributions (Doll & Jacquemin, 2019).

Considering Markov's property (Markov, 1906) each step in the MCMC chain depends on the previous step, which may result in autocorrelation, since model parameters are linked. In such cases, reparameterization was applied, as chain convergence can only be evaluated once a good burn-in is established and step correlations are eliminated (Doll & Jacquemin, 2019; Hastings, 1970). Chain convergence was assessed using the Gelman-Rubin test (Gelman & Rubin, 1992), comparing within and between chain variances, assuming convergence at values lower or equal to 1.1 ($\hat{R} \leq 1.1$) (Doll & Jacquemin, 2019). The Bayesian growth model was then plotted for each sex and compared with its frequentist model counterpart as previously described.

### VIII. Software, R packages and assumptions

The frequency of males and females across different size classes was plotted using the "FSA" (Simple Fisheries Stock Assessment Methods) package (Ogle et al., 2025). All back-calculation methods were applied to data using the "RFishBC" package (Ogle, 2023). Growth models were fit using the "minpack.lm" package (Elzhov et al., 2023). The frequentist growth model used for comparison with its Bayesian version was fit using the "AquaticLifeHistory" package (Smart, 2023). The MCMC method was used to fit Bayesian models with the "BayesGrowth" package (Carrillo-Colín et al., 2024; Smart & Grammer, 2021; Smart, 2023). All plots and graphs used in this thesis, unless stated otherwise, were created using the "ggplot2" package (Wickham, 2016). All the afore-mentioned packages, as well as associated packages for their proper functioning were used in R programming language version 4.4.3 (R Core Team, 2024). In all afore-mentioned statistical tests performed to evaluate assumptions, a confidence interval of 95% was always considered.

## 3. Results

### I. Samples

From the initial 294 sample pool, a total of 291 samples had an accepted age count, with three samples being discarded due to incompatibility with the afore-mentioned criteria

for age readings. Of these 291 samples, 137 samples were from males, while 154 were from females, meaning the number of samples for each sex was nearly even. The FL normality assumption was met based on Shapiro–Wilk's test for males (p-value = 0.651; W = 0.992) and females (p-value = 0.463; W = 0.991). Male specimens ranged from 99 to 230 cm FL (mean ± SD: 164.5 ± 21.8 cm), while females ranged from 101 to 213 cm FL (mean ± SD: 157.0 ± 18.7 cm). The highest density of samples for both sexes was comprised within the 120-190 cm FL range, and the lowest density of samples was present for FL < 120 cm and FL > 190 cm (Figure 3.1).

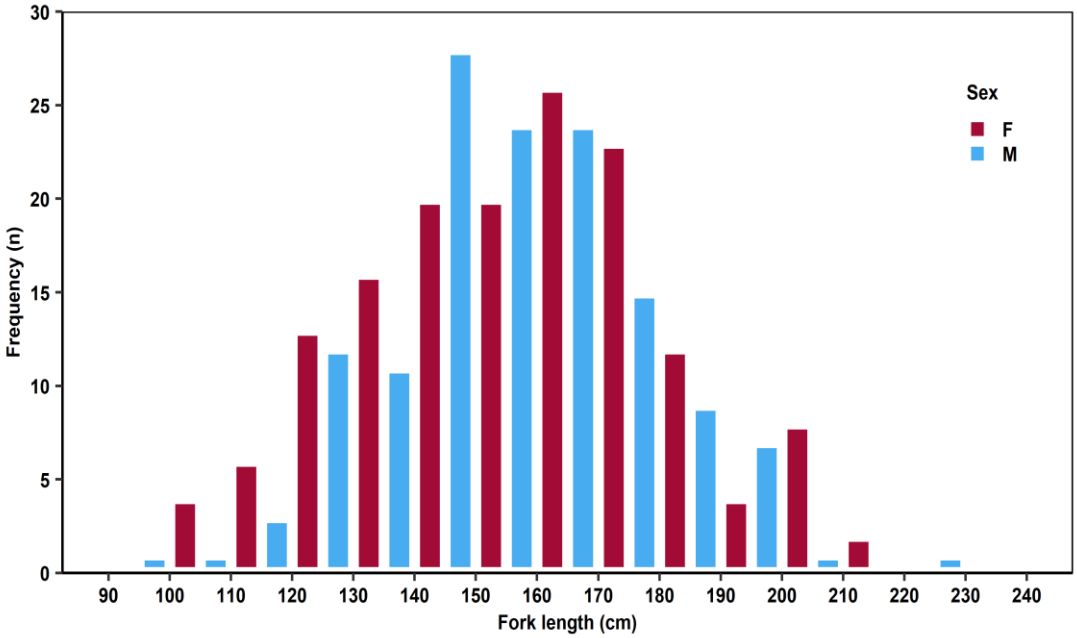


**Figure 3.1**- Frequency of occurrence (n) of male (n = 137) and female (n = 154) longfin mako sharks (*I. paucus*) in samples in 10 cm size classes according to their fork length (FL, cm). Male data is colored blue, while female data is colored magenta.

## II. Length-length relationship

The TL-FL relationship was highly significant (P< 0.001) with an $R^2$ of 0.98 (Figure 3.2) and the residual analysis revealed no trends or patterns in the residuals that could be considered problematic, (see Appendix A). The residuals were additionally tested for the normality and homoscedasticity assumptions, where the normality assumption failed for Shapiro-Wilk's test (p-value = 0.003; W = 0.959), despite the homoscedasticity assumption holding with Breusch-Pagan's test (p-value = 0.836; BP = 0.043). Kendall's Tau correlation was used to test the null hypothesis, which was rejected (p-value = $2.2 \times 10^{-16}$; $\tau = 0.891$).

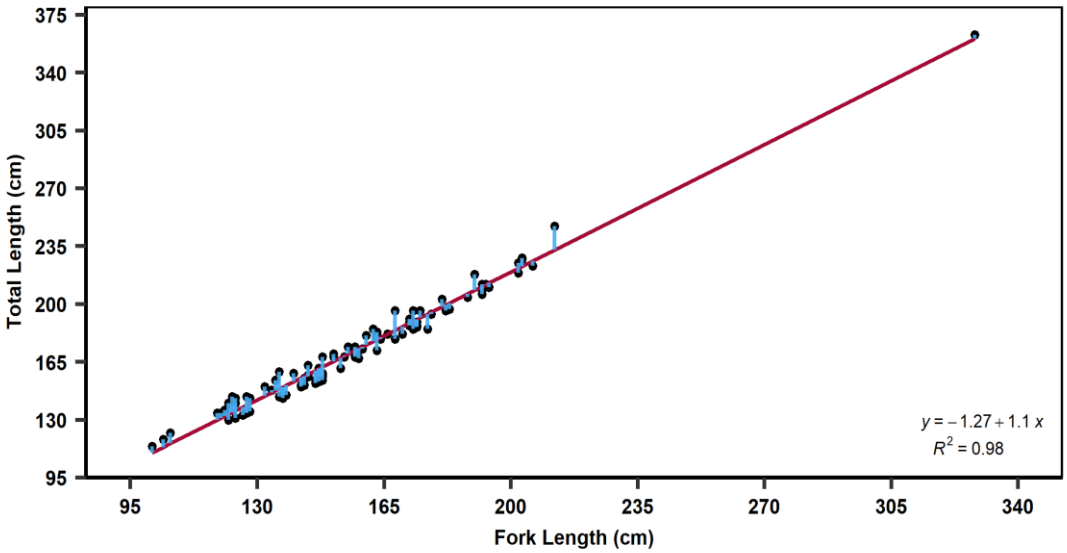


**Figure 3.2**- Linear regression between the fork length (FL, cm), and total length (TL, cm) of the longfin mako shark (*I. paucus*). Fitted residuals are colored blue, and the regression line in magenta. Points represent individuals for which both measurements were registered.

The linear regression equation was used to calculate the $L\infty$ and $L_0$ values, used with the MFL, and later, growth models as follows:

$$\mathbf{TL427 = (427 - 1.27) \div 1.1 \approx 387\ cm\ FL}$$

$$\mathbf{TL303 = (303 - 1.27) \div 1.1 \approx 276\ cm\ FL}$$

$$\mathbf{TL135 = (135 - 1.27) \div 1.1 \approx 122\ cm\ FL}$$

$$\mathbf{TL86 = (86 - 1.27) \div 1.1 \approx 77\ cm\ FL}$$

$$\mathbf{L_0 = (122 + 77) \div 2 = 99.3\ cm\ FL}$$

### III. Intra-reader bias plots

Pairwise comparisons were made between the triplicate age readings to assess the percent agreement, precision, and to detect systematic bias (Table 3.1). Between the first and second readings 71.8% of age estimates matched exactly, 17.5% of readings were one year over, and 10.7% were one year below the agreed age. In the first and third readings, 72.5% of age estimates matched exactly, while 12.7% of readings were one year over, and 14.8% were one year below the agreed age. Between the second and third readings the highest percentage agreement is seen, with 84.9% of readings matching exactly, 10% being one year over, and 5.2% one year under the agreed age. From McNemar's test statistically significant differences were found between the first and second readings (p-

value = 0.027; $\chi^2$ = 4.878) and the second and third readings (p-value = 0.034; $\chi^2$ = 0.450). The first and third readings, however, had no significant differences between them (p-value = 0.502; $\chi^2$ = 4.454). The estimated CV between the three readings was 5.621%, and the APE was 4.327%.

**Table 3.1**– Longfin mako shark (*I. paucus*) age reading comparisons with McNemar's test, including chi-square ($\chi^2$) values, and the percent of samples with a difference of -1, 0, and 1 year between readings (%).

| Compared Readings | $\chi^2$ | p-values | Difference of 0 (%) | Difference of +1 (%) | Difference of -1 (%) |
|---|---|---|---|---|---|
| 1st Reading Vs 2nd Reading | 4.878 | 0.027 | 71.8 | 17.5 | 10.7 |
| 1st Reading Vs 3rd Reading | 0.450 | 0.502 | 72.5 | 12.7 | 14.8 |
| 2nd Reading Vs 3rd Reading | 4.455 | 0.034 | 84.9 | 10 | 5.2 |

Bias plots were made to compare pairwise readings between the first, second, and third age estimates from counts. For the first and second readings (Figure 3.3) points between ages 0-5 are clustered near the 1:1 line and have narrow confidence interval (CI) bars. Beyond age 5, the points for the mean age estimates are below the 1:1 line, accompanied by a widening of the CI bars. This indicates that for those ages in the second reading, ages were overestimated in relation to the first reading.

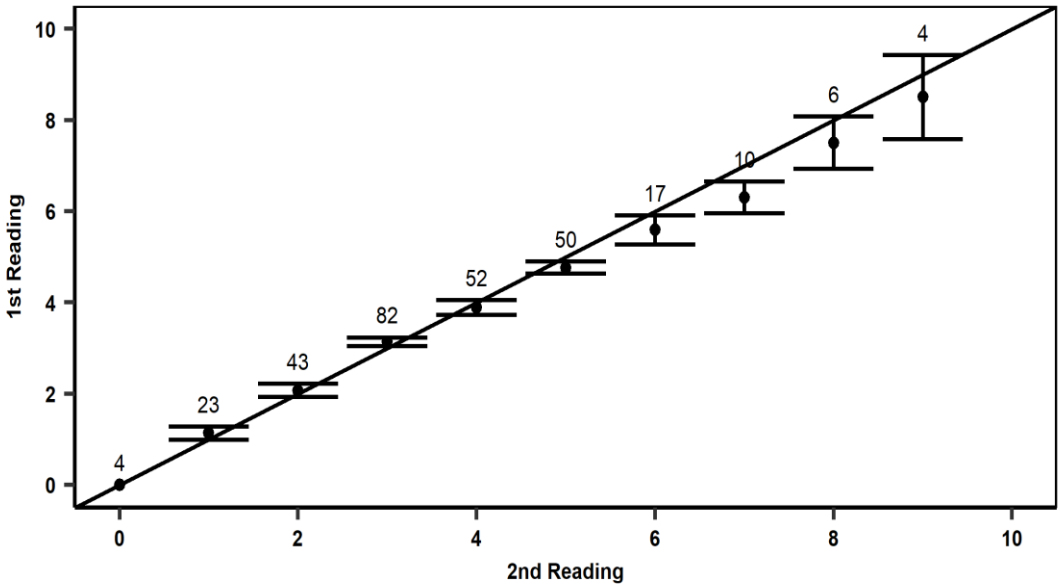


**Figure 3.3-** Bias plot showing pairwise comparisons of growth band counts between the first and second readings of longfin mako shark (*I. paucus*) vertebral sections. Each point represents the mean age assigned for age estimates. Vertical error bars represent the 95% confidence interval (CI). Sample sizes for each age are labeled over the error bars. The diagonal 1:1 line indicates a perfect agreement between readings.

Between the first and third readings (Figure 3.4), estimates for ages 0–5 and 9 were clustered near the 1:1 line, having narrow CI bars. Between ages 6–8, the mean age estimates showed a tendency to descend below the 1:1 line, with CI bars widening.

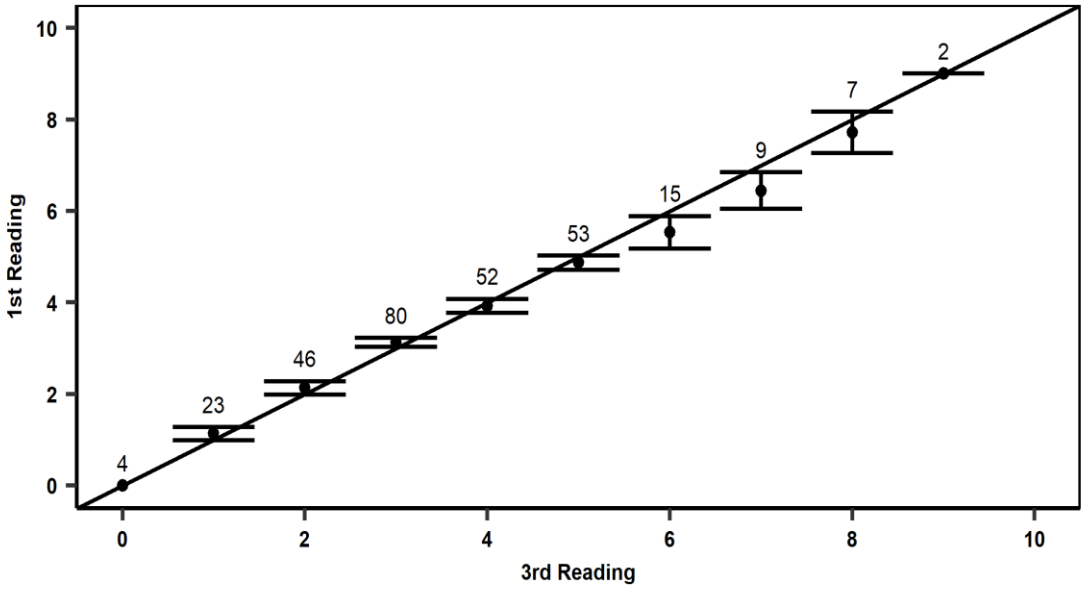


**Figure 3.4-** Bias plot showing pairwise comparisons of growth band counts between the first and third readings of longfin mako shark (*I. paucus*) vertebral sections. Each point represents the mean age assigned for age estimates. Vertical error bars represent the 95% confidence interval (CI). Sample sizes for each age are labeled over the error bars. The diagonal 1:1 line indicates a perfect agreement between readings.

When comparing the second and third readings (Figure 3.5), estimates from ages 0-7 and 9 were clustered near the 1:1 line and had narrow CI bars. For age 8, the mean age estimate, instead of being below the 1:1 line, is instead above it, with wider CI bars, but no consistent trend is seen, thus no major bias is present.

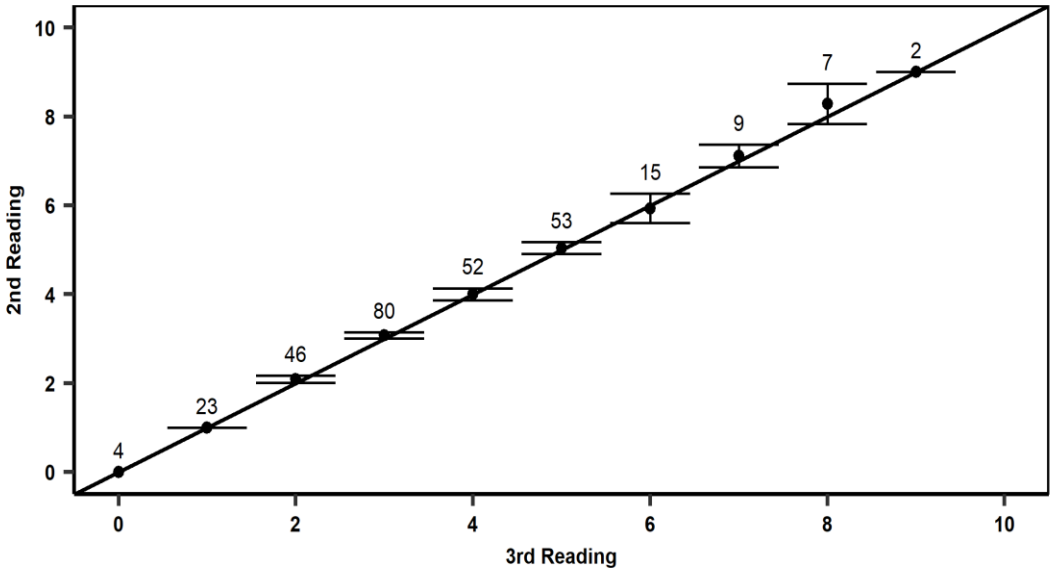


**Figure 3.5-** Bias plot showing pairwise comparisons of growth band counts between the second and third readings of longfin mako shark (*I. paucus*) vertebral sections. Each point represents the mean age assigned for age estimates. Vertical error bars represent the 95% confidence interval (CI). Sample sizes for each age are labeled over the error bars. The diagonal 1:1 line indicates a perfect agreement between readings.

## IV. Age estimates

Male and female *I. paucus* in samples ranged from 0 to 9 years of age, with the highest density of individuals being within the range of 1-6 years (Figure 3.6). A mean value of 4.316 mm was used to consistently detect the birth bands, based on VR measurements of samples within the defined birth FL and aged 0 (n = 4). For the agreed ages the normality assumption failed for both males (p-value = $4.78 \times 10^{-5}$; W = 0.948) and females (p-value = $2.15 \times 10^{-5}$; W = 0.949), despite the homogeneity of variances being met across most ages according to Levene's test (Table 3.2).

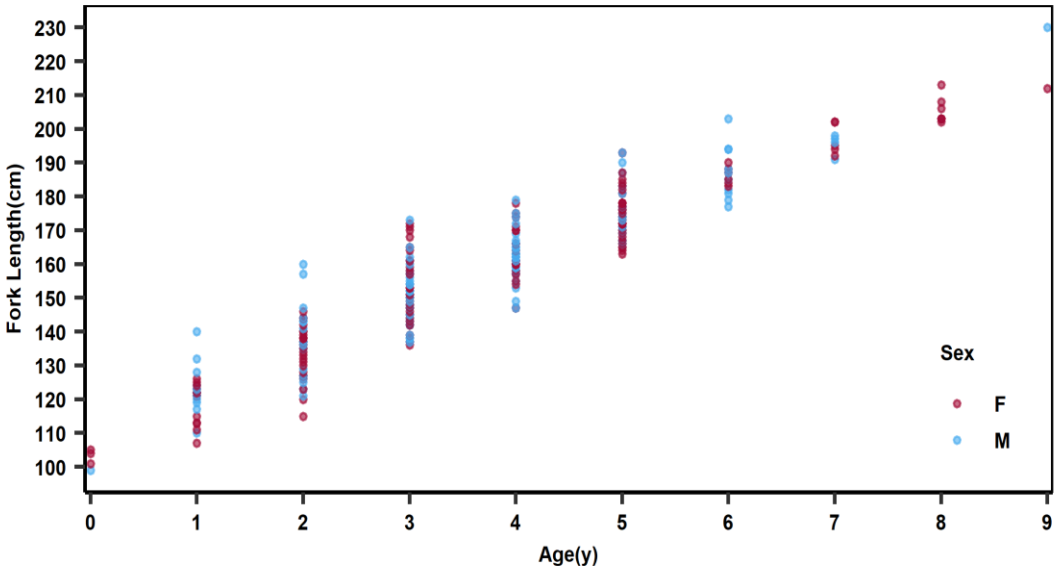


**Figure 3.6**- Correlation between the FL (fork length, cm) and age (years, y) of male and female longfin mako sharks (*I. paucus*. FL sizes ranged from 99 to 230 cm, with age counts ranging between 0-9 years old. Male data is colored blue, while female data is colored magenta.

**Table 3.2**- Levene's test results for equality of variances in FL (fork length, cm) at each agreed age count group of longfin mako sharks (*I. paucus*). **F-Value**: Levene's test F statistic; **df**: Degrees of freedom; **n**: Number of individuals of each sex; **M**: Males; **F**: Females.

| Agreed Age | n (M) | n (F) | df1 | df2 | F-value | p-value |
|---|---|---|---|---|---|---|
| 0 | 1 | 3 | 1 | 2 | 0.571 | 0.529 |
| 1 | 11 | 12 | 1 | 21 | 0.018 | 0.894 |
| 2 | 18 | 26 | 1 | 42 | 2.220 | 0.144 |
| 3 | 44 | 37 | 1 | 79 | 2.200 | 0.142 |
| 4 | 30 | 24 | 1 | 52 | 0.216 | 0.644 |
| 5 | 18 | 33 | 1 | 49 | 0.061 | 0.806 |
| 6 | 10 | 6 | 1 | 14 | 3.950 | 0.067 |
| 7 | 4 | 5 | 1 | 7 | 0.061 | 0.443 |
| 8 | 0 | 5 | NA | NA | NA | NA |
| 9 | 1 | 1 | NA | NA | NA | NA |

Due to the non-normal distribution of ages, a non-parametric Mann–Whitney U test was performed where for each comparison, none showed statistically significant length-at-age differences between males and females (Table 3.3).

**Table 3.3**- Mann–Whitney U test results for differences in FL (Fork length, cm) between longfin mako shark (*I. paucus*) sexes at each agreed age, as well as the mean FL of each sex. **U statistic**: Parameter reflecting differences in rank distributions between sexes (lower values, greater divergence); **n**: Number of individuals of each sex; **M**: Males**; F**: Females.

| Agreed Ages | Mean FL (M) | Mean FL (F) | n (M) | n (F) | U statistic | p-values |
|---|---|---|---|---|---|---|
| **0** | **99.0** | **103.3** | **1** | **3** | **3** | **0.500** |
| **1** | **123.3** | **118.5** | **11** | **12** | **49.5** | **0.324** |
| **2** | **136.6** | **134.1** | **18** | **26** | **218** | **0.720** |
| **3** | **149.8** | **152.9** | **44** | **37** | **963** | **0.159** |
| **4** | **162.5** | **163.0** | **30** | **24** | **365** | **0.937** |
| **5** | **176.1** | **174.8** | **18** | **33** | **281** | **0.760** |
| **6** | **187.0** | **186.2** | **10** | **6** | **31.5** | **0.913** |
| **7** | **195.5** | **197.0** | **4** | **5** | **11** | **0.902** |
| **8** | **NA** | **205.4** | **0** | **5** | **NA** | **NA** |
| **9** | **230.0** | **212.0** | **1** | **1** | **NA** | **NA** |

## V. Back-calculations

Data for *I. paucus* presented a linear relationship between FL and VR (Figure 3.7), with the linear regression model being slightly preferred, with lower BIC values, despite no AIC differences ($FL = 58.93 + 12.20 \times VR$, $R^2 = 0.840$, AIC = 2127, BIC = 2138), when compared to the quadratic regression model ($FL = 48.13 + 14.97 \times VR - 0.17 \times VR^2$, $R^2 = 0.840$, AIC = 2127, BIC = 2142). Additionally, the likelihood ratio test showed that the added complexity of the quadratic model did not present a significant improvement over the linear model's goodness-of-fit for the data (p-value = 0.217; F = 1.53).

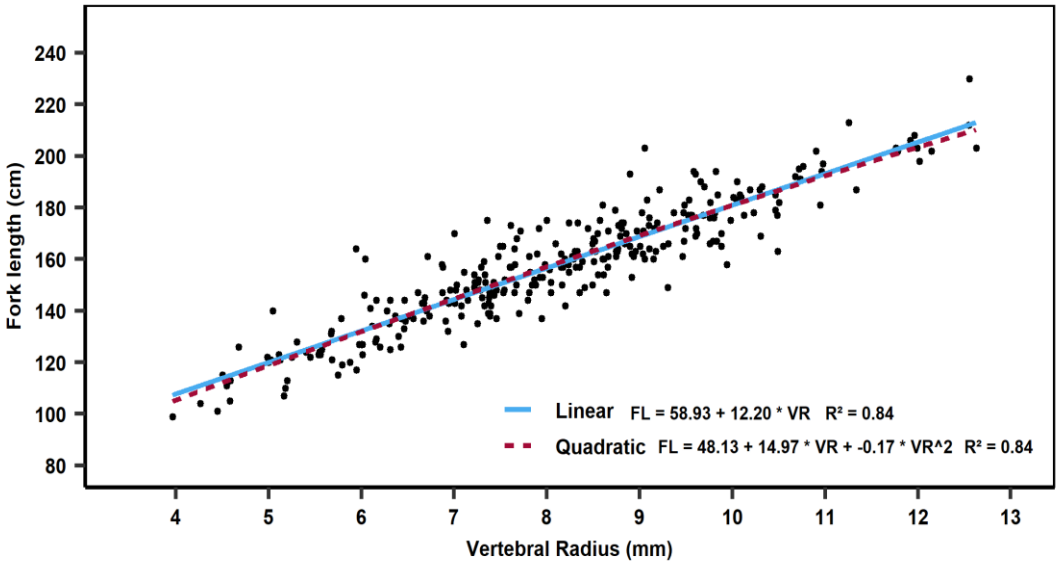


**Figure 3.7**- Correlation between the measured fork length (FL, cm) and vertebral radius (VR, mm) of longfin mako shark (*I. paucus*) samples. Each dot represents an individual observation. The solid blue line represents the linear regression, and the dashed magenta line represents the quadratic regression.

Considering the linear model was preferred over the quadratic model, the residuals of the linear equation were assessed. No major trends or patterns were observed, and the three small outliers were not considered significant (see Appendix B). The linear equation was therefore used to obtain $VR_0$ from $L_0$ as follows:

$$\boldsymbol{VR_0 = (99.30 - 58.93) \div 12.20 = 3.31 \text{ mm}}$$

Back-calculations were then performed using the aforementioned models, where the estimated mean back-calculated length-at-age was compared with the sample's estimated mean length-at-age for each sex (Figure 3.8; Figure 3.9). Out of all back-calculation methods (Table 3.4), the DL exhibited the highest MAD for both males and females from the mean sample length-at-age, in contrast with the LDL, which produced the lowest MAD for both sexes. The QDL followed closely behind the LDL, with the second lowest MAD for both sexes, being especially close for females. Lastly, the MFL produced the third lowest MAD values for each sex.

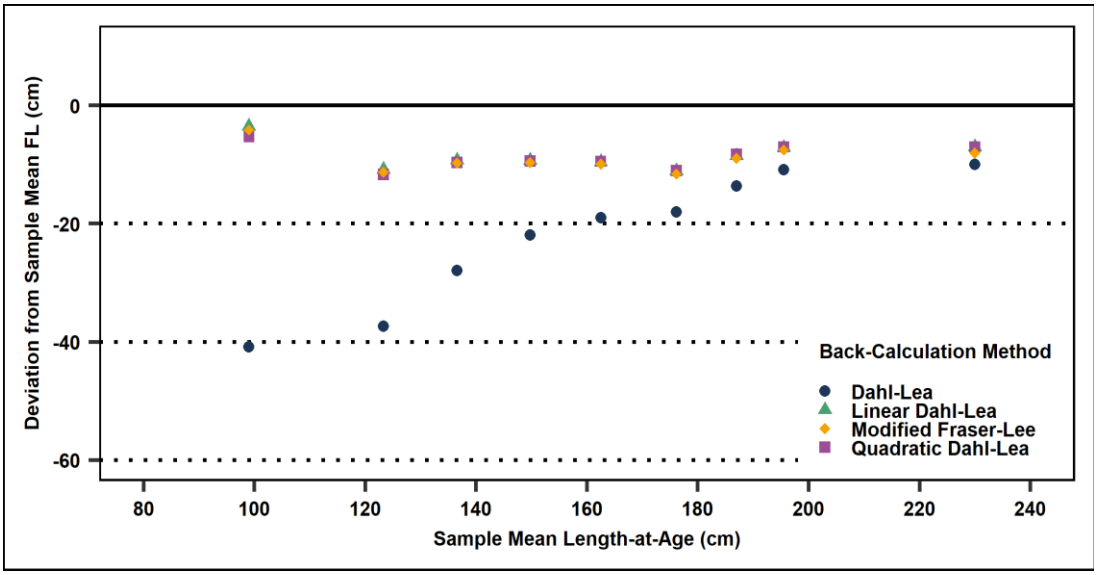


**Figure 3.8-** Deviation from sample mean fork length (FL, cm) of four different back-calculation method estimates from sampled length-at-age (cm) of male longfin mako sharks (*I. paucus*). Each point represents the mean back-calculated length-at-age difference for its respective model (blue circle: Dahl-Lea; green triangle: Linear Dahl-Lea; yellow prism: Modified Fraser-Lee; violet square: Quadratic Dahl-Lea). The horizontal black line at Y=0 represents a deviation of zero from the mean sampled length-at-age. No point is present for age 8, as no male individuals were 8 years old.

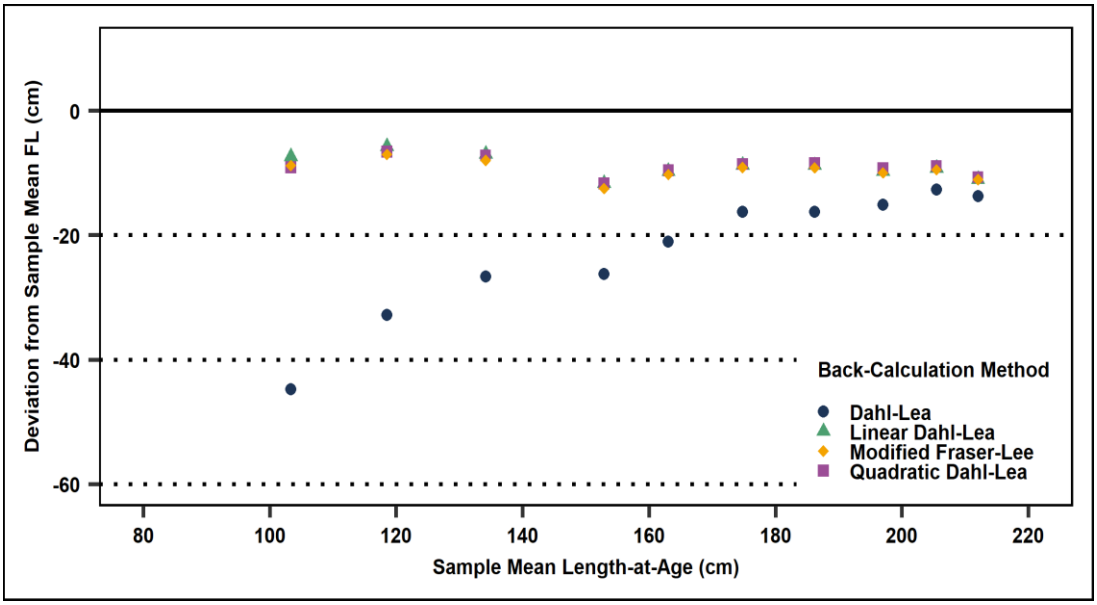


**Figure 3.9-** Deviation from the mean sample fork length (FL, cm) of four different back-calculation method estimates from the sampled length-at-age (cm) of female longfin mako sharks (*I. paucus*). Each point represents the mean back-calculated length-at-age for its respective model (blue circle: Dahl-Lea; green triangle: Linear Dahl-Lea; yellow prism: Modified Fraser-Lee; violet square: Quadratic Dahl-Lea). The horizontal black line at Y=0 represents a deviation of zero from the mean sampled length-at-age.

**Table 3.4**- Mean average deviation (MAD, cm) of observed vs back-calculated lengths for male and female longfin mako shark (*I. paucus*). **DL**: Dahl Lea; **LDL**: Linear Dahl Lea; **QDL**: Quadratic Dahl Lea; **MFL**: Biological intercept Fraser-Lee.

| Back-Calculation Models | MAD (Males) | MAD (Females) |
|---|---|---|
| **DL** | **22.20** | **22.50** |
| **LDL** | **8.46** | **8.87** |
| **QDL** | **8.74** | **8.98** |
| **MFL** | **8.95** | **9.50** |

Based on these MAD values, the decision was to utilize the LDL and QDL data for subsequent age and growth modeling, as these presented the lowest deviations between the mean back-calculated length-at-age and the observed mean length-at-age data.

## VI. Frequentist growth models

Growth models were fitted to the original sample data, as well as the LDL and QDL back-calculated data. The 3P-VBGF, 2P-VBGF, GOMP, LOG, and RICH models were used for males and females separately, as well as in combination. Each model was given a set of starting initial values, which were the same across all three datasets for each sex, most importantly, $L_0$ = 99.3 cm, and $L\infty$ = 387 cm. For each model, the parameter estimates, standard errors (SE), confidence intervals (CI), AIC, BIC, and degrees of freedom (df) were obtained.

For all models applied to the original sample data (Table 3.5), males had the highest estimates for $L\infty$ and $L_0$, while females had the highest $k$ estimates. The 3P-VBGF and GOMP had a high SE for the male $L\infty$, while RICH had a high SE across all parameters. Additionally, the 3P-VBGF had no computable 95% CI for the male $L\infty$, while RICH had no computable 95% CI's.

**Table 3.5-** Growth model parameter estimates for male, female, and combined longfin mako shark (*I. paucus*) original sample data. **3P-VBGF**: Three-parameter von Bertalanffy growth model; **2P-VBGF**: Two-parameter von Bertalanffy growth model; **GOMP**: Gompertz growth model; **LOG**: Logistic growth model; **RICH**: Richard's growth model**; SE**: Standard error; **95% CI**: 95% confidence interval; **M**: Males; **F**: Females; $L\infty$: Asymptotic maximum length (cm); $k$ = Relative growth coefficient; $L_0$ = Mean fork length at birth (cm); ***Fixed*** $L_0$: Fixed mean fork length at birth (cm)*;* $a$**:** Initial size variable; $t$: Time at inflection point; $b$: Curve shaping parameter; **NA**: Data unavailable.

| Growth Models (Samples) | Parameters | Estimates | | | SE | | | 95% CI | | | | | |
|---|---|---|---|---|---|---|---|---|---|---|---|---|---|
| | | Males | Females | Combined | Males | Females | Combined | Lower (M) | Upper (M) | Lower (F) | Upper (F) | Lower (Combined) | Upper (Combined) |
| 3P-VBGF | $L\infty$ | 558.153 | 280.450 | 316.311 | 380.570 | 24.398 | 33.975 | 312.000 | NA | 245.345 | 359.837 | 268.517 | 433.466 |
| | $k$ | 0.032 | 0.108 | 0.082 | 0.031 | 0.022 | 0.018 | -0.029 | 0.097 | 0.064 | 0.152 | 0.047 | 0.119 |
| | $L_0$ | 108.129 | 100.968 | 103.586 | 3.182 | 2.613 | 2.046 | 101.464 | 114.301 | 95.686 | 106.048 | 99.453 | 107.571 |
| 2P-VBGF Fixed $L_0 = 99.3$ | $L\infty$ | 291.555 | 270.353 | 277.287 | 26.924 | 14.344 | 12.942 | 250.054 | 372.761 | 246.521 | 305.833 | 255.152 | 308.338 |
| | $k$ | 0.102 | 0.119 | 0.113 | 0.018 | 0.013 | 0.011 | 0.067 | 0.140 | 0.093 | 0.146 | 0.092 | 0.135 |
| GOMP | $L\infty$ | 335.367 | 247.475 | 265.102 | 70.024 | 12.606 | 14.971 | 256.290 | 877.831 | 227.303 | 282.126 | 241.218 | 306.098 |
| | $k$ | 0.110 | 0.190 | 0.162 | 0.032 | 0.023 | 0.019 | 0.047 | 0.176 | 0.144 | 0.238 | 0.125 | 0.201 |
| | $a$ | 1.122 | 0.882 | 0.926 | 0.189 | 0.039 | 0.045 | 0.883 | 2.045 | 0.815 | 0.982 | 0.852 | 1.045 |
| LOG | $L\infty$ | 285.145 | 232.609 | 244.282 | 36.496 | 8.655 | 9.646 | 237.280 | 462.198 | 217.987 | 255.195 | 228.022 | 269.177 |
| | $k$ | 0.187 | 0.271 | 0.241 | 0.032 | 0.025 | 0.020 | 0.122 | 0.256 | 0.222 | 0.322 | 0.202 | 0.289 |
| | $t$ | 2.479 | 0.788 | 1.084 | 1.376 | 0.236 | 0.297 | 0.807 | 9.054 | 0.402 | 1.460 | 0.612 | 1.913 |
| RICH Fixed $L_0 = 99.3$ | $L\infty$ | 1661 | 300.525 | 994.500 | 87260 | 113.606 | 10810 | NA | NA | NA | NA | NA | NA |
| | $k$ | 0.001 | 0.081 | 0.004 | 0.157 | 0.108 | 0.089 | NA | NA | NA | NA | NA | NA |
| | $b$ | -1.036 | -0.351 | -1.114 | 1.628 | 1.145 | 0.956 | NA | NA | NA | NA | NA | NA |

For model selections (Table 3.6), the AIC for males was lowest for the 3P-VBGF (AIC = 964), but for females the lowest AIC was observed with the 2P-VBGF (AIC = 1064). For the combined sexes, AIC values were identical for the 3P-VBGF and RICH models (AIC = 2026), with no clear preference. Regarding the BIC, the lowest value for males was the 3P-VBGF (BIC = 976), while for females (BIC = 1073), and the combined sexes (BIC = 2039), the 2P-VBGF was preferred.

**Table 3.6-** AIC and BIC model comparisons for male, female, and combined data of longfin mako sharks (*I. paucus*) obtained from original sample data, including the degrees of freedom (df) of each model. **3P-VBGF**: Three-parameter von Bertalanffy growth model; **2P-VBGF**: Two-parameter von Bertalanffy growth model; **GOMP**: Gompertz growth model; **LOG**: Logistic growth model; **RICH**: Richard's growth model**.**

| Growth Models (Samples) | AIC | | | BIC | | | df |
|---|---|---|---|---|---|---|---|
| | Males | Females | Combined | Males | Females | Combined | |
| **3P-VBGF** | **964** | **1065** | **2026** | **976** | **1077** | **2041** | **4** |
| **2P-VBGF** | **969** | **1064** | **2028** | **978** | **1073** | **2039** | **3** |
| **GOMP** | **965** | **1066** | **2027** | **977** | **1078** | **2042** | **4** |
| **LOG** | **966** | **1067** | **2029** | **977** | **1079** | **2044** | **4** |
| **RICH** | **967** | **1065** | **2026** | **979** | **1077** | **2041** | **4** |

For the LDL back-calculation method (Table 3.7), male parameter estimates remained highest for $L\infty$ and $L_0$, with the exception of the 3P-VBGF $L_0$ estimate, which was higher for females along with all $k$ estimates. The 2P-VBGF had a high SE for $L\infty$, especially in males, and RICH had the highest SE across all parameters for males, as well as wide 95% CI's. Additionally, RICH remained the only model with no computable 95% CI's, except for females.

**Table 3.7-** Growth model parameter estimates for male, female, and combined longfin mako shark (*I. paucus*) using back-calculated data from the linear Dahl-Lea (LDL) method. **3P-VBGF**: Three-parameter von Bertalanffy growth model; **2P-VBGF**: Two-parameter von Bertalanffy growth model; **GOMP**: Gompertz growth model; **LOG**: Logistic growth model; **RICH**: Richard's growth model**; SE**: Standard error; **95% CI**: 95% confidence interval; **M**: Males; **F**: Females; $L\infty$: Asymptotic maximum length (cm); $k$ = Relative growth coefficient; $L_0$ = Mean fork length at birth (cm); ***Fixed*** $L_0$: Fixed mean fork length at birth (cm); $a$**:** Initial size variable; $t$: Time at inflection point; $b$: Curve shaping parameter; **NA**: Data unavailable.

| Growth Models (LDL) | Parameters | Estimates | | | SE | | | 95% CI | | | | | |
|---|---|---|---|---|---|---|---|---|---|---|---|---|---|
| | | Males | Females | Combined | Males | Females | Combined | Lower (M) | Upper (M) | Lower (F) | Upper (F) | Lower (Combined) | Upper (Combined) |
| 3P-VBGF | $L\infty$ | 363.466 | 307.800 | 324.100 | 44.731 | 16.950 | 17.350 | 298.195 | 508.656 | 279.721 | 348.608 | 294.910 | 365.630 |
| | $k$ | 0.061 | 0.080 | 0.073 | 0.012 | 0.008 | 0.007 | 0.037 | 0.085 | 0.064 | 0.096 | 0.060 | 0.087 |
| | $L_0$ | 96.075 | 96.170 | 96.090 | 0.585 | 0.455 | 0.365 | 94.914 | 97.230 | 95.278 | 97.065 | 95.373 | 96.808 |
| 2P-VBGF Fixed $L_0$ = 99.3 | $L\infty$ | 695.026 | 399.700 | 463.200 | 243.627 | 37.170 | 48.320 | 446.800 | 3792.000 | 342.377 | 496.449 | 389.324 | 592.151 |
| | $k$ | 0.024 | 0.050 | 0.040 | 0.010 | 0.007 | 0.006 | 0.004 | 0.044 | 0.036 | 0.063 | 0.029 | 0.051 |
| GOMP | $L\infty$ | 261.778 | 246.200 | 251.200 | 12.858 | 6.432 | 6.048 | 239.627 | 293.907 | 234.628 | 260.375 | 240.116 | 264.473 |
| | $k$ | 0.158 | 0.174 | 0.168 | 0.012 | 0.008 | 0.007 | 0.134 | 0.183 | 0.158 | 0.190 | 0.155 | 0.182 |
| | $a$ | 0.999 | 0.936 | 0.957 | 0.046 | 0.024 | 0.023 | 0.916 | 1.109 | 0.892 | 0.988 | 0.915 | 1.006 |
| LOG | $L\infty$ | 231.389 | 223.800 | 226.300 | 7.380 | 3.967 | 3.645 | 217.945 | 249.130 | 216.443 | 232.428 | 218.385 | 234.193 |
| | $k$ | 0.256 | 0.268 | 0.264 | 0.012 | 0.008 | 0.007 | 0.231 | 0.282 | 0.251 | 0.285 | 0.250 | 0.278 |
| | $t$ | 1.293 | 1.006 | 1.102 | 0.257 | 0.134 | 0.125 | 0.835 | 1.922 | 0.761 | 1.303 | 0.870 | 1.377 |
| RICH Fixed $L_0$ = 99.3 | $L\infty$ | 1043.036 | 234.069 | 258.697 | 7247.704 | 16.746 | 27.583 | NA | NA | 212.256 | 299.818 | NA | NA |
| | $k$ | 0.012 | 0.246 | 0.179 | 0.131 | 0.073 | 0.064 | NA | NA | 0.106 | 0.391 | NA | NA |
| | $b$ | -0.118 | 2.095 | 1.473 | 1.361 | 0.764 | 0.672 | NA | NA | 0.617 | 3.598 | NA | NA |

The AIC and BIC model evaluations (Table 3.8), were lowest for males, females and combined sexes with the 3P-VBGF, making it the most favored candidate for selection when compared to the other growth models, closely followed by the GOMP and LOG models.

**Table 3.8-** AIC and BIC model comparisons for male, female, and combined data of longfin mako sharks (*I. paucus*) obtained from back-calculated data using the linear Dahl-Lea (LDL) method, including the degrees of freedom (df) of each model. **3P-VBGF**: Three-parameter von Bertalanffy growth model; **2P-VBGF**: Two-parameter von Bertalanffy growth model; **GOMP**: Gompertz growth model; **LOG**: Logistic growth model; **RICH**: Richard's growth model**.**

| Growth Models (LDL) | AIC | | | BIC | | | df |
|---|---|---|---|---|---|---|---|
| | Males | Females | Combined | Males | Females | Combined | |
| 3P-VBGF | 4411 | 4842 | 9271 | 4428 | 4860 | 9292 | 4 |
| 2P-VBGF | 4438 | 4886 | 9345 | 4452 | 4900 | 9361 | 3 |
| GOMP | 4416 | 4844 | 9279 | 4434 | 4863 | 9300 | 4 |
| LOG | 4423 | 4851 | 9292 | 4441 | 4869 | 9313 | 4 |
| RICH | 4440 | 4880 | 9342 | 4458 | 4899 | 9363 | 4 |

For the QDL back-calculation method (Table 3.9), male parameter estimates, much like with the LDL, were highest for $L\infty$ and $L_0$, with the exception of the 3P-VBGF $L_0$ estimate, which was higher for females along with all $k$ estimates. The 2P-VBGF $L\infty$ had high SE's, especially in males, and SE's for the RICH male parameter estimates also remained high. No upper 95% CI was computable for the male $L\infty$ with the 2P-VBGF, and RICH remained the only model with no computable 95% CI's across all male parameter estimates.

**Table 3.9-** Growth model parameter estimates for male, female, and combined longfin mako shark (*I. paucus*) using back-calculated data from the quadratic Dahl-Lea (QDL) method. **3P-VBGF**: Three-parameter von Bertalanffy growth model; **2P-VBGF**: Two-parameter von Bertalanffy growth model; **GOMP**: Gompertz growth model; **LOG**: Logistic growth model; **RICH**: Richard's growth model**; SE**: Standard error; **95% CI**: 95% confidence interval; **M**: Males; **F**: Females; $L\infty$: Asymptotic maximum length (cm); $k$ = Relative growth coefficient; $L_0$ = Mean fork length at birth (cm); ***Fixed*** $L_0$: Fixed mean fork length at birth (cm); $a$**:** Initial size variable; $t$: Time at inflection point; $b$: Curve shaping parameter; **NA**: Data unavailable.

| Growth Models (QDL) | Parameters | Estimates | | | SE | | | 95% CI | | | | | |
|---|---|---|---|---|---|---|---|---|---|---|---|---|---|
| | | Males | Females | Combined | Males | Females | Combined | Lower (M) | Upper (M) | Lower (F) | Upper (F) | Lower (Combined) | Upper (Combined) |
| 3P-VBGF | $L\infty$ | 335.411 | 294.308 | 307.113 | 33.465 | 13.756 | 13.852 | 284.341 | 434.798 | 271.005 | 326.628 | 283.277 | 339.460 |
| | $k$ | 0.071 | 0.089 | 0.082 | 0.012 | 0.008 | 0.007 | 0.047 | 0.095 | 0.073 | 0.104 | 0.069 | 0.096 |
| | $L_0$ | 94.393 | 94.507 | 94.422 | 0.591 | 0.453 | 0.366 | 93.222 | 95.560 | 93.615 | 95.396 | 93.701 | 95.141 |
| 2P-VBGF Fixed $L_0$ = 99.3 | $L\infty$ | 994.580 | 438.900 | 534.300 | 584.160 | 49.930 | 72.900 | 530.901 | NA | 364.958 | 576.602 | 429.057 | 747.443 |
| | $k$ | 0.015 | 0.043 | 0.033 | 0.010 | 0.007 | 0.006 | -0.005 | 0.036 | 0.030 | 0.057 | 0.022 | 0.045 |
| GOMP | $L\infty$ | 252.771 | 240.800 | 244.800 | 10.880 | 5.595 | 5.244 | 233.678 | 279.450 | 230.588 | 253.039 | 235.089 | 256.258 |
| | $k$ | 0.171 | 0.186 | 0.180 | 0.012 | 0.008 | 0.007 | 0.147 | 0.196 | 0.170 | 0.202 | 0.167 | 0.194 |
| | $a$ | 0.981 | 0.931 | 0.949 | 0.040 | 0.021 | 0.020 | 0.908 | 1.076 | 0.891 | 0.977 | 0.911 | 0.991 |
| LOG | $L\infty$ | 225.995 | 220.500 | 222.400 | 6.458 | 3.543 | 3.249 | 214.054 | 241.366 | 213.811 | 228.151 | 216.150 | 229.411 |
| | $k$ | 0.272 | 0.283 | 0.279 | 0.012 | 0.008 | 0.007 | 0.247 | 0.298 | 0.266 | 0.300 | 0.264 | 0.293 |
| | $t$ | 1.171 | 0.963 | 1.037 | 0.216 | 0.116 | 0.107 | 0.781 | 1.696 | 0.748 | 1.217 | 0.835 | 1.272 |
| RICH Fixed $L_0$ = 99.3 | $L\infty$ | 361.375 | 224.953 | 239.757 | 249.435 | 12.454 | 17.262 | NA | NA | 207.999 | 265.813 | 217.159 | 300.696 |
| | $k$ | 0.090 | 0.309 | 0.250 | 0.137 | 0.079 | 0.069 | NA | NA | 0.163 | 0.464 | 0.122 | 0.383 |
| | $b$ | 0.771 | 2.810 | 2.278 | 1.417 | 0.812 | 0.712 | NA | NA | 1.290 | 4.396 | 0.943 | 3.634 |

According to the AIC and BIC model comparisons (Table 3.10), the 3P-VBGF was once again the overall preferred growth model, yielding the lowest values for both the sex-separated and combined sexes data, followed by the GOMP and LOG models.

**Table 3.10-** AIC and BIC model comparisons for male, female, and combined data of longfin mako sharks (*I. paucus*) obtained from back-calculated data using the quadratic Dahl-Lea (QDL) method, including the degrees of freedom (df) of each model. **3P-VBGF**: Three-parameter von Bertalanffy growth model; **2P-VBGF**: Two-parameter von Bertalanffy growth model; **GOMP**: Gompertz growth model; **LOG**: Logistic growth model; **RICH**: Richard's growth model**.**

| Growth Models (QDL) | AIC | | | BIC | | | df |
|---|---|---|---|---|---|---|---|
| | Males | Females | Combined | Males | Females | Combined | |
| 3P-VBGF | 4418 | 4831 | 9271 | 4436 | 4849 | 9292 | 4 |
| 2P-VBGF | 4482 | 4935 | 9438 | 4495 | 4949 | 9454 | 3 |
| GOMP | 4425 | 4836 | 9282 | 4443 | 4854 | 9303 | 4 |
| LOG | 4434 | 4845 | 9300 | 4451 | 4863 | 9321 | 4 |
| RICH | 4484 | 4924 | 9429 | 4502 | 4942 | 9450 | 4 |

Residual diagnostics were performed for the models with the most biologically appropriate parameter estimates for each sex (see Appendix C). For males and females, the standardized residual plots showed slight heteroscedasticity, while Q-Q plots pointed to some deviations from normality in residuals, but no outliers were present in data.

Likelihood ratio tests were used to compare the sex-separated growth models with combined growth models for the three datasets (Table 3.11). In all tested comparisons, no p-value was statistically significant, and as such, no improvement is seen in curves by fitting a sex-separated growth model over a combined growth model to represent the length-at-age data.

Nonetheless, the decision was to include the growth model curves for males and females separated, to allow for better interpretability of the results and for transparency.

**Table 3.11-** Likelihood ratio test (LRT) results comparing sex-separated growth models to combined growth models of longfin mako sharks (*I. paucus*) for the original sample data, linear Dahl-Lea (LDL) back-calculated data, and quadratic Dahl-Lea (QDL) back-calculated data. **RSS**: Residual sum of squares; **Comb.**: Combined; **Sep.**: Separated; **df**: Degrees of freedom; **Samples**: Original sample data; **LDL**: Linear Dahl-Lea; **QDL**: Quadratic Dahl-Lea; **3P-VBGF**: Three-parameter von Bertalanffy growth model; **2P-VBGF**: Two-parameter von Bertalanffy growth model; **GOMP**: Gompertz growth model; **LOG**: Logistic growth model; **RICH**: Richard's growth model**.**

| Data | Growth Models | RSS (Comb.) | RSS (Sep.) | $\chi^2$ | df | p-values | LRT Results |
|---|---|---|---|---|---|---|---|
| **Samples** | **2P-VBGF** | **17762** | **17728** | **0.538** | **3** | **0.910** | **False** |
| **Samples** | **3P-VBGF** | **17509** | **17273** | **3.882** | **4** | **0.422** | **False** |
| **Samples** | **GOMP** | **17583** | **17339** | **4.010** | **4** | **0.405** | **False** |
| **Samples** | **LOG** | **17690** | **17447** | **3.978** | **4** | **0.409** | **False** |
| **Samples** | **RICH** | **17550** | **17502** | **0.796** | **4** | **0.939** | **False** |
| **LDL** | **2P-VBGF** | **71406** | **71164** | **3.692** | **3** | **0.297** | **False** |
| **LDL** | **3P-VBGF** | **67569** | **67428** | **2.277** | **4** | **0.685** | **False** |
| **LDL** | **GOMP** | **67970** | **67862** | **1.735** | **4** | **0.784** | **False** |
| **LDL** | **LOG** | **68548** | **68548** | **1.304** | **4** | **0.861** | **False** |
| **LDL** | **RICH** | **71152** | **70834** | **4.875** | **4** | **0.300** | **False** |
| **QDL** | **2P-VBGF** | **76405** | **76118** | **4.097** | **3** | **0.251** | **False** |
| **QDL** | **3P-VBGF** | **67559** | **67424** | **2.179** | **4** | **0.703** | **False** |
| **QDL** | **GOMP** | **68125** | **68023** | **1.633** | **4** | **0.803** | **False** |
| **QDL** | **LOG** | **69005** | **68928** | **1.223** | **4** | **0.874** | **False** |
| **QDL** | **RICH** | **75797** | **75503** | **4.239** | **4** | **0.374** | **False** |

For the original sample data, LDL back-calculated data, and QDL back-calculated data all fitted models for male and female *I. paucus* displayed similar curve shapes. With the original sample data, male curves (Figure 3.10) overlapped between ages 2-6, and across nearly the entire range of ages for females (Figure 3.11).

The 3P-VBGF, GOMP, and LOG model curves overlapped for males between ages 0-2 and 6-9, producing higher FL estimates when compared to the 2P-VBGF and RICH models with a fixed $L_0$.

For females, the LOG and GOMP models had slightly higher FL estimates between ages 0-2 while the 3P-VBGF estimated a lower FL for this interval. Although model curves overlapped across most ages, beyond age 7, a minimal dispersal of growth curves starts occurring.

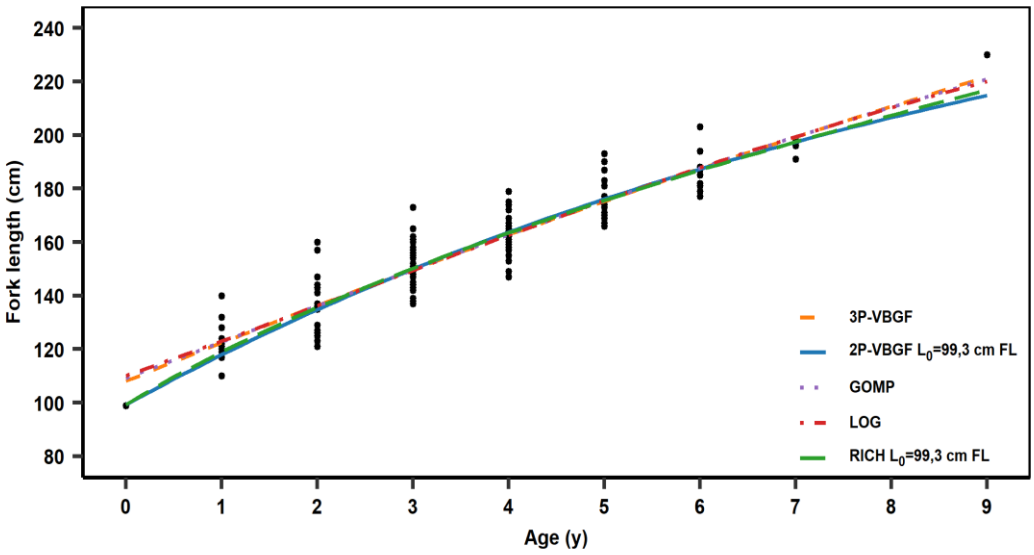


**Figure 3.10**- Growth model curves for the original vertebral band counts of male longfin mako shark (*I. paucus*) samples. The vertical black dots represent individual observations at each given age (years, y) with a respective fork length (FL, cm). The orange dashed line represents the three-parameter von Bertalanffy growth model (3P-VBGF). The full blue line represents the two-parameter von Bertalanffy growth model with a fixed mean length at birth ($L_0$ = 99.3 cm) (2P-VBGF). The purple dashed line represents the Gompertz growth model (GOMP). The dashed red line represents the Logistic growth model (LOG). The green full line represents the Richards growth model with a fixed $L_0$ = 99.3 cm (RICH).

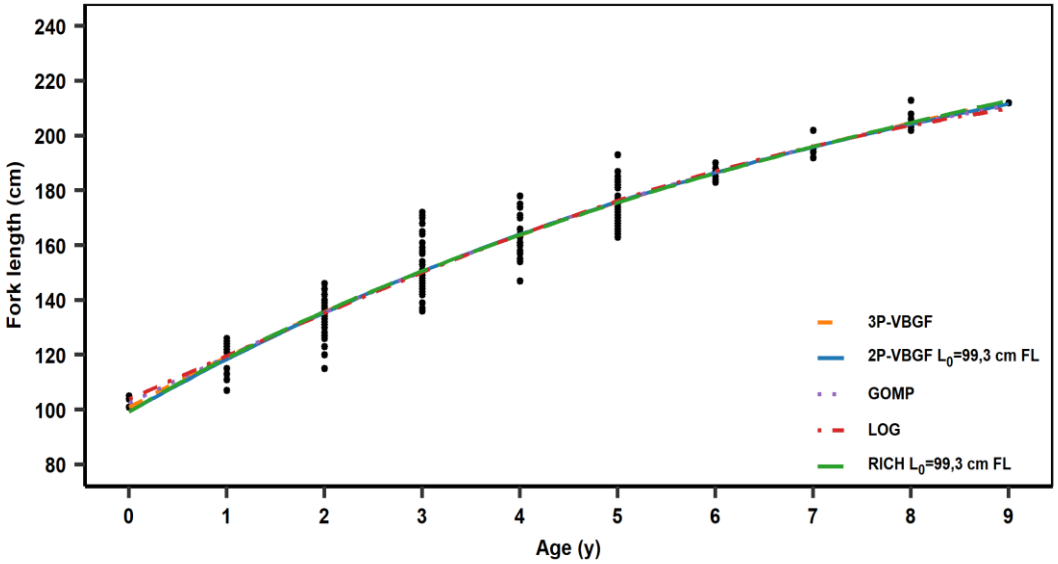


**Figure 3.11**- Growth model curves for the original vertebral band counts of female longfin mako shark (*I. paucus*) samples. The vertical black dots represent individual observations at each given age (years, y) with a respective fork length (FL, cm). The orange dashed line represents the three-parameter von Bertalanffy growth model (3P-VBGF). The full blue line represents the two-parameter von Bertalanffy growth model with a fixed mean length at birth ($L_0$ = 99.3 cm) (2P-VBGF). The purple dashed line represents the Gompertz growth model (GOMP). The dashed red line represents the Logistic growth model (LOG) . The green full line represents the Richards growth model with a fixed $L_0$ = 99.3 cm (RICH).

For the LDL back-calculated data, male curves (Figure 3.12) overlapped between ages 2-6, while for females (Figure 3.13), this overlap extended from ages 2-7. For both sexes, between ages 0-2, the 3P-VBGF, GOMP, and LOG curves overlapped, producing lower FL estimates when compared to the fixed $L_0$ of the 2P-VBGF and RICH.

Male curves for the 2P-VBGF and RICH maintained this overlap through ages 6-9, yielding higher FL estimates, whereas the 3P-VBGF, GOMP, and LOG curves became increasingly dispersed, estimating progressively lower FL values.

For females, this consistent overlap ends beyond age 7, with the curves of all models dispersing, producing progressively lower FL estimates.

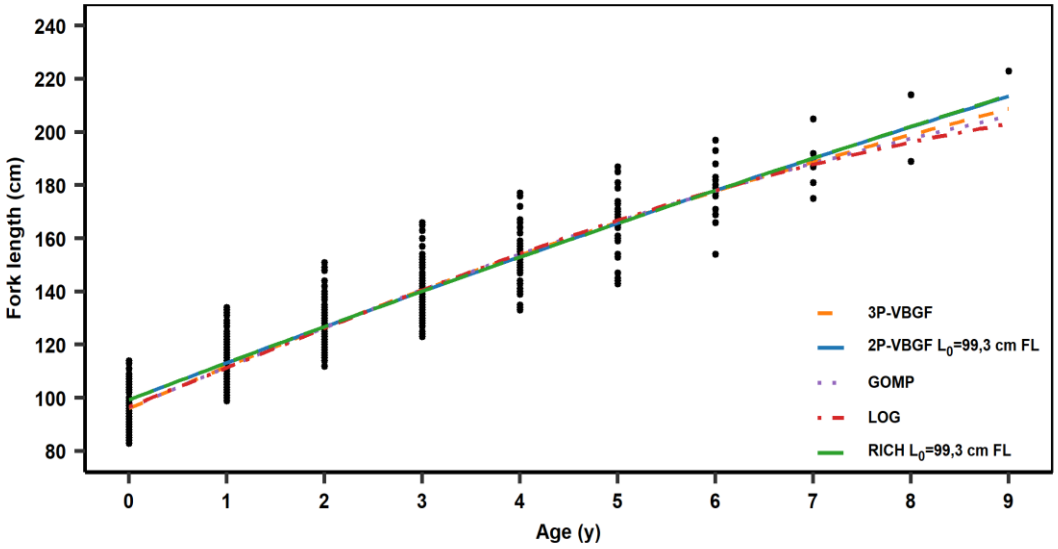


**Figure 3.12**– Growth model curves for the back-calculated linear Dahl-Lea (LDL) data of male longfin mako shark (*I. paucus*) samples. The vertical black dots represent individual observations at each given age (years, y) with a respective fork length (FL, cm). The orange dashed line represents the three-parameter von Bertalanffy growth model (3P-VBGF). The full blue line represents the two-parameter von Bertalanffy growth model with a fixed mean length at birth ($L_0$ = 99.3 cm) (2P-VBGF). The purple dashed line represents the Gompertz growth model (GOMP). The dashed red line represents the Logistic growth model (LOG). The green full line represents the Richards growth model with a fixed $L_0$ = 99.3 cm (RICH).

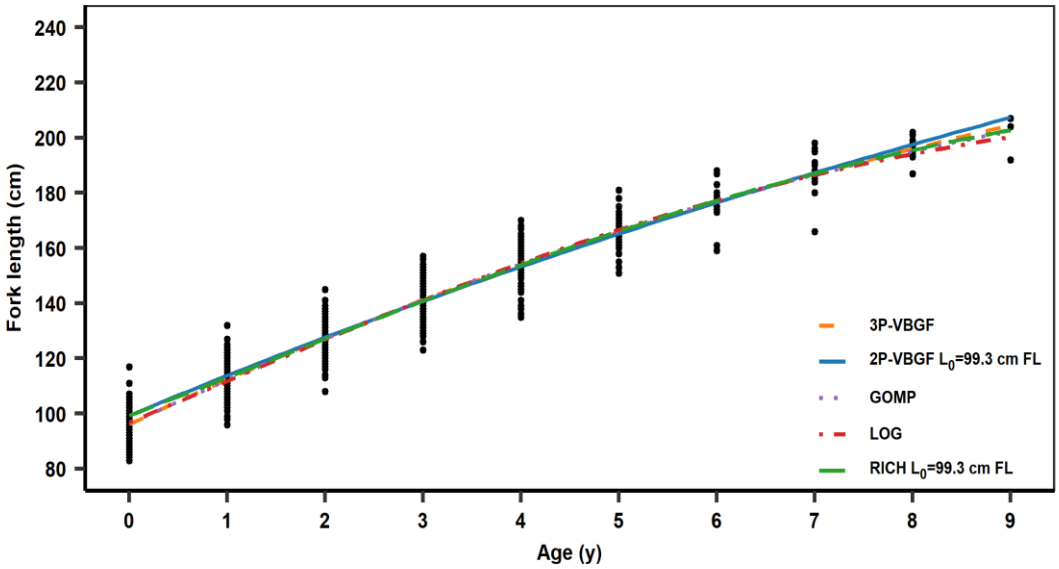


**Figure 3.13**– Growth model curves for the back-calculated linear Dahl-Lea (LDL) data of female longfin mako shark (*I. paucus*) samples. The vertical black dots represent individual observations at each given age (years, y) with a respective fork length (FL, cm). The orange dashed line represents the three-parameter von Bertalanffy growth model (3P-VBGF). The full blue line represents the two-parameter von Bertalanffy growth model with a fixed mean length at birth ($L_0$ = 99.3 cm) (2P-VBGF). The purple dashed line represents the Gompertz growth model (GOMP). The dashed red line represents the Logistic growth model (LOG). The green full line represents the Richards growth model with a fixed $L_0$ = 99.3 cm (RICH).

Finally, for the QDL back-calculated data, male curves (Figure 3.14) overlapped between ages 2–6, while for females (Figure 3.15), this overlap is seen from ages 2–7, meaning estimates were rather consistent in this interval across all models. For both sexes, between ages 0–2, the 3P-VBGF, GOMP, and LOG curves overlapped, producing lower FL estimates when compared to the 2P-VBGF and RICH fixed $L_0$.

For males, the 2P-VBGF and RICH curves maintained their overlap between ages 6-7, while at age 8 they start diverging, but yielded the highest FL estimates, while the 3P-VBGF, GOMP, and LOG curves became increasingly dispersed, with progressively lower FL estimates.

In females, beyond age 7 all curves disperse, with the 2P-VBGF estimating the highest FL values, while the 3P-VBGF, RICH, GOMP, and LOG progressively estimated lower FL values.

Considering the values obtained with AIC and BIC (Table 3.8, Table 3.9, Table 3.10) for the original sample data and back-calculated data (LDL and QDL), the 3P-VBGF, GOMP, and LOG models were selected to use with a Bayesian framework. These models consistently performed well across sexes, aside from female individuals in the original sample data, where the 2P-VBGF performed best.

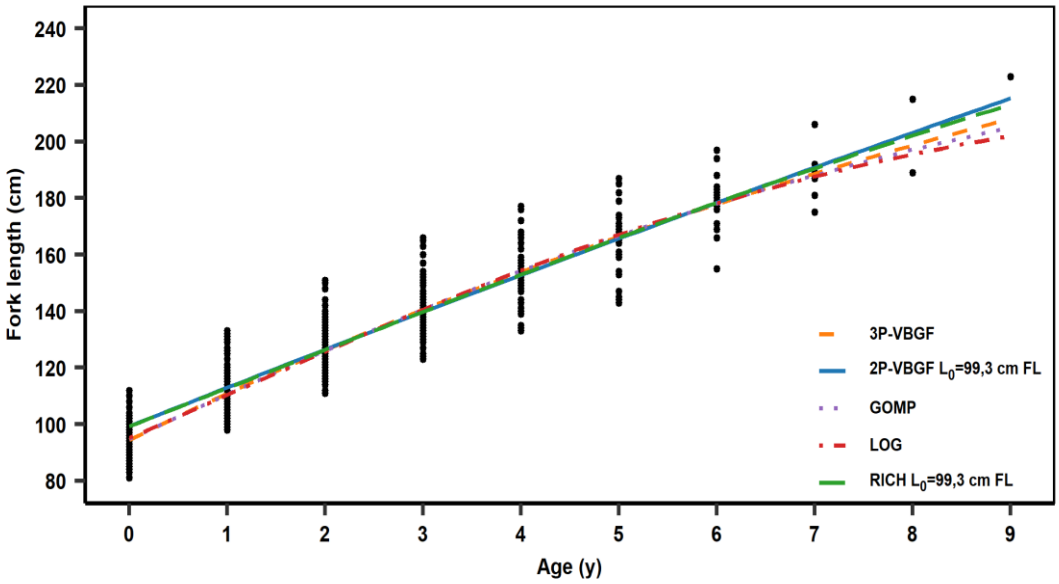


**Figure 3.14**– Growth model curves for the back-calculated quadratic Dahl-Lea (QDL) data of male longfin mako shark (*I. paucus*) samples. The vertical black dots represent individual observations at each given age (years, y) with a respective fork length (FL, cm). The orange dashed line represents the three-parameter von Bertalanffy growth model (3P-VBGF). The full blue line represents the two-parameter von Bertalanffy growth model with a fixed mean length at birth ($L_0$ = 99.3 cm) (2P-VBGF). The purple dashed line represents the Gompertz growth model (GOMP). The dashed red line represents the Logistic growth model (LOG). The green full line represents the Richards growth model with a fixed $L_0$ = 99.3 cm (RICH).

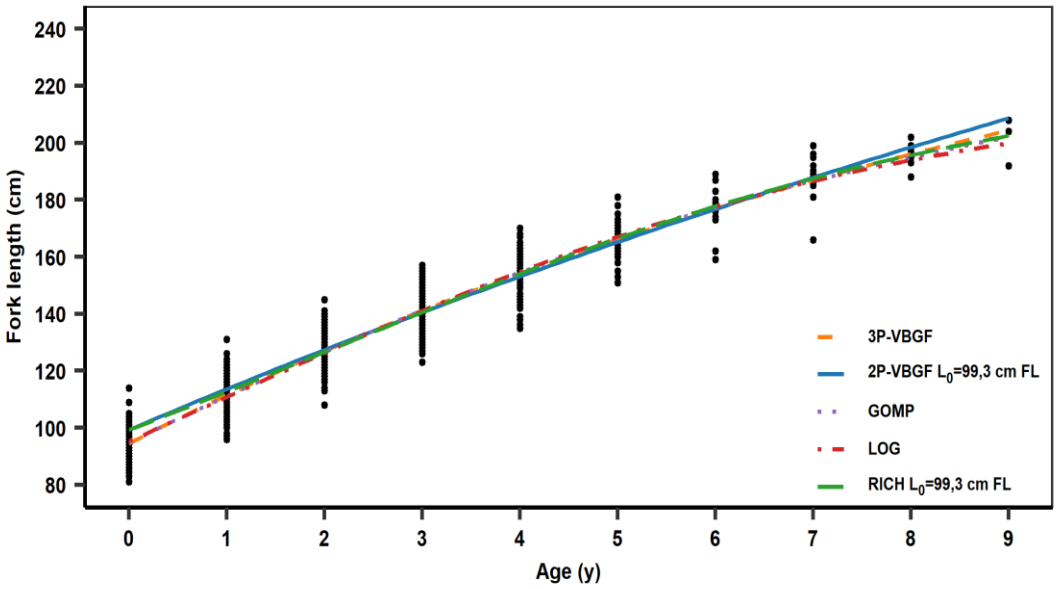


**Figure 3.15**– Growth model curves for the back-calculated quadratic Dahl-Lea (QDL) data of female longfin mako shark (*I. paucus*) samples. The vertical black dots represent individual observations at each given age (years, y) with a respective fork length (FL, cm). The orange dashed line represents the three-parameter von Bertalanffy growth model (3P-VBGF). The full blue line represents the two-parameter von Bertalanffy growth model with a fixed mean length at birth ($L_0$ = 99.3 cm) (2P-VBGF). The purple dashed line represents the Gompertz growth model (GOMP). The dashed red line represents the Logistic growth model (LOG). The green full line represents the Richards growth model with a fixed $L_0$ = 99.3 cm (RICH).

## VII. Bayesian framework models

A Bayesian approach was also applied to data from readings. For this analysis, the 3P-VBGF, GOMP, and LOG models were fitted separately for males and females using Bayesian inference. These were selected based on their previous biological plausibility and goodness-of-fit to the original sample data and back-calculation data for length-at-age modelling.

Models were then compared using LOOIC to estimate out-of-sample predictive performance. Of the three selected models, the 3P-VBGF had the lowest LOOIC values for both males (LOOIC = 963.684) and females (LOOIC = 1065.284) (Table 3.12). GOMP was closely behind, with slightly higher values for each sex, while LOG had the highest values for both. Although LOOIC differences were minimal between models, the model weight was highest for the 3P-VBGF for both males (0.44), and especially females (0.49), supporting its further analysis with the Bayesian framework.

**Table 3.12**- Comparison of Bayesian models for male and female longfin mako shark (*I. paucus*) sample data using the Leave-One-Out information criterion (LOOIC). Evaluation was conducted for the three-parameter von Bertalanffy (3P-VBGF), Gompertz (GOMP), and Logistic (LOG) growth models, including their respective model weight. **SE**: Standard error.

| | LOOIC | | SE (LOOIC) | | Model Weight | |
|---|---|---|---|---|---|---|
| **Growth Models** | **Males** | **Females** | **Males** | **Females** | **Males** | **Females** |
| **3P-VBGF** | **963.684** | **1065.284** | **18.249** | **19.349** | **0.44** | **0.49** |
| **GOMP** | **963.895** | **1066.316** | **18.229** | **19.224** | **0.40** | **0.29** |
| **LOG** | **965.711** | **1066.934** | **17.998** | **19.189** | **0.16** | **0.22** |

Parameters were estimated for both males and females by fitting a Bayesian 3P-VBGF using the MCMC method (Table 3.13). Male parameter estimates were higher for $L\infty$ and $L_0$, while $k$ had a lower estimate ($L\infty$ = 389.20 cm; $k$ = 0.060 yr$^{-1}$; $L_0$ = 105.74 cm) when compared to females ($L\infty$ = 319.900 cm; k = 0.090 yr$^{-1}$; $L_0$ = 102.88 cm). This trend was also consistent for the lower and upper 95% credibility intervals (CrI), with males having higher $L\infty$ and $L_0$ values, but a lower $k$ compared to females. Gelman-Rubin's diagnostic ($\hat{R} = 1 \leq 1.1$) determined that all MCMC chains converged successfully for each estimated parameter.

**Table 3.13**- Bayesian parameter estimates for male and female longfin mako sharks (*I. paucus*) using the three-parameter von Bertalanffy growth model (3P-VBGF) with the Markov Chain Monte Carlo method (MCMC). **SE**: Standard error; **sd(Posterior)**: Standard deviation of posterior**;** $\hat{R}$: Gelman-Rubin convergence diagnostic; **95% CrI**: 95% credibility interval**;** $L\infty$**:** Asymptotic maximum length (cm); $k$ = Relative growth coefficient; $L_0$ = Mean fork length at birth (cm).

| Models | Parameters | Estimates | SE (Estimates) | sd (Posterior) | $\hat{R}$ | 95% CrI (Lower) | 95% CrI (Upper) |
|---|---|---|---|---|---|---|---|
| **3P-VBGF (Males)** | **L∞** | **389.200** | **0.610** | **44.710** | **1** | **307.000** | **480.140** |
| | **k** | **0.060** | **0.001** | **0.010** | **1** | **0.040** | **0.090** |
| | **L0** | **105.740** | **0.030** | **2.240** | **1** | **101.080** | **109.980** |
| **3P-VBGF (Females)** | **L∞** | **319.900** | **0.540** | **37.140** | **1** | **261.670** | **405.880** |
| | **k** | **0.090** | **0.001** | **0.020** | **1** | **0.050** | **0.130** |
| | **L0** | **102.880** | **0.030** | **2.430** | **1** | **97.850** | **107.400** |

For males (Figure 3.16), the CrI was narrower between ages 2-5, coinciding with a higher sample density, while the CrI was widest between ages 0-1 and 6-9. In females (Figure 3.17), the CrI was narrower between ages 2-6, and widens between ages 0-1 and 7-9, where the lowest sample density is present.

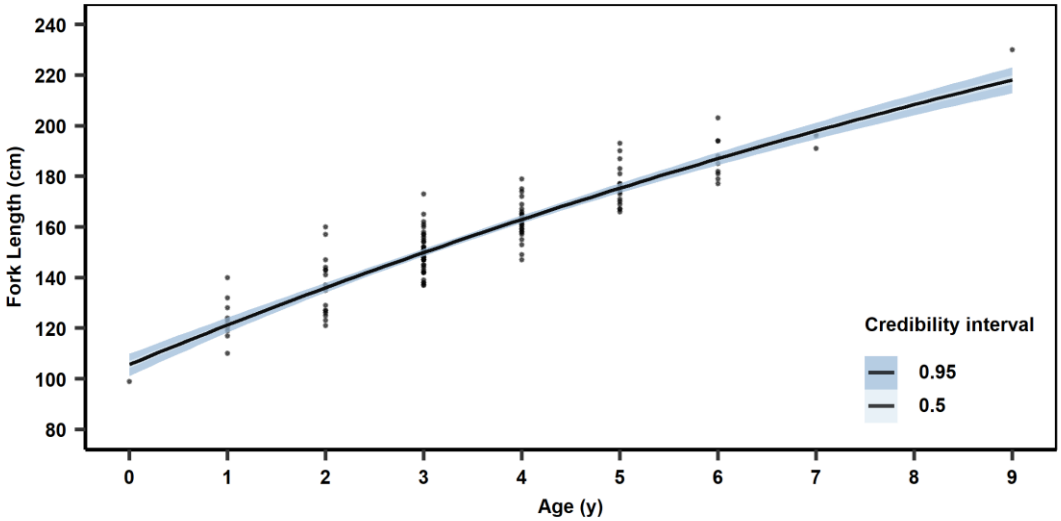


**Figure 3.16-** Fitted Bayesian three-parameter von Bertalanffy growth model (3P-VBGF) for male longfin mako shark (*I. paucus*) sample data using posterior mean parameter estimates obtained using Markov Chain Monte Carlo (MCMC). Vertical dots represent individual observations at each age (years, y) with a respective fork length (FL, cm). The full black line represents the fitted 3P-VBGFgrowth curve. The dark and light blue ribbons represent the upper and lower 95% credibility intervals (CrI), respectively.

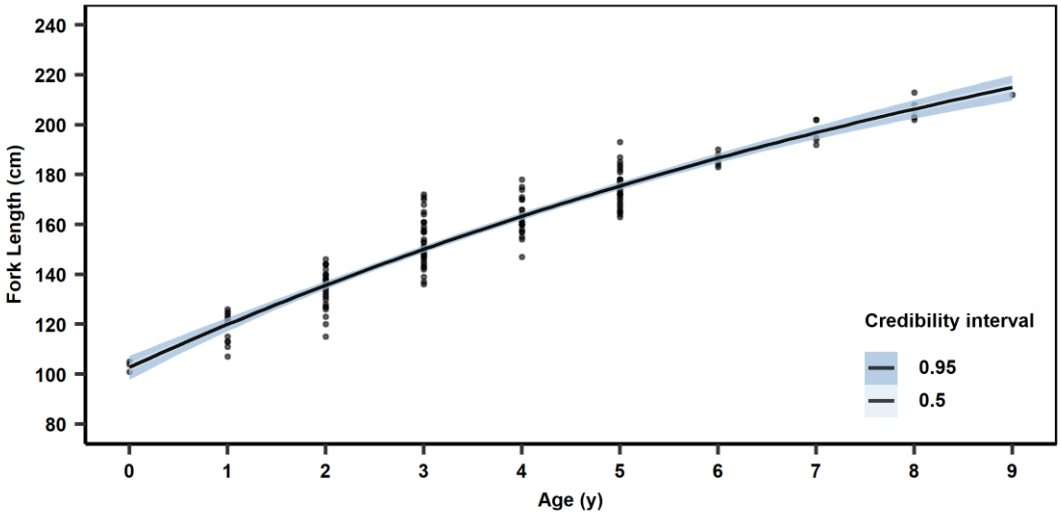


**Figure 3.17**- Fitted Bayesian three-parameter von Bertalanffy growth model (3P-VBGF) for female longfin mako shark (*I. paucus*) sample data using posterior mean parameter estimates obtained from Markov Chain Monte Carlo (MCMC). Vertical dots represent individual observations at each age (years, y) with a respective fork length (FL, cm). The full black line represents the fitted 3P-VBGF growth curve. The dark and light blue ribbons represents the upper 95% credibility intervals (CrI), respectively.

Prior and posterior probability density distributions for each parameter were then compared for male and female *I. paucus*. For the male $L\infty$ parameter (Figure 3.18), the posterior distribution estimates ranged between a 300-500 cm interval, while the prior had its distribution over a broader range of 150-600 cm due to its informative but not too restrictive nature.

In females (Figure 3.19), however, the posterior distribution for $L\infty$ had a narrower interval with a sharp peak and slightly right skewed distribution when compared to its prior and male posterior distributions, comprised between a 290-340 cm interval.

As for the prior distribution, a similar interval to the male prior distribution is seen since both were assigned the same priors. For both sexes (Figure 3.20; Figure 3.21), the posterior distributions for $L_0$ were equally narrow with a sharp peak and concentrated between a 95-110 cm interval. Prior distributions for $L_0$ followed a similarly flat and dispersed trend over a range of 50-150 cm for both sexes.

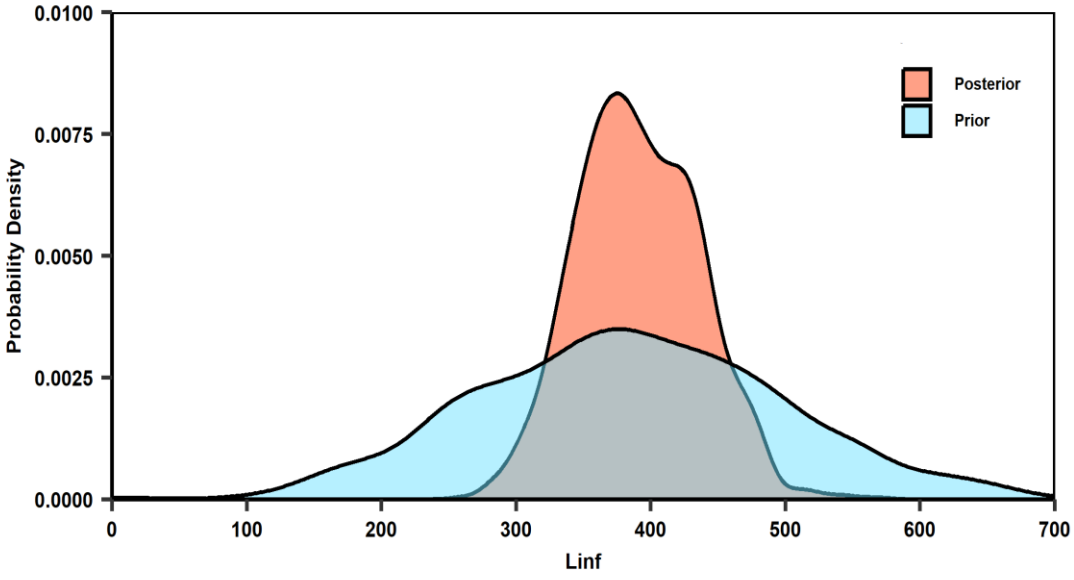


**Figure 3.18**- Prior and posterior probability density distributions of the asymptotic maximum length ($L\infty$, cm) from the Bayesian three-parameter von Bertalanffy growth model (3P-VBGF) fitted to male longfin mako shark (*I. paucus*) data. The prior distribution in blue shows the pre-data assumptions, while the posterior distribution in salmon was estimated using Markov Chain Monte Carlo (MCMC) sampling, incorporating observed data.

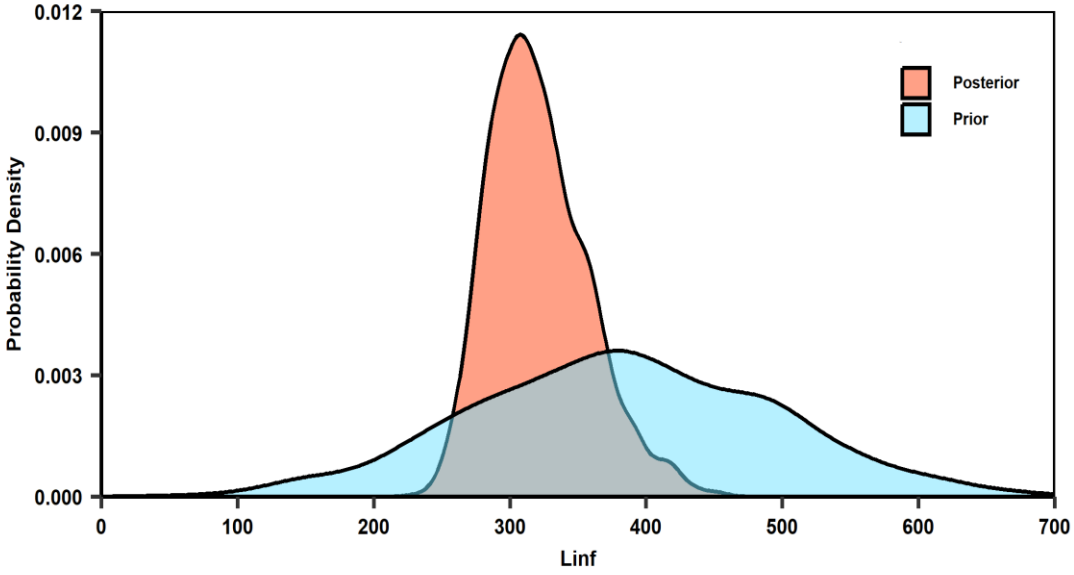


**Figure 3.19**- Prior and posterior probability density distributions of the asymptotic maximum length ($L\infty$, cm) from the Bayesian three-parameter von Bertalanffy growth model (3P-VBGF) fitted to female longfin mako shark (*I. paucus*) data. The prior distribution in blue shows the pre-data assumptions, while the posterior distribution in salmon was estimated using Markov Chain Monte Carlo (MCMC) sampling, incorporating observed data.

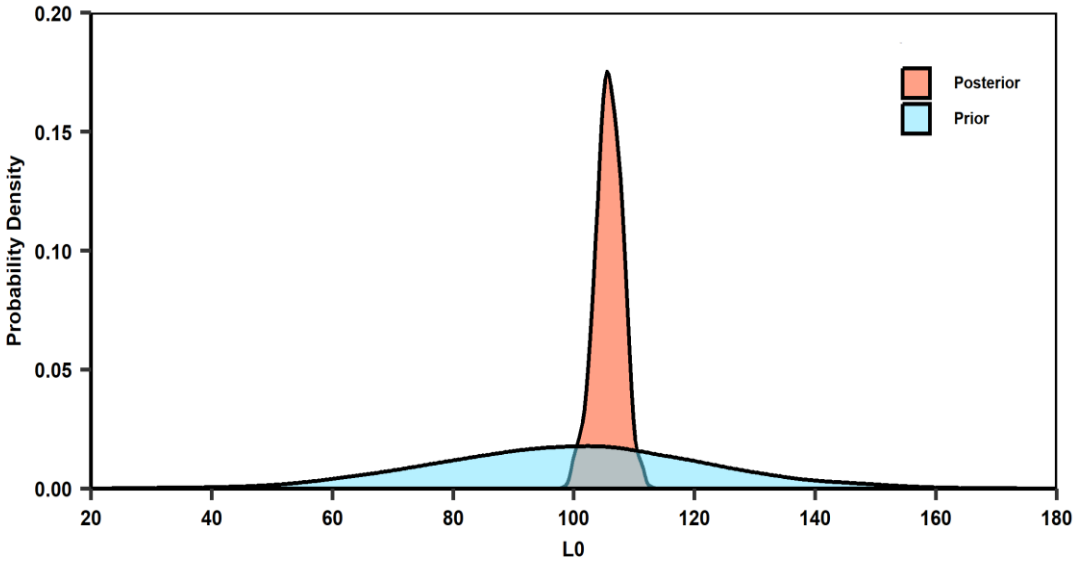


**Figure 3.20**- Prior and posterior probability density distributions of the mean fork length at birth ($L_0$, cm) from the Bayesian three-parameter von Bertalanffy growth model (3P-VBGF) fitted to male longfin mako shark (*I. paucus*) data. The prior distribution in blue shows the pre-data assumptions, while the posterior distribution in salmon was estimated using Markov Chain Monte Carlo (MCMC) sampling, incorporating observed data.

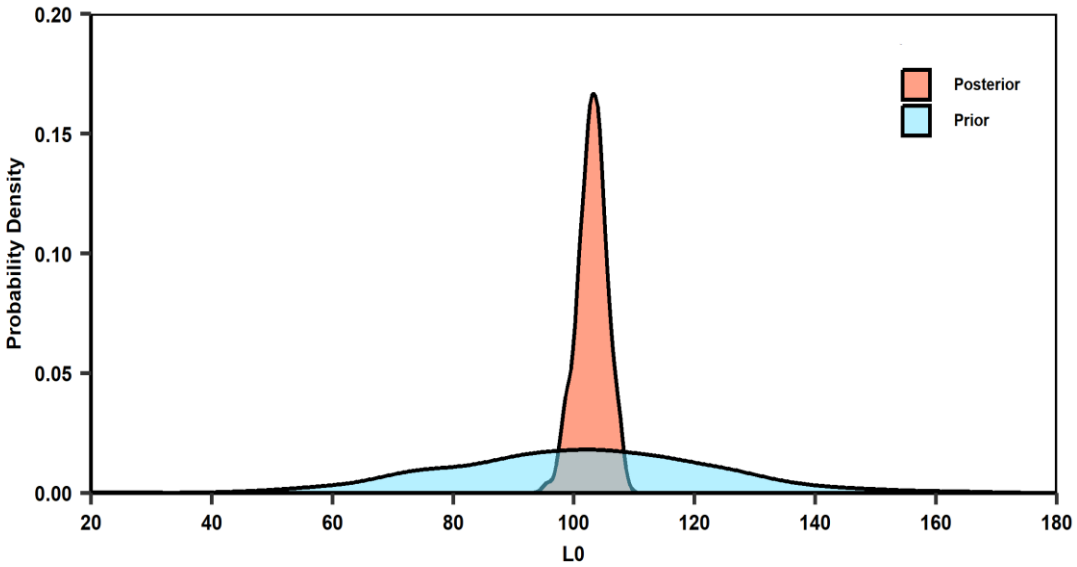


**Figure 3.21**- Prior and posterior probability density distributions of the mean fork length at birth ($L_0$, cm) from the Bayesian three-parameter von Bertalanffy growth model (3P-VBGF) fitted to male longfin mako shark (*I. paucus*) data. The prior distribution in blue shows the pre-data assumptions, while the posterior distribution in salmon was estimated using Markov Chain Monte Carlo (MCMC) sampling, incorporating observed data.

The frequentist and Bayesian 3P-VBGF curves were plotted for comparison across sexes, with both models exhibiting similar curve shapes. For male *I. paucus* (Figure 3.22), the model curves overlapped between ages 1-6, aligning with the higher sample density.

At ages 0-1 and 6-9 the frequentist 3P-VBGF estimated higher FL values, while the Bayesian 3P-VBGF produced lower FL estimates. In contrast for females (Figure 3.23), despite the curves also overlapping between ages 1-6, the opposite trend was observed at ages 0-1 and 7-9, with the Bayesian 3P-VBGF producing higher FL values, while the frequentist 3P-VBGF yielded lower FL estimates.

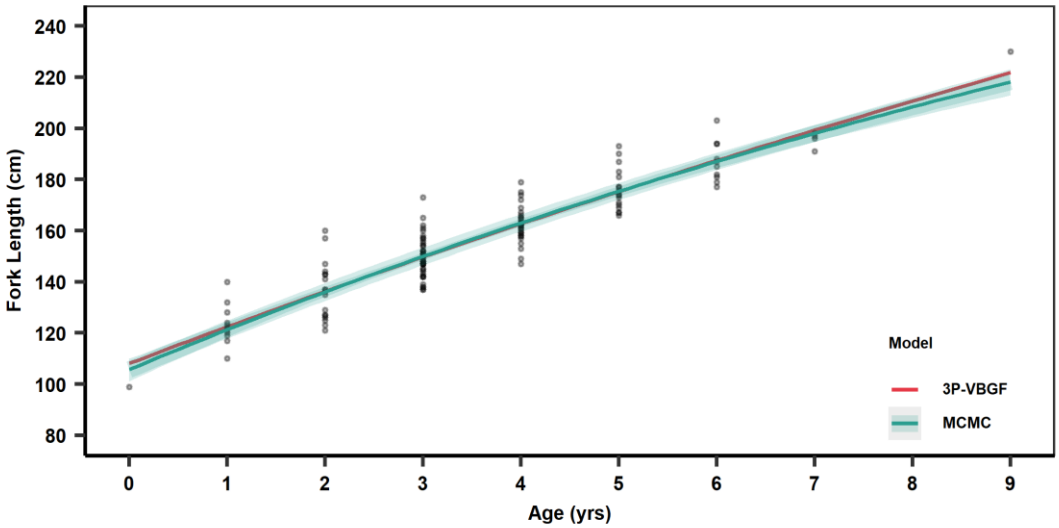


**Figure 3.22**- Length-at-age curves for the male longfin mako shark (*I. paucus*) data. The vertical black dots represent individual observations at each given age (years, y) with a respective fork length (FL, cm). The red line represents the frequentist three-parameter von Bertalanffy growth curve (3P-VBGF), while the green line represents the Bayesian 3P-VBGF growth curve using posterior mean parameter estimates. The bright green ribbon represents the 95% credibility interval (CrI) for the Bayesian 3P-VBGF.

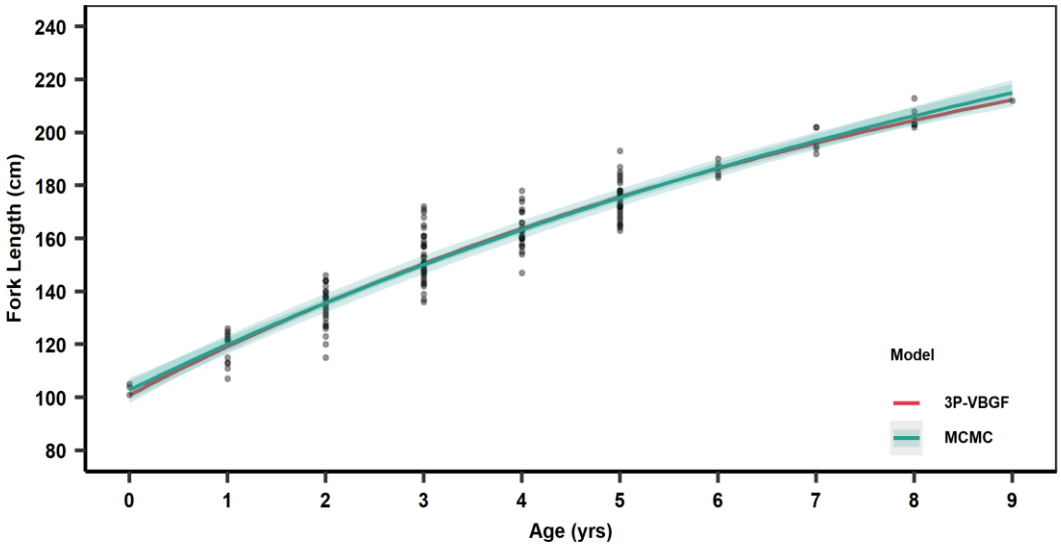


**Figure 3.23**- Length-at-age curves for the female longfin mako shark (*I. paucus*) data. The vertical black dots represent individual observations at each given age (years, y) with a respective fork length (FL, cm). The red line represents the frequentist three-parameter von Bertalanffy growth curve (3P-VBGF), while the green line represents the Bayesian 3P-VBGF growth curve using posterior mean parameter estimates. The bright green ribbon represents the 95% credibility interval (CrI) for the Bayesian 3P-VBGF.

## 4. Discussion

### I. Sample composition

The samples used in this study were *I. paucus* from the Equatorial Atlantic Ocean, which while constituting a great addition to the lack information on the species, does not extrapolate to *I. paucus* in other oceanic regions, such as the Pacific and Indian Oceans, as well as the Mediterranean and Arabian seas. Further research on *I. paucus* populations from different geographic regions is thus heavily encouraged.

Additionally, the sample pool does not represent the complete FL range known for *I. paucus*, with the majority of individuals being juveniles and only five males, aged 6–9, and two females, aged 8–9, being mature according to FL comparisons with reported median TL-at-maturity reported in Ruiz-Abierno et al. (2021a). Lacking small juveniles and large mature individuals in both sexes, even with a moderate sample size of 294 individuals, posed significant challenges when modelling growth, as a representation of the full FL range is often more critical than a large sample size (Smart et al., 2012).

The size at birth ranges from 77 to 122 cm FL, the smallest individual of 99 cm FL in the sample being included in this range, however, few individuals with lengths below 120 cm FL were available in the sample pool, for both sexes, but in particular for females.

Regarding the upper limit of the size distribution, no individual was above 230 cm FL, which when considering the largest female reported was 387 cm FL and the largest male 276 cm FL, there is a severe lack of information on larger sizes for both sexes. Due to restrictions imposed by CITES (CITES, 2019) the acquisition of additional samples is now extremely difficult, hindering the expansion of biological material and databases, as well as future research on the life history of elasmobranchs, such as *I. paucus*.

This absence, or low sample size, within size classes may have generated biased growth parameter estimates, with the lack of large individuals possibly leading to an underestimated $L\infty$, while a lack of juveniles may have led to poor $L_0$ estimates, consequently affecting $k$, and ultimately reducing the biological realism of growth curves (Smart et al., 2012).

**II. Age estimates and bias**

Due to the inconsistent visibility of the *corpus calcareum* angle change in *I. paucus* vertebrae, the use of the VR from individuals within the 99-124 cm FL range was invaluable to locate birth bands and improve the consistency of age counts (Casto et al., 1999; Gilmore, 1983; Goldman et al., 2005; Natanson et al., 2002).

As stated by Campana (2005), values for the CV and APE should be below the 7.6% and 5.5% threshold, respectively, mentioning some studies report values for CV beyond 10%. In this study, a CV of 5.6% and an APE of 4.3% are reported, making the internal consistency and precision of readings acceptable (Beamish & Fournier, 1981; Campana, 2005).

Significant differences were found with McNemar's test between the first and second readings, as well as the second and third readings, but no significant differences were found between the first and third readings. This may suggest some inconsistencies were introduced with the second reading, possibly attributed to human error, bias, or temporary deviation from the established ageing criteria (Campana, 2005).

While secondary readers are not a necessity to ensure consistent readings, a secondary reader for *I. paucus* ageing would have contributed to a more in-depth evaluation of inconsistencies (Campana, 2005). Plots provided visual support for statistical evidences, where between the first and second readings, a slight negative directional bias is seen beyond age 5, where the second reading tended to underestimate age compared to the first.

With the second and third readings, however, results from McNemar's test are not consistent with what is seen, since most values were tightly clustered near the 1:1 line, with no visible patterns, suggesting greater consistency than other reading comparisons. Despite the plot comparing the first and third readings showing a similar negative directional bias pattern between ages 6-8 to that of the first and second readings, McNemar's test did not flag these differences as statistically significant. These discordances can be attributed to a smaller number of discordant pairs at each age, which reduced the power of McNemar's test to detect subtle directional differences in data (Beamish & Fournier, 1981; Campana, 2005).

Campana (2005) emphasizes that statistical significance alone is not always reliable when detecting ageing bias, as small statistically significant differences may lack biological importance, while trends can signal real disagreement, even when the CI overlaps the 1:1 line. This emphasizes the importance of the assessment of age readings both visually and statistically for *I. paucus* vertebrae, as well as other elasmobranch species (Campana, 2005).

The "split banding" phenomenon was commonly observed in vertebrae of both *I. paucus* sexes, which introduced further complexity to age interpretations (Goldman et al., 2005). Despite only three samples being discarded due to incompatibility with the established criteria, an uneven distribution of data across age classes was evident, with most samples being between 120-190 cm FL, corresponding to the 1-6 years of age interval.

Males had both the largest and smallest samples in the dataset, with the smallest male being aged 0 with an FL of 99 cm, while the largest male was aged 9, with a 230 cm FL. For females, the smallest female was aged 0 and had a 101 cm FL, while the largest was 213 cm FL and aged 8 years old. For samples of both sexes, neither had an FL close to the reported minimum and maximum sizes in the literature of 387 cm FL for females (Castro, 2011) and 276 cm FL for males (Wakida-Kusunoki & de Anda-Fuente, 2012). While this was the case, the data was still sufficient to proceed with the approaches previously addressed in this work.

Additionally, no statistically significant differences in length-at-age were seen between male and female *I. paucus* based on the Mann-Whitney U test results, despite sexual dimorphism being reported in some elasmobranch species (Gayford et al., 2023).

### III. Age validation

While age estimates were precise, this does not ensure that readings were accurate, particularly without age validation techniques (Goldman, 2005). For *I. paucus*, this age validation remains unknown, highlighting a critical gap in knowledge for the confirmation of age estimates. Studies on other lamnid sharks, like *I. oxyrinchus* and the porbeagle shark (*Lamna nasus*) have demonstrated the utility of age validation tools, such as bomb radiocarbon ($\Delta^{14}C$) and oxytetracycline (OTC) tag-recapture.

The first application of $\Delta^{14}C$ dating to a long-lived shark was for *L. nasus* in the northwest Atlantic Ocean by Campana et al. (2002), where $\Delta^{14}C$ uptake in vertebrae reflected known marine $\Delta^{14}C$ trends, supporting annual band deposition in individuals up to 26 years of age. Natanson et al. (2002) validated this annual deposition rate for *L. nasus* in the northwest Atlantic Ocean, but only up to 11 years of age, with limited validation for older individuals.

For *I. oxyrinchus*, Pratt and Casey (1983) proposed a two band pair per year deposition rate, contrasting with Cailliet et al. (1983) who assumed annual deposition rates of band pairs. Ardizzone et al. (2006) and Natanson et al., 2006 supported Cailliet et al. (1983) based on the alignment of $\Delta^{14}C$ timelines between *I. oxyrinchus* and *L. nasus*, where variations were attributed to dietary and geographical distribution differences. Dietary overlaps also occur between *I. paucus* and *I. oxyrinchus* diets, such as *Dosidicus gigas* (Bustamante et al., 2009; Vetter et al., 2008), suggesting that certain aspects of $\Delta^{14}C$ deposition patterns in *I. oxyrinchus* may apply to *I. paucus*.

Kinney et al. (2016) and Wells et al. (2013) used the OTC tag-recapture method to determine that two band pairs were deposited per year up to six years of age in *I. oxyrinchus* off the coast of south California, transitioning to one band pair per year beyond that age.

While both $\Delta^{14}C$ and OTC tag-recapture are strong methods, it is important to acknowledge that to date, no existing method validates age across a species' entire lifespan (Natanson et al., 2018). $\Delta^{14}C$ is also expensive and for validation to occur sharks must have been born during the post-bomb $^{14}C$ increase period (from 1960 to 1970) while also remaining in the oceans' mixed layer for part of their life (Goldman & Cailliet, 2004).

Additionally, $\Delta^{14}C$ validation assumes a consistent formation of band pairs, which may only occur for a portion of a species life history (Natanson et al., 2018). With *I. paucus* being a migratory species, and its diet being generalistic, inconsistencies may be present in the periodicity of band pair formations (Bowman, 2000; Bustamante et al., 2009; Estupiñán-Montaño & Delgado-Huertas, 2022; Gong et al., 2023).

Despite OTC tag-recapture being an effective age validation technique for chondrichthyan fishes, its reliability decreases when recapture windows are short (Campana, 2005; Goldman, 2005; Wells et al., 2013). While longer recapture intervals are ideal, these are often impractical, as individuals become increasingly difficult to recapture

and recover over extended time periods (Goldman & Cailliet, 2004). Age readings may also become increasingly more difficult with older individuals, as bands may be reabsorbed or deposited in narrower intervals, affecting the effectiveness of the OTC tag-recapture (Wells et al., 2013).

Estimates for *I. paucus* ages reported in this study were considered to be bi-annual up to five years and annual thereafter as validated by Kinney et al., 2016; Wells et al., 2013 for *I. oxyrinchus*. While the use of congeners as proxies is a common practice in elasmobranch age and growth research, inherent uncertainty is introduced from growth dynamic differences, band pair deposition rates, and life history traits between species (Chin et al., 2013). Estimates for *I. paucus* ages reported in this study would thus benefit from research employing the $\Delta^{14}C$ and/or OTC tag-recapture methods, to validate these band deposition rates and improve the reliability of age readings.

**IV. Back-calculations**

The TL/FL model presented a strong fit to the data ($R^2 = 0.98$),supporting its suitability to transform length-at-birth and maximum lengths from TL in the literature to FL, used in this study. This length-length equation may also be useful for use in standardization of reported sizes to ICCAT, as currently no TL/FL relationship is available for *I. paucus* (Mas et al., 2022). This performance was similar to other TL/FL linear regressions reported for *I. oxyrinchus*, *L. nasus*, and other shark species, where values for $R^2 \geq 0.95$ were common (Mas et al., 2014; Natanson et al., 2014; Rosa et al., 2021).

The linear FL/VR model was preferred over the quadratic model based on the BIC and likelihood ratio test, despite both fitting the data equally well ($R^2_{Linear} = R^2_{Quadratic} = 0.840$). The linear model offered a slightly better statistical fit, with its selection being further supported by the lower MAD of back-calculated lengths when using the LDL back-calculation method (Francis, 1990).

A consistent underestimation of the back-calculated mean length-at-age in relation to the observed mean length-at-age was observed for all back-calculation methods, especially at younger ages, with the DL method showing the highest MAD. These underestimations are consistent with Lee's phenomenon, which typically results in lower back-calculated lengths at younger ages compared to observed values, often due to selective mortality and

sampling bias (Lee, 1920). As stated by Campana (1990) and Francis (1990), the DL back-calculation method assumes that growth is isometric between FL and VR, which is unlikely for a species with slowing non-linear growth, like *I. paucus*. This isometric correlation likely caused an underestimation of FL at younger ages, based on the measured VR, explaining the observed pattern.

Despite these limitations, the LDL method yielded the lowest MAD from the observed mean length-at-age, which when combined with the better statistical fit of the linear FL/VR regression, suggests that it is more biologically and statistically appropriate for modelling growth than the QDL. This shows that the added complexity of the quadratic FL/VR regression and its equation parameters did not translate to better results when performing back-calculations with the QDL.

Other studies have reported on the outcomes of back-calculation methods, with varying results for different species and data. Rosa et al. (2017) found that while using the same methods, the QDL produced the most biologically realistic back-calculations for the *S. zygaena*, while Harry et al. (2010) reports on the LDL producing the most accurate results for the milk shark (*Rhizoprionodon acutus*).

In the present study, back-calculated lengths with the LDL and QDL methods were limited to younger age classes (age ≤ 9), with ages older than 8 years remaining underrepresented. Although these methods addressed issues for individuals below 120 cm, they do not account for the scarcity of larger specimens.

## V. Frequentist growth models for the original data

As the first study to model growth for *I. paucus* in the Equatorial Atlantic Ocean and worldwide, the multi-model approach recommended by Cailliet et al. (2006) was essential to evaluate model fits, parameter convergence, and robustness across data.

The limitations of the original sample data for younger age classes could have affected growth model parameter estimates, affecting their biological realism (Cerna & Licandeo, 2009; Smart et al., 2012). In all models fitted to the original data, males had consistently higher $L\infty$ and $L_0$ estimates while females had consistently higher $k$ estimates. This would suggest that males achieve a larger maximum size while growing slower, and females have a faster growth rate, but smaller maximum size.

The 3P-VBGF had issues converging for male data, with large $L\infty$ SE, a negative lower 95% CI for k, and a lacking upper 95% CI estimate for $L\infty$. Despite these issues, it still had the lowest BIC and shared the lowest AIC with RICH for males. The RICH failed to converge for individual and grouped sex data, producing no 95% CIs, suggesting a poor goodness-of-fit to data. In contrast, the 2P-VBGF showed the strongest performance, yielding the lowest SE for males, females, and combined, while having narrow 95% CIs and the lowest values for AIC and BIC for females and combined.

A trend is seen in male data, with higher SEs and wider 95% CIs, highlighting the aforementioned sensitivity of parameter estimates to the data structure. For males, all models except those with a fixed $L_0$, estimated higher $L_0$ values with high associated SEs. In contrast, female models slightly underestimated $L_0$, but had lower SEs, and values closer to the expected $L_0$, suggesting $L_0$ estimates are more biologically plausible than those of males.

For the male $L\infty$ and $k$, the lack of samples at age 8 and the inclusion of a single large male at age 9 may have skewed the 3P-VBGF, GOMP, and LOG curves, resulting in an overextended exponential growth phase. This likely resulted in the overestimation of $L\infty$, and underestimation of $k$, since these parameters are inversely proportional, while uncertainty resulted in wider 95% CIs and increased SEs (Jensen, 1997). In females, model fits were more consistent, however, the limited data beyond age 6 could have led to an earlier end of the exponential growth phase, leading to the lower $L\infty$ and higher $k$ values, and thus faster growth but unrealistic small maximum sizes.

Across multiple oceanic regions, females in lamniform shark species frequently grow larger than males, while exhibiting slower growth rates, based on current data. In the western South Atlantic Ocean, Barreto et al. (2016) reported slightly higher L∞ and lower k for *I. oxyrinchus* females with the 2P-VBGF, assuming a two-band pair deposition rate until five years of age (Males: $L\infty$ = 291.57 cm FL, $k$ = 0.200 $y^{-1}$; Females: $L\infty$ = 309.79 cm, $k$ = 0.130 $y^{-1}$). A similar trend was observed in the western North Atlantic by Natanson et al. (2006), where males were best fit by the 3P-VBGF ($L\infty$ = 253 cm FL, $k$ = 0.125 $y^{-1}$, $L_0$ = 72 cm FL), and females by the GOMP ($L\infty$ = 366 cm FL, $k$ = 0.087 $y^{-1}$, $L_0$ = 88 cm FL), with growth being similar for both sexes until 11 years of age.

In the western and central North Pacific Ocean, Semba et al. (2009) observed a comparable pattern for *I. oxyrinchus* with the 3P-VBGF and annual band pair deposition

rates (Males: $L\infty$ = 231 cm PCL, $k$ = 0.160 $y^{-1}$, $L_0$ = 59.7 cm PCL; Females: $L\infty$ = 308 cm PCL, $k$ = 0.090 $y^{-1}$, $L_0$ = 88 cm PCL), but growth was only similar until seven years of age. In the southeast Pacific Ocean, Cerna and Licandeo (2009) reported similar results with the 2P-VBGF and annual band pair deposition rates (Males: $L\infty$ = 231 cm TL, $k$ = 0.160 $y^{-1}$; Females: $L\infty$ = 308 cm TL, $k$ = 0.090 $y^{-1}$).

A similar pattern was reported for *A. superciliosus* in the tropical Northeast Atlantic Ocean by Fernandez-Carvalho et al. 2011 with the 3P-VBGF using an annual band pair deposition rate (Males: $L\infty$ = 206 cm FL, $k$ = 0.18 $y^{-1}$, $L0$ = 93 cm FL; Females: $L\infty$ = 293 cm FL, k = 0.06 y–1 and $L0$ = 111 cm FL).

Additionally, for salmon sharks (*Lamna ditropis*), Goldman and Musick, 2006 report a similar trend in the Northeast Pacific Ocean with the 3P-VBGF (Males: $L\infty$ = 182.8 cm PCL, $k$ = 0.230 $y^{-1}$; Females: $L\infty$ = 207.4 cm PCL, $k$ = 0.170 $y^{-1}$). Likewise, Rosa et al. (2021) documented this same sexual dimorphism for the crocodile shark (*Pseudocarcharias kamoharai*) in the tropical Atlantic Ocean with the 2P-VBGF and an annual band pair deposition rate (Males: $L\infty$ = 94.6 cm FL, $k$ = 0.180 $y^{-1}$; Females: $L\infty$ = 105.6 cm FL, $k$ = 0.140 $y^{-1}$).

This highlights the impact of data gaps in both sexes, and while convergence was possible for some models, the produced estimates for $L\infty$ and $k$ are unlikely to be biologically realistic in both cases. The statistical results of the LRT comparing sex-separated and combined growth models additionally support that no significant differences in size between males and females were present for the data to justify presenting sex-separate growth curves, other than transparency. It is likely, however, that the absence of sexual dimorphism seen *I. paucus* data could deviate from commonly observed patterns in other lamnids, reinforcing the need for additional research to assess the realism of said deviations.

### VI. Frequentist growth models for LDL and QDL back-calculated data

Using the LDL and QDL back-calculation methods significantly improved model fits and parameter estimates for the 3P-VBGF, which became the best fitting model. While true, model selection criteria should be approached with caution, as parameter estimates may not reflect biological realism (Katsanevakis, 2006).

$L\infty$ estimates remained highest for males, and $k$ estimates for females, while $L_0$ estimates became closer for both sexes. Although RICH managed to estimate parameters for females with the LDL, and for females and combined sexes with the QDL, female $L\infty$ estimates were rather low. Similarly, while the GOMP and LOG managed to produce parameter estimates for females, these were far too low to be considered realistic for *I. paucus*. The 2P-VBGF fit worsened for males, with the LDL producing biologically unrealistic estimates, and QDL producing even less plausible results.

When comparing the produced LDL and QDL back-calculated data growth curves with the original sample data curves for males, the non-fixed $L_0$'s remained close to the calculated $L_0$. On the other hand, beyond age 6, model curves have a more evident dispersal for the LDL and QDL, influenced by changes in $k$ and $L\infty$ estimates. In females, for the LDL and QDL back-calculated data curves, the same trend is observed for non-fixed $L_0$'s, suggesting a similar, size-at-birth to that of male *I. paucus*.

With the original sample curves, these overlapped for most ages, but with the LDL and QDL, the introduction of additional data points, especially at ages 6-7, allowed for more flexibility when estimating growth parameters. While exploring the LDL and QDL produced interesting results, considering parameter estimates and that model curves were rather similar in both cases, the LDL method is preferred, based on the lower MAD and linear FL/VR regression.

Perhaps most curious, is that the 2P-VBGF became the poorest-fitting model for females with high SEs and wide 95% CIs but produced the most biologically realistic $L\infty$ estimates (LDL = 400 cm FL; QDL = 438 cm FL). Considering the similar growth patterns observed across other lamniform sharks, and that the 2P-VBGF produced biologically plausible estimates for females, it is reasonable to assume that the 3P-VBGF may have produced biologically realistic estimates for males (LDL = 363 cm FL ; QDL = 335 cm FL), even if the largest reported male is only 303 cm TL (275.848 cm FL), thus being less reliable (Wakida-Kusunoki & de Anda-Fuente, 2012).

If so, $k$ estimates from the LDL (3P-VBGF Males: $k = 0.061\ y^{-1}$; 2P-VBGF Females: $k = 0.050\ y^{-1}$) and QDL (3P-VBGF Males: $k = 0.071\ y^{-1}$; 2P-VBGF Females: $0.043\ y^{-1}$) highlight a rather slow growth rate for *I. paucus* when compared to aforementioned age-and-growth studies on other species, especially for females. While a mere hypothesis, this slow growth coupled with a K life strategy and low reproductive potential could lead to

rapid declines in population size for *I. paucus* due to overexploitation, requiring urgent attention (Cortés, 2008).

## VII. Bayesian approach

The main goal of applying a Bayesian framework was to further explore the lack of individuals with FL>180 cm in the original data, since the LDL managed to address issues for smaller sizes (Smart & Grammer, 2021). While using the same priors for both sexes can bias posterior estimates, since data on *I. paucus* is rather scarce this simplification is justifiable (Doll & Jacquemin, 2019).

The slightly lower LOOIC and superior model weight of the Bayesian 3P-VBGF justified its selection for use with the Bayesian framework, as a lower LOOIC and higher model weight suggested a better out-of-sample predictive performance (Vehtari et al., 2017). While MCMC chains converged successfully, the issues seen in the frequentist approach persisted with the Bayesian 3P-VBGF, which estimated higher $L\infty$ values for males ($L\infty$ = 389.2 cm FL) than females ($L\infty$ = 319.9 cm FL).

Values for $k$ were slightly higher for males ($k$ = 0.060 $y^{-1}$) and lower for females ($k$ = 0.090 $y^{-1}$) when compared to the original sample estimates (Males: $k$ = 0.032 $y^{-1}$; Females: $k$ = 0.108 $y^{-1}$) , but the growth rate for females remained higher than for males. Bayesian $L_0$ estimates (Males: $L_0$ = 105.740 cm FL; Females: $L_0$ = 102.880 cm FL) were, however, slightly lower than the original data $L_0$ for males ($L_0$ = 108.129 cm FL), while for females it was slightly higher ($L_0$ = 100.968 cm FL). Relative to the LDL data, both male and female $L_0$ estimates (Males: $L_0$ = 105.740 cm FL; Females: $L_0$ = 102.880 cm FL) were slightly higher than LDL estimated values (Males: $L_0$ = 96.075 cm FL; Females: $L_0$ = 96.170 cm FL), while also associated with wide 95% CrIs, following the original data model trend.

Although the results were generally consistent with those from frequentist models, the prior-posterior distributions allow for a good visualization of limitations previously stated. For the male $L\infty$, while the given prior was rather wide, the probability density suggested, based on data, that it is most likely that males are anywhere between 350-440 cm FL, while females are most likely between 290-330 cm FL. These wider posteriors, especially in males, support that data constraints from the lack of large individuals is

causing the observed uncertainty with $L\infty$ estimates and is likely why males are estimated to achieve much larger sizes than females. On the other hand, while female posteriors were more constricted, based on the largest reported size, the female predicted $L\infty$ is not biologically accurate.

For $L_0$, a very narrow posterior probability density with higher values is seen for males and females, where both are most likely to be between 99-105 cm FL. This further supports the idea, much like the LDL, that both sexes are likely to have a very similar mean length-at-birth, but LDL back-calculation parameters are likely to be more realistic, since it is a more appropriate method when lacking young individuals.

When comparing the frequentist original sample 3P-VBGF to the Bayesian 3P-VBGF of males, the Bayesian 3P-VBGF estimated smaller sizes between ages 0-1 and 6-9, but the original sample 3P-VBGF is contained within the 95% CrI. For females, the opposite trend is seen at these age intervals, but much like in the original sample and LDL curves, between ages 6-9 the female growth curves asymptote much earlier than male curves, thus leading to L∞ and k underestimations.

While the Bayesian framework has contributed to studies with limited shark sample data and proven useful in this study to visualize uncertainty and explore posterior distributions, the frequentist LDL approach likely produced the most biologically plausible parameter estimates for both sexes.

## 5. Conclusion

This study presents the first reported attempt to estimate growth parameters for *I. paucus* in the Equatorial Atlantic Ocean, contributing with valuable data to the current scientific understanding of this elusive species. Through the application of the LDL back-calculation method, alongside both frequentist and Bayesian modeling approaches, this research offers novel insights into this species life history traits. These findings provide support in making decisions and assessing stocks, based on scientific information, contributing to a more efficient management of longfin mako sharks. Nonetheless, knowledge gaps remain present, opening a door of possibilities to future research, with a strong emphasis on the need for age validation and length-at-age studies in other oceanic regions, especially including data on larger individuals. Addressing these gaps is the key

to improving the accuracy of future demographic models, strengthening conservation efforts for this poorly understood shark species.

## 6. References


Adams, D. H., Borucinska, J. D., Maillett, K., Whitburn, K., & Sander, T. E. (2014). Mortality due to a retained circle hook in a longfin mako shark *Isurus paucus* (Guitart-Manday). Journal of Fish Diseases, 38(7), 621–628. https://doi.org/10.1111/jfd.12277

Akaike, H. (1973). Information Theory and an Extension of the Maximum Likelihood Principle. In B. N. Petrov & F. Csáki (Eds.), Proceedings of the Second International Symposium on Information Theory, Tsahkadsor, Armenia, USSR, September 2-8, 1971 (pp. 267–281). Akademiai Kiadó, Budapest, Hungary.

Anderson, O., Small, C., Croxall, J., Dunn, E., Sullivan, B., Yates, O., & Black, A. (2011). Global seabird bycatch in longline fisheries. Endangered Species Research, 14(2), 91–106. https://doi.org/10.3354/esr00347

Andrade, I., Rosa, D., Muñoz-Lechuga, R., & Coelho, R. (2019). Age and growth of the blue shark (*Prionace glauca*) in the Indian Ocean. Fisheries Research, 211, 238–246. https://doi.org/10.1016/j.fishres.2018.11.019

Anscombe, F. J. (1973). Graphs in Statistical Analysis. The American Statistician, 27(1), 17. https://doi.org/10.2307/2682899

Ardizzone, D., Cailliet, G. M., Natanson, L. J., Andrews, A. H., Kerr, L. A., & Brown, T. A. (2006). Application of bomb radiocarbon chronologies to shortfin mako (*Isurus oxyrinchus*) age validation. *Special Issue: Age and Growth of Chondrichthyan Fishes: New Methods, Techniques and Analysis*, 355-366. https://doi.org/10.1007/978-1-4020-5570-6_15

Arif, S., & MacNeil, M. A. (2022). Predictive models aren't for causal inference. Ecology Letters, 25(8), 1741–1745. https://doi.org/10.1111/ele.14033

Barreto, R. R., De Farias, W. K. T., Andrade, H., Santana, F. M., & Lessa, R. (2016). Age, Growth and Spatial Distribution of the Life Stages of the Shortfin Mako, *Isurus oxyrinchus* (Rafinesque, 1810) Caught in the Western and Central Atlantic. *PLoS ONE*, *11*(4), e0153062. https://doi.org/10.1371/journal.pone.0153062

Barreto, R. R., Lessa, R. P., Hazin, F. H., & Santana, F. M. (2011). Age and growth of the blacknose shark, *Carcharhinus acronotus* (Poey, 1860) off the northeastern Brazilian Coast. Fisheries Research, 110(1), 170–176. https://doi.org/10.1016/j.fishres.2011.04.003

Bayes, T. (1763). An essay towards solving a problem in the doctrine of chances (R. Price, Ed.). Philosophical Transactions of the Royal Society of London, **53**, 370–418. https://doi.org/10.1098/rstl.1763.0053

Beamish, R. J., & Fournier, D. A. (1981). A method for comparing the precision of a set of age determinations. *Canadian Journal of Fisheries and Aquatic Sciences*, *38*(8), 982-983. https://doi.org/10.1139/f81-132

Bowman, R. E. (2000). Food of northwest Atlantic fishes and two common species of squid. NOAA Technical Memorandum NMFS-NE ; 155.

Breusch, T. S., & Pagan, A. R. (1979). A Simple Test for Heteroscedasticity and Random Coefficient Variation. Econometrica, 47(5), 1287. https://doi.org/10.2307/1911963

Brody, S. (1945). Bioenergetics and growth, with special reference to the efficiency complex in domestic animals. Reinhold Publishing Corporation.

Bustamante, C., Concha, F., Balbontín, F., & Lamilla, J. (2009). Southernmost record of Isurus paucus Gitart Manday, 1966 (Elasmobranchii: Lamnidae) in the southeast Pacific Ocean. Revista de Biología Marina y Oceanografía, 44(2). https://doi.org/10.4067/S0718-19572009000200025

Cailliet, G., Martin, L. K., Harvey, J., Kusher, D., & Welden, B. A. (1983). Preliminary studies on the age and growth of blue, *Prionace glauca*, common thresher, *Alopias vulpinus*, and shortfin mako, *Isurus oxyrinchus*, sharks from California waters. NOAA Tech. Rep. NMFS, 8, 179–188.

Cailliet, G. M., Smith, W. D., Mollet, H. F., & Goldman, K. J. (2006). Age and growth studies of chondrichthyan fishes: the need for consistency in terminology, verification, validation, and growth function fitting. Environmental Biology of Fishes, 77(3–4), 211–228. https://doi.org/10.1007/s10641-006-9105-5

Campana, S. E. (1990). How Reliable are Growth Back-Calculations Based on Otoliths? Canadian Journal of Fisheries and Aquatic Sciences, 47(11), 2219–2227. https://doi.org/10.1139/f90-246

Campana, S. E. (2005). Accuracy, precision and quality control in age determination, including a review of the use and abuse of age validation methods. Journal of Fish Biology, 59(2), 197–242. https://doi.org/10.1111/j.1095-8649.2001.tb00127.x

Campana, S. E., Natanson, L. J., & Myklevoll, S. (2002). Bomb dating and age determination of large pelagic sharks. *Canadian Journal of Fisheries and Aquatic Sciences*, *59*(3), 450-455. https://doi.org/10.1139/f02-027

Cardeñosa, D., Shea, S. K., Zhang, H., Fischer, G. A., Simpfendorfer, C. A., & Chapman, D. D. (2022). Two thirds of species in a global shark fin trade hub are threatened with extinction: Conservation potential of international trade regulations for coastal sharks. Conservation Letters, 15(5). https://doi.org/10.1111/conl.12910

Carlander, K. D. (1969). Life History Data on Freshwater Fishes of the United States and Canada, Exclusive of the Perciformes. In Handbook of Freshwater Fishery Biology (Vol. 1).

Carlson, J. K., Middlemiss, A. M., & Neer, J. A. (2007). A revised age and growth model for blacknose shark, *Carcharhinus acronotus*, from the eastern Gulf of Mexico using X-radiography. *Gulf of Mexico Science*, 25(1), 82–87. https://doi.org/10.18785/goms.2501.06

Carrier, J. C., Simpfendorfer, C. A., Heithaus, M. R., & Yopak, K. E. (2022). Biology of Sharks and Their Relatives. CRC Press. https://doi.org/10.1201/9781003262190

Carrillo-Colín, L. D., Márquez-Farías, J. F., & Zamora-García, O. G. (2024). Bayesian estimation of the age and growth of the pelagic thresher shark (*Alopias pelagicus*) from the Mexican Pacific. Environmental Biology of Fishes, 107(9), 927–943. https://doi.org/10.1007/s10641-024-01592-5

Castro, J. I. (2011). The Sharks of North America. Oxford University Press, USA.

Castro, J. I., Woodley, C. M., & Brudek, R. L. (1999). A preliminary evaluation of the status of shark species (Issue 380). https://agris.fao.org/search/en/records/65ddd31f0f3e94b9e5c5481d

Cerna, F., & Licandeo, R. (2009). Age and growth of the shortfin mako (*Isurus oxyrinchus*) in the south-eastern Pacific off Chile. *Marine and Freshwater Research*, *60*(5), 394. https://doi.org/10.1071/mf08125

Chang, C.-H., Shao, K.-T., Lin, Y.-S., Tsai, A.-Y., Su, P.-X., & Ho, H.-C. (2013). The complete mitochondrial genome of the shortfin mako, *Isurus oxyrinchus* (Chondrichthyes, Lamnidae). Mitochondrial DNA, 26(3), 475–476. https://doi.org/10.3109/19401736.2013.834430

Chin, A., Simpfendorfer, C., Tobin, A., & Heupel, M. (2013). Validated age, growth and reproductive biology of *Carcharhinus melanopterus*, a widely distributed and exploited reef shark. *Marine and Freshwater Research*, *64*(10), 965. https://doi.org/10.1071/mf13017

CITES, (2019). *Eighteenth meeting of the Conference of the Parties (CoP18), Geneva (Switzerland), 17–28 August 2019*. Convention on International Trade in Endangered Species of Wild Fauna and Flora. https://cites.org/eng/cop/18

Coelho, R., Fernandez-Carvalho, J., Amorim, S., & Santos, M. N. (2011). Age and growth of the smooth hammerhead shark, *Sphyrna zygaena* , in the Eastern Equatorial Atlantic Ocean, using vertebral sections. Aquatic Living Resources, 24(4), 351–357. https://doi.org/10.1051/alr/2011145

Compagno, L. J. V. (2001). Sharks of the world. An annotated and illustrated catalogue of shark species known to date. Volume 2. Bullhead, mackerel and carpet sharks (Heterodontiformes, Lamniformes and Orectolobiformes). FAO Species Catalogue for Fishery Purposes, 2, 109–117.

Compagno, L. J. V. (2008). Pelagic Elasmobranch Diversity. In Sharks of the Open Ocean (pp. 14–23). Wiley. https://doi.org/10.1002/9781444302516.ch2

Cortés, E. (1999). Standardized diet compositions and trophic levels of sharks. ICES Journal of Marine Science, 56(5), 707–717. https://doi.org/10.1006/jmsc.1999.0489

Cortés, E. (2008). Life History Patterns and Correlations in Sharks. Reviews in Fisheries Science, 8(4), 299–344. https://doi.org/10.1080/10408340308951115

Cortés, E., Domingo, A., Miller, P., Forselledo, R., Mas, F., Arocha, F., Campana, S., Coelho, R., da Silva, C., Hazin, F., Holtzhausen, H., Keene, K., Lucena Frédou, F.,

Ramirez, K., Santos, M. N., Semba, Y., Yokawa, K., Medeiros, M., Irmãos, N.-Dois, & Brasil. (2015). Expanded ecological risk assessment of pelagic sharks caught in Atlantic pelagic longline fisheries. *Collective Volume of Scientific Papers (ICCAT)*, 71, 2637–2688.

D'Alberto, B. M., Chin, A., Smart, J. J., Baje, L., White, W. T., & Simpfendorfer, C. A. (2016). Age, growth and maturity of oceanic whitetip shark (*Carcharhinus longimanus*) from Papua New Guinea. Marine and Freshwater Research, 68(6), 1118. https://doi.org/10.1071/MF16165

Dedman, S., Moxley, J. H., Papastamatiou, Y. P., Braccini, M., Caselle, J. E., Chapman, D. D., Cinner, J. E., Dillon, E. M., Dulvy, N. K., Dunn, R. E., Espinoza, M., Harborne, A. R., Harvey, E. S., Heupel, M. R., Huveneers, C., Graham, N. A. J., Ketchum, J. T., Klinard, N. V., Kock, A. A., … Heithaus, M. R. (2024). Ecological roles and importance of sharks in the Anthropocene Ocean. Science, 385(6708). https://doi.org/10.1126/science.adl2362

Dodrill, J. W., & Gilmore, R. G. (1979). First North American continental record of the longfin mako (*Isurus paucus* Guitart Manday). Florida Scientist, 52–58.

Doll, J. C., & Jacquemin, S. J. (2019). Bayesian model selection in fisheries management and ecology. *Journal of Fish and Wildlife Management*, *10*(2), 691-707. https://doi.org/10.3996/042019-JFWM-024

Elzhov, T. V, Mullen, K. M., Spiess, A., & Bolker, B. (2023). minpack.lm: R Interface to the Levenberg-Marquardt Nonlinear Least-Squares Algorithm Found in MINPACK, Plus Support for Bounds. https://CRAN.R-project.org/package=minpack.lm

Emmons, S. M., D'Alberto, B. M., Smart, J. J., & Simpfendorfer, C. A. (2021). Age and growth of tiger shark (*Galeocerdo cuvier*) from Western Australia. Marine and Freshwater Research. https://doi.org/10.1071/MF20291

Estupiñán-Montaño, C., Delgado-Huertas, A. Longfin Mako Shark, *Isurus paucus*, in the Eastern Tropical Pacific: First Evidence of Trophic Ontogeny Based on the Isotopic Analysis of Long-term Tissues. *Thalassas* **38**, 49–55 (2022). https://doi.org/10.1007/s41208-022-00404-w

Fabens, A. J. (1965). Properties and fitting of the Von Bertalanffy growth curve. Growth, 29 3, 265–289. https://api.semanticscholar.org/CorpusID:5110718

Fernandez-Carvalho, J., Coelho, R., Erzini, K., & Santos, M. N. (2011). Age and growth of the bigeye thresher shark, *Alopias superciliosus*, from the pelagic longline fisheries in the tropical northeastern Atlantic Ocean, determined by vertebral band counts. *Aquatic Living Resources*, *24*(4), 359–368. https://doi.org/10.1051/alr/2011046

Francis, R. I. C. C. (1990). Back-calculation of fish length: a critical review. Journal of Fish Biology, 36(6), 883–902. https://doi.org/10.1111/j.1095-8649.1990.tb05636.x

Froese, R., & D. Pauly. (2025). FishBase. *Isurus paucus* Guitart, 1966.

Gallagher, A. J., Orbesen, E. S., Hammerschlag, N., & Serafy, J. E. (2014). Vulnerability of oceanic sharks as pelagic longline bycatch. Global Ecology and Conservation, 1, 50–59. https://doi.org/10.1016/j.gecco.2014.06.003

Garrick, J. A. F. (1967). Revision of Sharks of Genus Isurus with Description of a New Species (Galeoidea, Lamnidae). Proceedings of the United States National Museum, 118(3537), 663–690. https://doi.org/10.5479/si.00963801.118-3537.663

Gayford, J. H. (2023). The evolution of sexual dimorphism in Chondrichthyes: drivers, uncertainties, and future directions. *Environmental Biology of Fishes*, *106*(6), 1463–1475. https://doi.org/10.1007/s10641-023-01425-x

Gelman, A., & Rubin, D. B. (1992). Inference from iterative simulation using multiple sequences. *Statistical Science, 7*(4), 457–472. https://doi.org/10.1214/ss/1177011136

Gelman, A., Hwang, J., & Vehtari, A. (2013). Understanding predictive information criteria for Bayesian models. Statistics and Computing, 24(6), 997–1016. https://doi.org/10.1007/s11222-013-9416-2

Gervelis, B. J., & Natanson, L. J. (2013). Age and Growth of the Common Thresher Shark in the Western North Atlantic Ocean. Transactions of the American Fisheries Society, 142(6), 1535–1545. https://doi.org/10.1080/00028487.2013.815658

Gilman, E., Clarke, S., Brothers, N., Alfaro-Shigueto, J., Mandelman, J., Mangel, J., Petersen, S., Piovano, S., Thomson, N., Dalzell, P., Donoso, M., Goren, M., & Werner, T. (2008). Shark interactions in pelagic longline fisheries. Marine Policy, 32(1), 1–18. https://doi.org/10.1016/j.marpol.2007.05.001

Gilmore, R. G. (1983). Observations on the Embryos of the Longfin Mako, *Isurus paucus*, and the Bigeye Thresher, *Alopias superciliosus*. Copeia, 1983(2), 375. https://doi.org/10.2307/1444380

Gompertz, B. (1825). On the nature of the function expressive of the law of human mortality, and on a new mode of determining the value of life contingencies. Philosophical Transactions of the Royal Society of London, **115**, 513–583. https://doi.org/10.1098/rstl.1825.0026

Goldman, K. (2005). Age and growth of elasmobranch fishes. FAO Fisheries Technical Paper, 474.

Goldman, K. J., Branstetter, S., & Musick, J. A. (2006). A re-examination of the age and growth of sand tiger sharks, *Carcharias taurus*, in the western North Atlantic: the importance of ageing protocols and use of multiple back-calculation techniques (pp. 241–252). https://doi.org/10.1007/978-1-4020-5570-6_4

Goldman, K., & Cailliet, G. (2004). Age Determination and Validation in Chondrichthyan Fishes (pp. 399–447). https://doi.org/10.1201/9780203491317.pt3

Goldman, K. J., & Musick, J. A. (2006). Growth and maturity of salmon sharks (*Lamna ditropis*) in the eastern and western North Pacific, and comments on back-calculation methods. *Fishery Bulletin*, *104*(2), 278.

Gong, Y., Huang, X., Li, Z., Shen, Y., Li, Y., Zhu, J., & Wu, F. (2023). Plastic ingestion and trophic transfer in an endangered top predator, the longfin mako shark (*Isurus paucus*), from the tropical western Pacific Ocean. Environmental Science and Pollution Research, 30(49), 107365–107370. https://doi.org/10.1007/s11356-023-25532-5

Grant, M. I., Smart, J. J., White, W. T., Chin, A., Baje, L., & Simpfendorfer, C. A. (2018). Life history characteristics of the silky shark *Carcharhinus falciformis* from the central west Pacific. Marine and Freshwater Research, 69(4), 562. https://doi.org/10.1071/MF17163

Guitart Manday, D. J. (1966). Nuevo nombre para una especie de tiburón del género Isurus: (Elasmobranchii: Isuridae) de aguas cubanas. Poeyana, Series A, Instituto de Biología. No. 15: 1-9.

Hairston, N. G., Smith, F. E., & Slobodkin, L. B. (1960). Community Structure, Population Control, and Competition. The American Naturalist, 94(879), 421–425. https://doi.org/10.1086/282146

Harry, A. V., Macbeth, W. G., Gutteridge, A. N., & Simpfendorfer, C. A. (2011). The life histories of endangered hammerhead sharks (Carcharhiniformes, Sphyrnidae) from the east coast of Australia. Journal of Fish Biology, 78(7), 2026–2051. https://doi.org/10.1111/j.1095-8649.2011.02992.x

Hastings, W. K. (1970). *Monte Carlo sampling methods using Markov chains and their applications*. Biometrika, 57(1), 97–109. https://doi.org/10.1093/biomet/57.1.97

Hemida, F., & Capapé, C. (2008). On the occurrence of the longfin mako, *Isurus paucus* (Chondrichthyes: Isuridae) off the Algerian coast (southwestern Mediterranean). Acta Adriatica, 49, 185–189.

Hernandez-Llamas, A., & Ratkowsky, D. (2004). Growth of fishes, crustaceans and molluscs: -estimation of the von Bertalanffy, Logistic, Gompertz and Richards curves and a new growth model. Marine Ecology Progress Series, 282, 237–244. https://doi.org/10.3354/meps282237

Heupel, M., Knip, D., Simpfendorfer, C., & Dulvy, N. (2014). Sizing up the ecological role of sharks as predators. Marine Ecology Progress Series, 495, 291–298. https://doi.org/10.3354/meps10597

Hsu, H. H., Joung, S. J., Hueter, R. E., & Liu, K. M. (2014). Age and growth of the whale shark (*Rhincodon typus*) in the north-western Pacific. Marine and Freshwater Research, 65(12), 1145. https://doi.org/10.1071/MF13330

Hueter, R. E., Manire, C. A., Tyminski, J. P., Hoenig, J. M., & Hepworth, D. A. (2006). Assessing Mortality of Released or Discarded Fish Using a Logistic Model of Relative Survival Derived from Tagging Data. Transactions of the American Fisheries Society, 135(2), 500–508. https://doi.org/10.1577/T05-065.1

ICCAT (2021). Rec. 21-09, Recommendation by ICCAT on the conservation of the North Atlantic stock of shortfin mako caught in association with ICCAT fisheries.

Jensen, A. L. (1997). Origin of relation between K and Linf and synthesis of relations among life history parameters. *Canadian Journal of Fisheries and Aquatic Sciences*, *54*(5), 987–989. https://doi.org/10.1139/f97-007

Kai, M. (2021). Are the current IUCN category and CITES listing appropriate for the conservation and management of shortfin mako, *Isurus oxyrinchus*, in the North Pacific Ocean? Marine Policy, 134, 104790. https://doi.org/10.1016/j.marpol.2021.104790

Katsanevakis, S. (2006). Modelling fish growth: Model selection, multi-model inference and model selection uncertainty. *Fisheries Research*, *81*(2–3), 229–235. https://doi.org/10.1016/j.fishres.2006.07.002

Kendall, M. G. (1938). A NEW MEASURE OF RANK CORRELATION. Biometrika, 30(1–2), 81–93. https://doi.org/10.1093/biomet/30.1-2.81

Kinney, M. J., Wells, R. J. D., and Kohin, S. (2016). Oxytetracycline age validation of an adult shortfin mako shark *Isurus oxyrinchus* after 6 years at liberty. Journal of Fish Biology 89, 1828–1833. https://doi.org/10.1111/JFB.13044

Lee, R. M. (1920). *A review of the methods of age and growth determination in fishes by means of scales*. HM Stationery Office.

Levene, H. (1960). Robust Tests for Equality of Variances. In I. Olkin (Ed.), Contributions to Probability and Statistics: Essays in Honor of Harold Hotelling (pp. 278–292). Stanford University Press.

Lopez, S., Meléndez, R., & Barría, P. (2010). Preliminary diet analysis of the blue shark *Prionace glauca* in the eastern South Pacific. Revista de Biología Marina y Oceanografía, 45, 745–749. https://doi.org/10.4067/S0718-19572010000400017

Mandelman, J. W., Cooper, P. W., Werner, T. B., & Lagueux, K. M. (2008). Shark bycatch and depredation in the U.S. Atlantic pelagic longline fishery. Reviews in Fish Biology and Fisheries, 18(4), 427–442. https://doi.org/10.1007/s11160-008-9084-z

Mann, H. B., & Whitney, D. R. (1947). On a Test of Whether one of Two Random Variables is Stochastically Larger than the Other. The Annals of Mathematical Statistics, 18(1), 50–60. https://doi.org/10.1214/aoms/1177730491

Markov, A. A. (1906). Extension of the limit theorems of probability theory to a sum of variables connected in a chain. *Reprinted in Appendix B of "An Introduction to Probability Theory and Its Applications," Vol. 1 by William Feller.*

Martin, S. L., Stohs, S. M., & Moore, J. E. (2015). Bayesian inference and assessment for rare-event bycatch in marine fisheries: a drift gillnet fishery case study. Ecological Applications, 25(2), 416-429. https://doi.org/10.1890/14-0059.1

Mas, F., Forselledo, R., & Domingo, A. (2014). Length-length relationships for six pelagic shark species commonly caught in the southwestern Atlantic Ocean. *Collect. Vol. Sci. Pap. ICCAT*, *70*(5), 2441-2445.

MAS F., DOMINGO A.,FORSELLEDO R. & MILLER P. 2022. CHAPTER 2.2.1.11:LONGFIN MAKO SHARK. In: ICCAT. 2006-2016. ICCAT Manual. ISBN (Electronic ed.): 978-92-990055-0-7.

McNemar, Q. (1947). Note on the Sampling Error of the Difference Between Correlated Proportions or Percentages. Psychometrika, 12(2), 153–157. https://doi.org/10.1007/BF02295996

Montero-Quintana, A. N., Ocampo-Valdez, C. F., Vázquez-Haikin, J. A., Sosa-Nishizaki, O., & Osorio-Beristain, M. (2021). Whale shark (*Rhincodon typus*) predatory flexible feeding behaviors on schooling fish. Journal of Ethology, 39(3), 399–410. https://doi.org/10.1007/s10164-021-00717-y

Mucientes, G., Bañón, R., & Queiroz, N. (2013). Updated distribution range of longfin mako *Isurus paucus* (Lamniformes: Lamnidae) in the North Atlantic. Journal of Applied Ichthyology, 29(5), 1163–1165. https://doi.org/10.1111/jai.12203

Natanson, L. J., Adams, D. H., Winton, M. V., & Maurer, J. R. (2014). Age and growth of the bull shark in the western North Atlantic Ocean. *Transactions of the American Fisheries Society, 143*(3), 732–743. https://doi.org/10.1080/00028487.2014.892537

Natanson, L. J., Kohler, N. E., Ardizzone, D., Cailliet, G. M., Wintner, S. P., & Mollet, H. F. (2006). Validated age and growth estimates for the shortfin mako, *Isurus oxyrinchus*, in the North Atlantic Ocean. *Special Issue: Age and Growth of Chondrichthyan Fishes: New Methods, Techniques and Analysis*, 367-383. https://doi.org/10.1007/978-1-4020-5570-6_16

Natanson, L. J., Mello, J. J., & Campana, S. E. (2002). Validated age and growth of the porbeagle shark (*Lamna nasus*) in the western North Atlantic Ocean. *FISHERY BULLETIN-NATIONAL OCEANIC AND ATMOSPHERIC ADMINISTRATION*, *100*(2), 266-278.

Natanson, L. J., Skomal, G. B., Hoffmann, S. L., Porter, M. E., Goldman, K. J., & Serra, D. (2018). Age and growth of sharks: do vertebral band pairs record age?. *Marine and Freshwater Research*, *69*(9), 1440-1452. https://doi.org/10.1071/MF17279

National Oceanic, & Atmospheric Administration, N. C. for E. I. (2025). Fishing gear: Pelagic longlines.

Navia, A. F., Cortés, E., & Mejía-Falla, P. A. (2010). Topological analysis of the ecological importance of elasmobranch fishes: A food web study on the Gulf of Tortugas, Colombia. Ecological Modelling, 221(24), 2918–2926. https://doi.org/10.1016/j.ecolmodel.2010.09.006

Nelson, J. S., Grande, T. C., & Wilson, M. V. H. (2016). Fishes of the World. Wiley. https://doi.org/10.1002/9781119174844

Ogle, D. H. (2023). RFishBC: Back-Calculation of Fish Length.

Ogle, D. H., Doll, J. C., Wheeler, A. P., & Dinno, A. (2025). FSA: Simple Fisheries Stock Assessment Methods.

Oktaviyani, S., Kurniawan, W., & Fahmi, F. (2022). Estimating shark body sizes from fins as the future monitoring strategy for shark fin trade in Indonesia. Indian Journal of Fisheries, 69(2). https://doi.org/10.21077/ijf.2022.69.2.114601-08

Pan, B., Zhu, J., Lin, Q., Geng, Z., Wu, F., & Zhang, Y. (2024). Study on the catch, bycatch and discard of Chinese pelagic longline fisheries in the Atlantic Ocean. Aquaculture and Fisheries, 9(2), 280–286. https://doi.org/10.1016/j.aaf.2022.03.002

Pratt HL, Casey JG (1983) Age and growth of the shortfin mako *Isurus oxyrinchus*, using four methods. Can J Fish Aquat Sci 40:1944–1957

Queiroz, N., Humphries, N. E., Mucientes, G., Hammerschlag, N., Lima, F. P., Scales, K. L., Miller, P. I., Sousa, L. L., Seabra, R., & Sims, D. W. (2016). Ocean-wide tracking of pelagic sharks reveals extent of overlap with longline fishing hotspots. Proceedings of the

National Academy of Sciences, 113(6), 1582–1587. https://doi.org/10.1073/pnas.1510090113

R Core Team. (2024). R: A Language and Environment for Statistical Computing. https://www.R-project.org/

Raoult, V., Peddemors, V. M., Zahra, D., Howell, N., Howard, D. L., de Jonge, M. D., & Williamson, J. E. (2016). Strontium mineralization of shark vertebrae. Scientific Reports, 6(1), 29698. https://doi.org/10.1038/srep29698

Régnier, T., Dodd, J., Benjamins, S., Gibb, F. M., & Wright, P. J. (2021). Age and growth of the Critically Endangered flapper skate, *Dipturus intermedius*. Aquatic Conservation: Marine and Freshwater Ecosystems, 31(9), 2381–2388. https://doi.org/10.1002/aqc.3654

Richards, F. J. (1959). A Flexible Growth Function for Empirical Use. Journal of Experimental Botany, 10(2), 290–301. https://doi.org/10.1093/jxb/10.2.290

Ricker, W. E. (1975). Computation and Interpretation of Biological Statistics of Fish Populations (Vol. 191). Fishery Research Board of Canada.

Ridewood, W. G. (1921). On the Calcification of the Vertebral Centra in Sharks and Rays. Philosophical Transactions of the Royal Society. Series B-Biology, 210, 311–407.

Rigby, C. L., Barreto, R., Carlson, J., Fernando, D., Fordham, S., Francis, M. P., Jabado, R. W., Liu, K. M., Marshall, A., Pacoureau, N., Romanov, E., Sherley, R. B., & Winker, H. (2018). *Isurus paucus*. In IUCN Red List of Threatened Species. https://doi.org/10.2305/IUCN.UK.2019-1.RLTS.T60225A3095898.en

Rodríguez-García, C., Gonçalves Neto, J. B., García-Romero, C., Domínguez-Bustos, Á. R., & Cabrera-Castro, R. (2024). Feeding habits of two shark species: velvet belly, *Etmopterus spinax* (Linnaeus, 1758) and blackmouth catshark, *Galeus melastomus* (Rafinesque, 1810), present in fishing discards in the Gulf of Cádiz. Environmental Biology of Fishes, 107(2), 159–172. https://doi.org/10.1007/s10641-024-01519-0

Roff, G., Doropoulos, C., Rogers, A., Bozec, Y.-M., Krueck, N. C., Aurellado, E., Priest, M., Birrell, C., & Mumby, P. J. (2016). The Ecological Role of Sharks on Coral Reefs. Trends in Ecology & Evolution, 31(5), 395–407. https://doi.org/10.1016/j.tree.2016.02.014

Rosa, D., Coelho, R., Fernandez-Carvalho, J., & Santos, M. N. (2017). Age and growth of the smooth hammerhead, *Sphyrna zygaena* , in the Atlantic Ocean: comparison with other hammerhead species. Marine Biology Research, 13(3), 300–313. https://doi.org/10.1080/17451000.2016.1267366

Rosa, D., Gago, M., Fernandez-Carvalho, J., & Coelho, R. (2021). Life history parameters of the crocodile shark, *Pseudocarcharias kamoharai* , in the tropical Atlantic Ocean. Journal of the Marine Biological Association of the United Kingdom, 101(4), 753–763. https://doi.org/10.1017/S0025315421000588

Ruiz-Abierno, A., Márquez-Farías, J. F., Rojas-Corzo, A., Miller, V., Angulo-Valdés, J. A., & Hueter, R. E. (2021b). Seasonal Abundance and Size Structure of Sharks Taken in the Pelagic Longline Fishery off Northwestern Cuba. Marine and Coastal Fisheries, 13(3), 275–291. https://doi.org/10.1002/mcf2.10152

Ruiz-Abierno, A., Márquez-Farías, J., Trápaga-Roig, M., & Hueter, R. (2021a). Length at maturity of two pelagic sharks ( *Isurus paucus* and *Carcharhinus longimanus* ) found off northern Cuba. Bulletin of Marine Science, 97(1), 77–88. https://doi.org/10.5343/bms.2020.0033

Saigal, M., Shueh Yi, H. N., Rameez, N. A., van Manen, S., Van Anh, B. T., Arora, V. P., Han, K. D. M., Lee, J. Q. T., Syaddad, A., Tan, C. K., Lim, E. X. Y., & Wainwright, B. J. (2024). Beneath the surface: DNA barcoding of shark fins in Singapore. Royal Society Open Science, 11(9). https://doi.org/10.1098/rsos.240532

Sales, G., Giffoni, B. B., Fiedler, F. N., Azevedo, V. G., Kotas, J. E., Swimmer, Y., & Bugoni, L. (2010). Circle hook effectiveness for the mitigation of sea turtle bycatch and capture of target species in a Brazilian pelagic longline fishery. Aquatic Conservation: Marine and Freshwater Ecosystems, 20(4), 428–436. https://doi.org/10.1002/aqc.1106

Santos, C. C., Rosa, D., Gonçalves, J. M. S., & Coelho, R. (2023). A review of reported effects of pelagic longline fishing gear configurations on target, bycatch and vulnerable species. Aquatic Conservation: Marine and Freshwater Ecosystems, 34(1). https://doi.org/10.1002/aqc.4027

Santos, C. C., Santos, M. N., Rosa, D., & Coelho, R. (2024). Leader material and bait effects on target and bycatch species caught in an Atlantic Ocean pelagic longline fishery. Fisheries Research, 278, 107093. https://doi.org/10.1016/j.fishres.2024.107093

Schneider, C. A., Rasband, W. S., & Eliceiri, K. W. (2012). NIH Image to ImageJ: 25 years of image analysis. Nature Methods, 9(7), 671–675. https://doi.org/10.1038/nmeth.2089

Schwarz, G. (1978). Estimating the Dimension of a Model. The Annals of Statistics, 6(2). https://doi.org/10.1214/aos/1176344136

Sellheim, N. (2020). The CITES appendix II-Listing of mako sharks — Revisiting counter arguments. Marine Policy, 115, 103887. https://doi.org/10.1016/j.marpol.2020.103887

Semba, Y., Nakano, H., & Aoki, I. (2009). Age and growth analysis of the shortfin mako, *Isurus oxyrinchus*, in the western and central North Pacific Ocean. *Environmental Biology of Fishes*, *84*, 377-391. https://doi.org/10.1007/s10641-009-9447-x

Shapiro, S. S., & Wilk, M. B. (1965). An analysis of variance test for normality (complete samples). Biometrika, 52(3–4), 591–611. https://doi.org/10.1093/biomet/52.3-4.591

Siegfried, K. I., & Sansó, B. (2006). Two Bayesian methods for estimating parameters of the von Bertalanffy growth equation. Environmental Biology of Fishes, 77(3–4), 301–308. https://doi.org/10.1007/s10641-006-9112-6

Smart, J. (2023). *BayesGrowth: Estimate Fish Growth using MCMC Analysis* (Version 1.0.0) [Computer software]. https://github.com/jonathansmart/BayesGrowthcran.r-project.org

Smart, J. J., & Grammer, G. L. (2021). Modernising fish and shark growth curves with Bayesian length-at-age models. PLOS ONE, 16(2), e0246734. https://doi.org/10.1371/journal.pone.0246734

Smart, J. J., Harry, A. V., Tobin, A. J., & Simpfendorfer, C. A. (2012). Overcoming the constraints of low sample sizes to produce age and growth data for rare or threatened sharks. *Aquatic Conservation Marine and Freshwater Ecosystems*, *23*(1), 124–134. https://doi.org/10.1002/aqc.2274

Thorson, J. T., & Simpfendorfer, C. A. (2009). Gear selectivity and sample size effects on growth curve selection in shark age and growth studies. Fisheries Research, 98(1–3), 75–84. https://doi.org/10.1016/j.fishres.2009.03.016

Varghese, S. P., Unnikrishnan, N., Gulati, D. K., & Ayoob, A. E. (2017). Size, sex and reproductive biology of seven pelagic sharks in the eastern Arabian Sea. Journal of the Marine Biological Association of the United Kingdom, 97(1), 181–196. https://doi.org/10.1017/S0025315416000217

Vehtari, A., Gelman, A., & Gabry, J. (2017). Practical Bayesian model evaluation using leave-one-out cross-validation and WAIC. *Statistics and Computing*, 27(5), 1413–1432. https://doi.org/10.1007/s11222-016-9696-4

Verhulst, P. F. (1838). Notice sur la loi que la population suit dans son accroissement. Correspondance Mathématique et Physique, 10, 113–121.

Vetter, R., Kohin, S., Preti, A., Mcclatchie, S. A. M., & Dewar, H. (2008). Predatory interactions and niche overlap between mako shark, *Isurus oxyrinchus*, and jumbo squid, *Dosidicus gigas*, in the California Current. *Reports/California Cooperative Oceanic Fisheries Investigations*, *49*, 142-156.

Vigliola, L., & Meekan, M. G. (2009). The Back-Calculation of Fish Growth From Otoliths (pp. 174–211). https://doi.org/10.1007/978-1-4020-5775-5_6

Von Bertalanffy, L. (1938). A Quantitative Theory of Organic Growth (Inquiries on Growth Laws II). Human Biology, 10(2), 181–213.

Wakida-Kusunoki, A. T., & de Anda-Fuente, D. (2012). Presence of longfin mako shark *Isurus paucus* (Chondrichthyes: Lamnidae) in the south-eastern Gulf of Mexico, Tabasco, Mexico. Marine Biodiversity Records, 5, e92. https://doi.org/10.1017/S1755267212000723

Ward, P., Epe, S., Kreutz, D., Lawrence, E., Robins, C., & Sands, A. (2009). The effects of circle hooks on bycatch and target catches in Australia's pelagic longline fishery. Fisheries Research, 97(3), 253–262. https://doi.org/10.1016/j.fishres.2009.02.009

Ward-Paige, C. A. (2017). A global overview of shark sanctuary regulations and their impact on shark fisheries. Marine Policy, 82, 87–97. https://doi.org/10.1016/j.marpol.2017.05.004

Wells, R. J. D., Smith, S. E., Kohin, S., Freund, E., Spear, N. & Ramon, D. A. (2013). Age validation of juvenile Shortfin Mako (*Isurus oxyrinchus*) tagged and marked with

oxytetracycline off southern California. Fishery Bulletin 111, 147–160. https://doi.org/10.7755/FB.111.2.3

Whitenack, L. B., & Gottfried, M. D. (2010). A morphometric approach for addressing tooth-based species delimitation in fossil mako sharks, Isurus (Elasmobranchii: Lamniformes). Journal of Vertebrate Paleontology, 30(1), 17–25. https://doi.org/10.1080/02724630903409055

Wickham, H. (2016). ggplot2. Springer International Publishing. https://doi.org/10.1007/978-3-319-24277-4

Wilk, M. B., & Gnanadesikan, R. (1968). Probability plotting methods for the analysis for the analysis of data. Biometrika, 55(1), 1–17. https://doi.org/10.1093/biomet/55.1.1

Wilks, S. S. (1938). The Large-Sample Distribution of the Likelihood Ratio for Testing Composite Hypotheses. The Annals of Mathematical Statistics, 9(1), 60–62.

Zenetos, A., Gofas, S., Verlaque, M., Cinar, M. E., Garcia Raso, J. E., Bianchi, C. N., Morri, C., Azzurro, E., Bilecenoglu, M., Froglia, C., Siokou, I., Violanti, D., Sfriso, A., San Martin, G., Giangrande, A., Katagan, T., Ballesteros, E., Ramos-Espla, A. A., Mastrototaro, F., Streftaris, N. (2011). Errata to the Review Article (Medit. Mar. Sci. 11/2, 2010, 381-493): “Alien species in the Mediterranean Sea by 2010. A contribution to the application of European Union’s Marine Strategy Framework Directive (MSFD). Part I. Spatial distribution.” Mediterranean Marine Science, 12(2), 509. https://doi.org/10.12681/mms.49

## Appendix A

## Length-Length Regression Residual Diagnostics

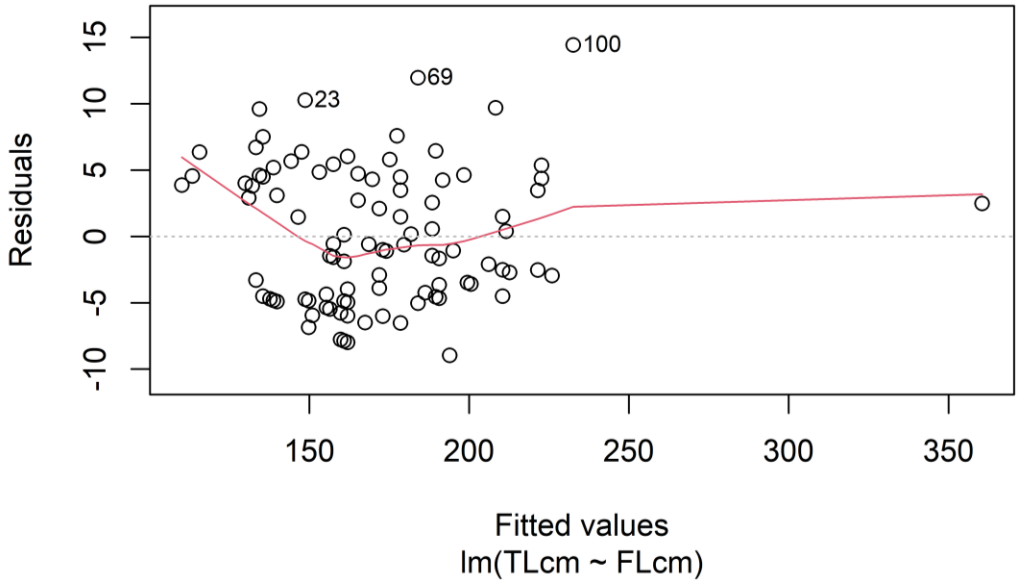


**Figure A1 -** Residual plot from the length-length regression of fork length (FL, cm) and total length (TL, cm). Each point represents the residual for an observation plotted against its fitted value. The dashed horizontal line indicates zero residuals, while the red smooth line shows the trend in residuals. Labeled points (23, 69, 100) indicate observations with relatively large residuals or potential influence. The scatter suggests that model assumptions of homoscedasticity and linearity are not met.

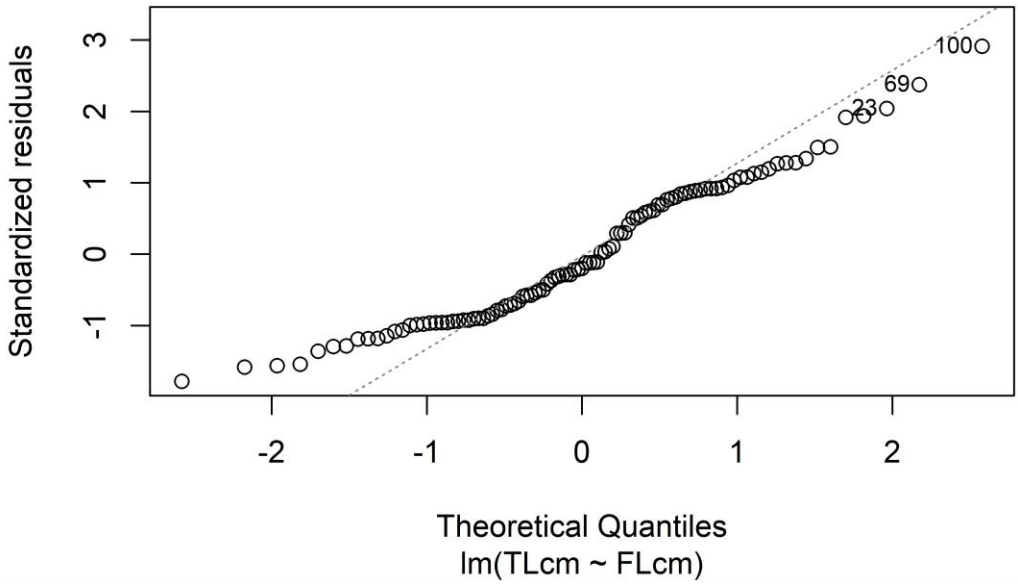


**Figure A2** - Q–Q plot from the length-length regression of fork length (FL, cm) and total length (TL, cm). The points compare the distribution of standardized residuals against the theoretical quantiles of a normal distribution. The dashed line represents the expected 1:1 relationship under normality. Labeled points (23, 69, 100) show some deviation at the upper tail, and the residuals do not follow a normal distribution.

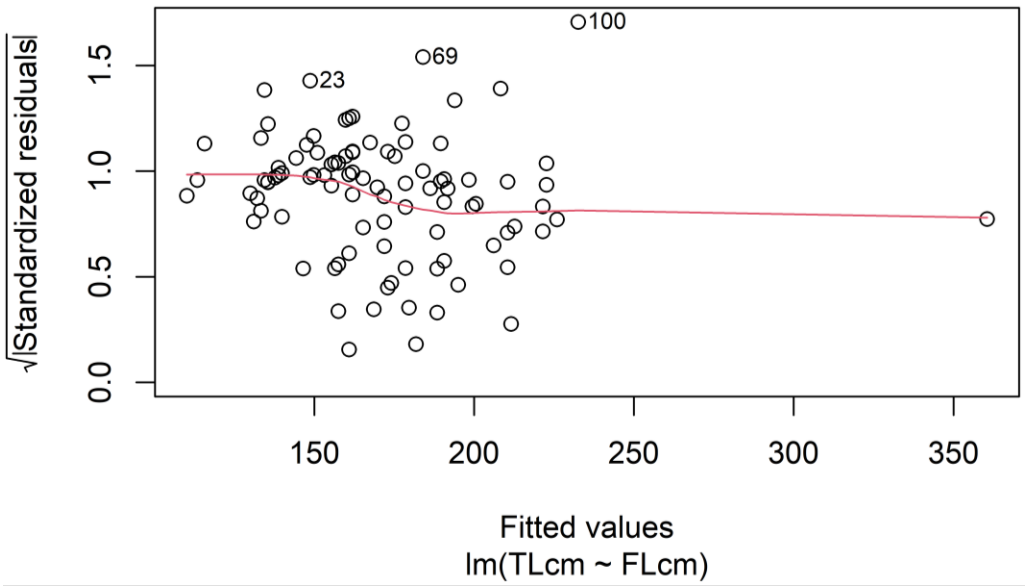


**Figure A3** - Scale–location plot from the length-length regression of fork length (FL, cm) and total length (TL, cm). The square-root of the standardized residuals is plotted against fitted values. The red line indicates the trend in spread across fitted values. The relatively horizontal pattern suggests approximate homoscedasticity, although minor deviations are present, likely due to labeled points (23, 69, 100).

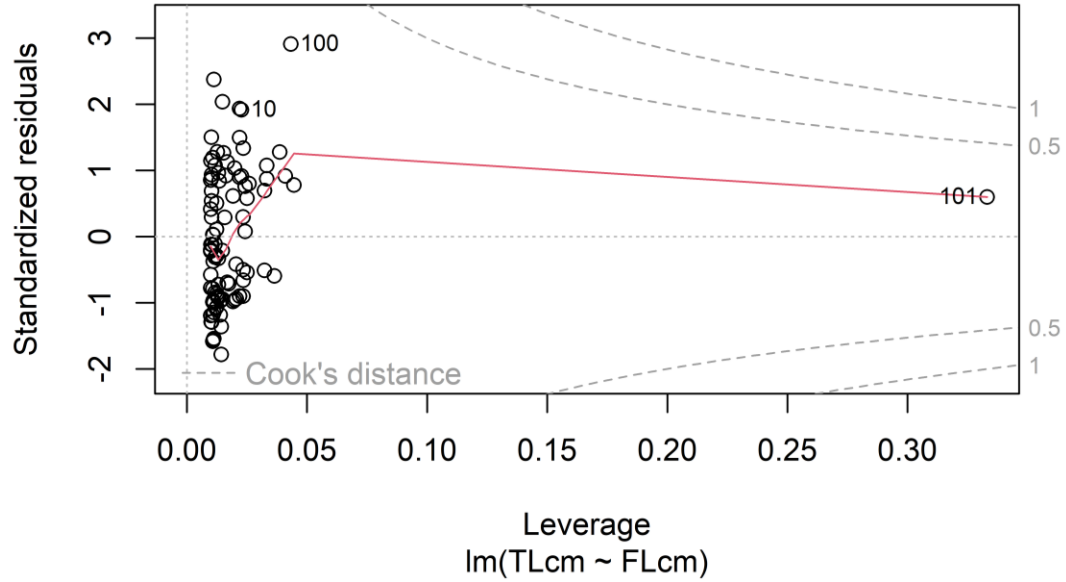


**Figure A4** - Residuals vs. leverage plot from the length-length regression of fork length (FL, cm) and total length (TL, cm). Dashed lines indicate Cook's distance, which helps identify observations with potential influence on the model. Labeled points (10, 100, 101) are potentially influential, though overall the model does not appear to be dominated by single observations.

## Appendix B

## Linear Regression Residual Diagnostics

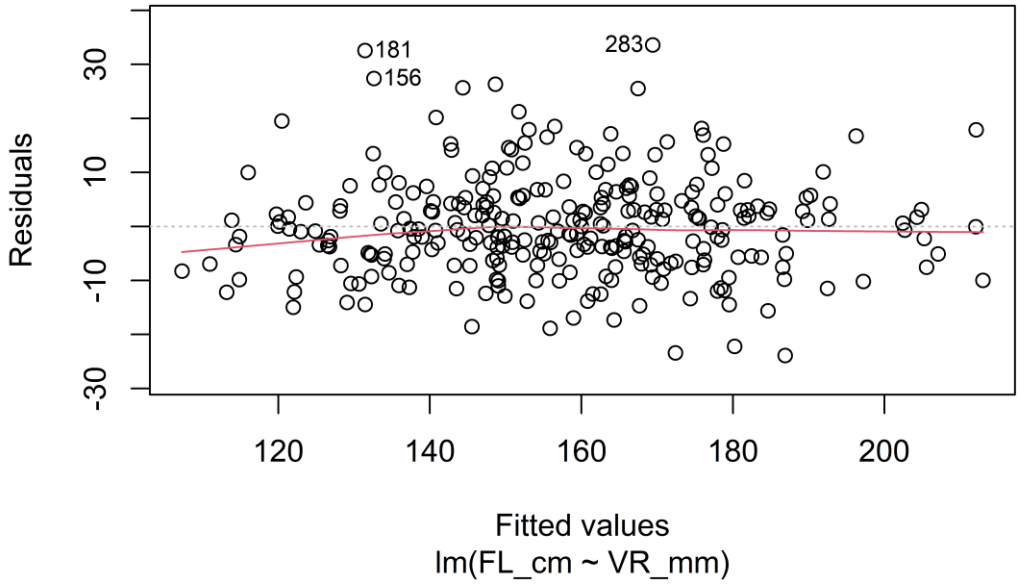


**Figure B1** - Residual plot from the linear regression of fork length (FL, cm) and vertebral radius (VR, mm). Each point represents the residual for an observation plotted against its fitted value. The dashed horizontal line indicates zero residuals, while the red smooth line shows the trend in residuals. Labeled points (156, 181, 2830) indicate observations with relatively large residuals or potential influence. The generally horizontal scatter suggests that model assumptions of homoscedasticity and linearity are approximately met.

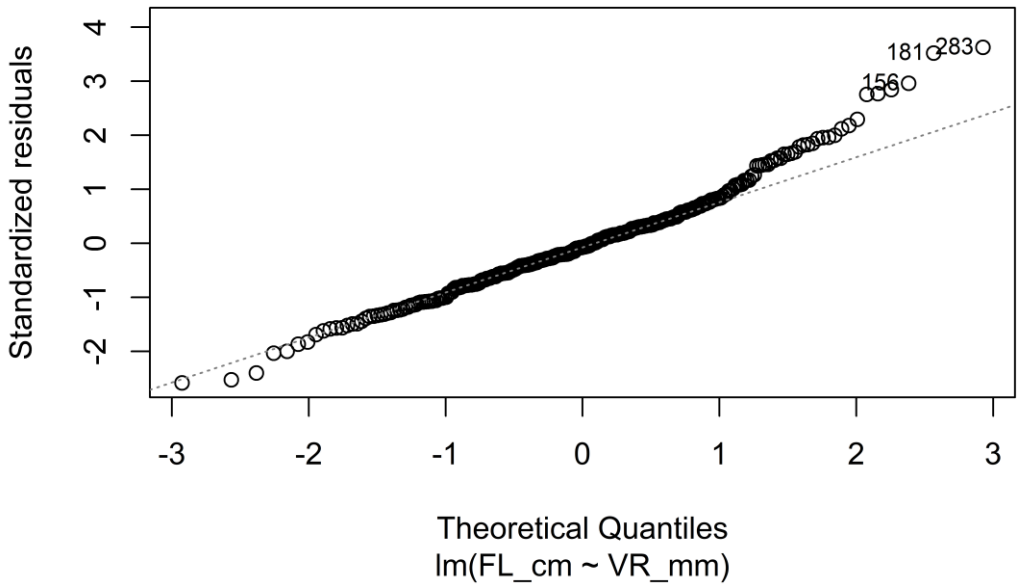


**Figure B2** - Q–Q plot from the linear regression of fork length (FL, cm) on ventral radius (VR, mm). The points compare the distribution of standardized residuals against the theoretical quantiles of a normal distribution. The dashed line represents the expected 1:1 relationship under normality. Labeled points (156, 181, 2830) show some deviation at the upper tail, but overall the residuals follow a roughly normal distribution.

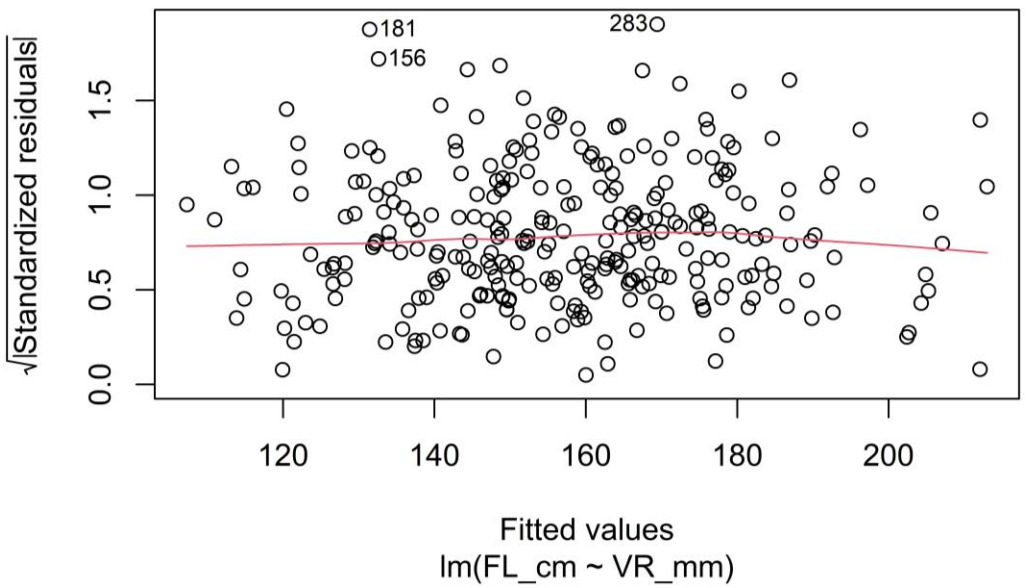


**Figure B3** - Scale–location plot from the linear regression of fork length (FL, cm) on vertebral radius (VR, mm). The square-root of the standardized residuals is plotted against fitted values. The red line indicates the trend in spread across fitted values. The relatively horizontal pattern suggests approximate homoscedasticity, although minor deviations are present, likely due to labeled points (156, 181, 2830).

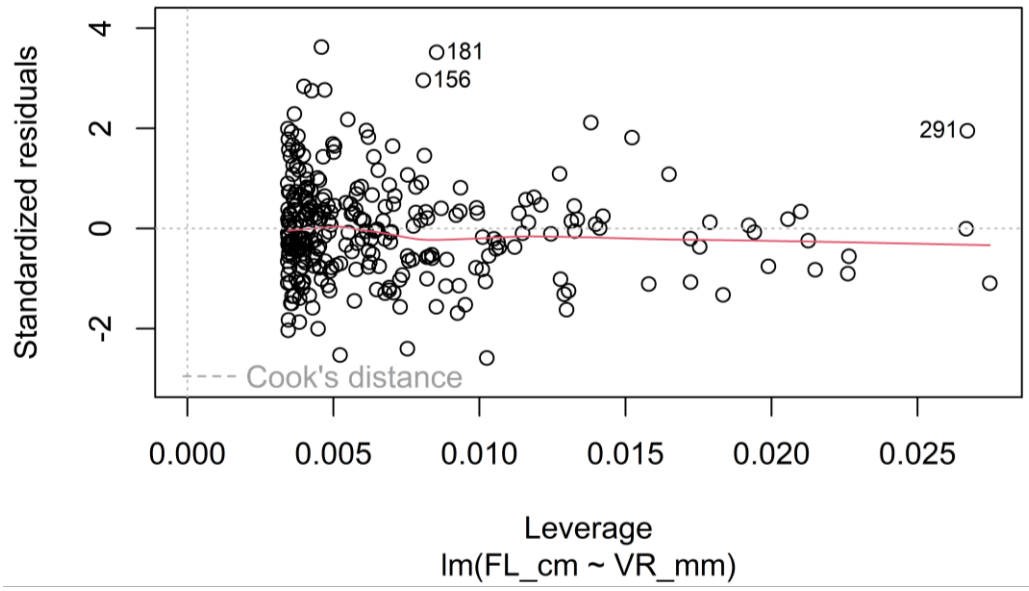


**Figure B4** - Residuals vs. leverage plot from the linear regression of fork length (FL, cm) on ventral radius (VR, mm). Dashed lines indicate Cook's distance, which helps identify observations with potential influence on the model. Labeled points (156, 181, 2830) are potentially influential, though overall the model does not appear to be dominated by single observations.

# Appendix C

## Residual Diagnostics for Growth Models

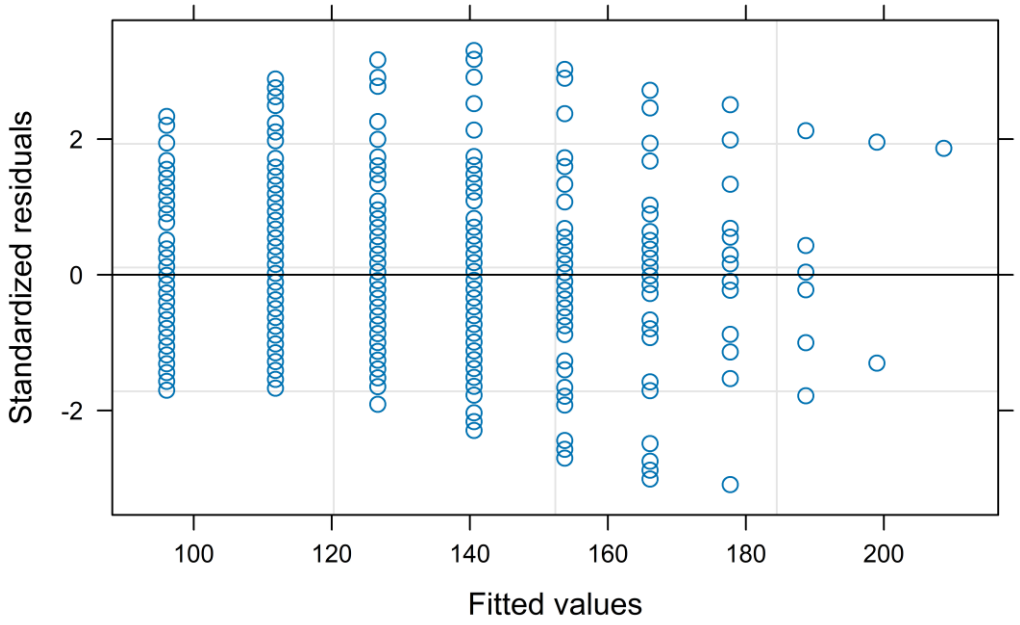


**Figure C1** – Residuals versus fitted values for male *I. paucus* using the three-parameter von Bertalanffy growth model (3P-VBGF). The plot shows slight heteroscedasticity, indicating that the variance of residuals changes moderately across fitted values.

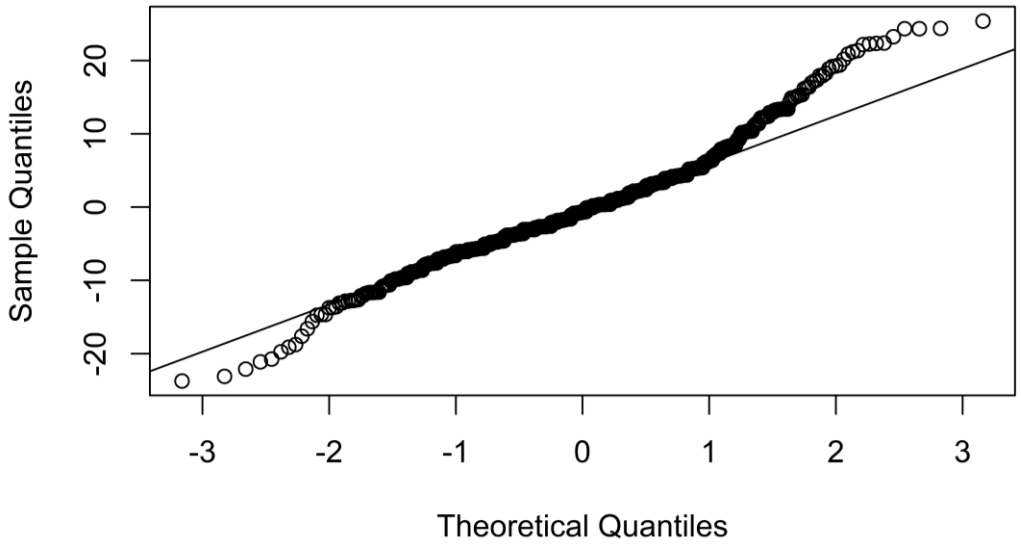


**Figure C2** – Normal Q–Q plot of standardized residuals for male *I. paucus* using the three-parameter von Bertalanffy growth model (3P-VBGF). Residuals generally follow a normal distribution, with slight deviations at the tails indicating minor departures from normality in extreme residuals.

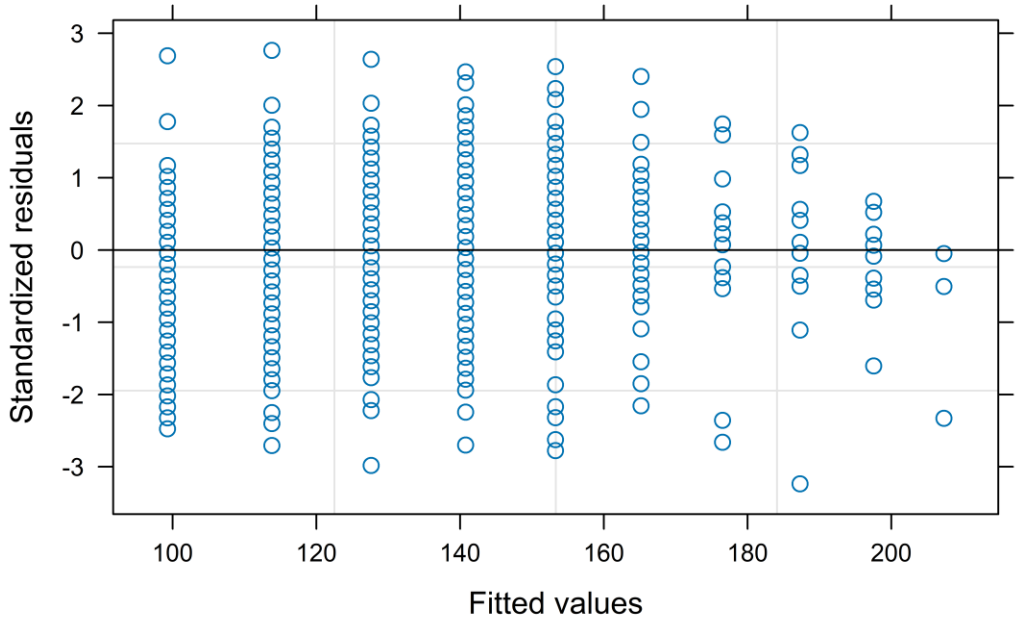


**Figure C3** – Residuals versus fitted values for female *I. paucus* using the two-parameter von Bertalanffy growth model (2P-VBGF). The plot shows slight heteroscedasticity, indicating that the variance of residuals changes modestly across fitted values.

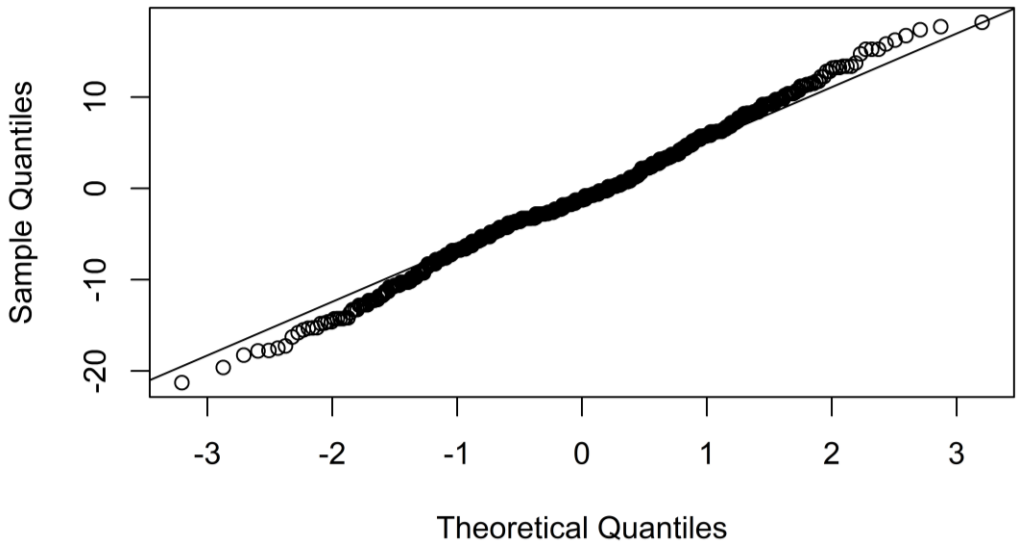


**Figure C4** - Normal Q–Q plot of standardized residuals for female *I. paucus* using the two-parameter von Bertalanffy growth model (2P-VBGF). Residuals generally follow a normal distribution, with slight deviations at the tails indicating minor departures from normality in extreme residuals.